

Size effects on flow stress and springback behaviour in micro metal forming

A thesis submitted in partial fulfilment of the requirements
for the award of the degree of

Master of Engineering (Research)

From

University of Technology Sydney

By

Mandeep Singh

Mandeepsingh@student.uts.edu.au

B. Tech, M. Tech

School of Mechanical and Mechatronic Engineering

Faculty of Engineering and Information Technology

Certificate of original authorship

I, [Mandeep Singh], declare that this thesis is submitted in fulfilment of the requirements for the award of Master of Engineering (Research) in the Faculty of Engineering and Information Technology at the University of Technology Sydney.

This thesis is wholly my own work unless otherwise reference or acknowledged. In addition, I certify that all information sources and literature used are indicated in the thesis.

This document has not been submitted for qualifications at any other academic institution.

This research is supported by the Australian Government Research Training Program.

Production Note:

Signature: Signature removed prior to publication.

Date: 22/02/2019

Acknowledgement

Firstly, I would like to express my sincere appreciation and deepest gratitude to my supervisor, Dr. Dongbin Wei (Associate Professor), for the opportunity he offered, and for his valuable guidance, support, encouragement and friendship during my Masters of engineering (Research) candidature. It has been a great pleasure working with him.

I am deeply grateful to Dr. Jinchen Ji for his strong guidance, valuable discussion and close supervision. Without his support, it would be difficult to achieve this goal.

I am deeply thankful to Dr. GL Samuel and Indian Institute of Technology, Madras to give me an opportunity to do a joint research collaboration work under the UTS '2018 FEIT HDR Students Research Collaboration Experience award'. I would like to convey my appreciation from the bottom of my heart and my gratitude to Dr. GL Samuel for his absolute help, support and warmth towards me. Many thanks as well to Mr. CK Golpalakrishnan and Mr. Srikanth who contributed to design and carry out instrumental analysis in my experimental works at IIT, Madras- India.

I would like to acknowledge senior mechanical engineer Vahik Avakian and Chris Chapman for their help and support in the laboratory and the administrative support from Kara and David as well. I also would like to thank to Mr. Alexander Angeloski from technical support services who gave me enormous help and assistance.

Family is always have been a source of my inspiration, without my family support, I would not have achieved my goals and no words can describe the appreciation for my family for supporting me and encouraging me to enhance my knowledge. At this point, I would definitely like to take this opportunity to express my gratefulness towards, my sister Gurpreet Kaur, brother-in-law Hardeep Singh and my parents for their sacrifices, love, patience, understanding and selfless dedication. They are all to me. Cheers for everything!

Special thanks to my DAD and MOM, love you.

Mandeep Singh

List of Publications

1. **Singh, M.**, Hossain, A. Mishra, P.K. 2019. “Effects of grain size on surface roughness of thin pure Cooper sheets in metal micro forming” *Test Engineering and Management*. Vol. 82, pp. 12673-12678.

<http://www.testmagzine.biz/index.php/testmagzine/article/view/2878>

2. **Singh, M.**, Hossian, A. & Wei, D. 2019 “A Hybrid Model for Studying the Size Effects on Flow Stress in Micro-Forming with the Consideration of Grain Hardening”, *Key Engineering Materials*, Vol. 794, pp. 97-104.

<https://doi.org/10.4028/www.scientific.net/KEM.794.97>

3. **Singh, M.** & Wei, D. 2018 “Size effects in Micro Forming: A review”, *International Review of Mechanical Engineering (IREME)* ISSN 1970-8734, Special issue (print form).

<https://www.scribd.com/document/385504833/Mandeep2018-Dongbin>

4. **Singh, M.**, Sharma, S & Sharma, S. 2017 “Criticality of Micro-Forming Process - A Review”, *International Journal of Emerging Trends in Engineering and Development*. 7(4), pp.191-198. RS publication.

Table of contents

Acknowledgement	iii
List of Publications	iv
Table of Contents	v
List of Figures	viii
List of Tables	xii
List of Abbreviations and Symbols	xiii
Abstract	xv
Chapter 1. Introduction	1
1.1 Research background	1
1.2 Significances of research	3
1.3 Outline of the thesis	4
Chapter 2. Literature review	5
2.1 Size effects	5
2.2 Size effects in micro forming processes	9
2.3 Summary and objectives of this research	20
Chapter 3. Material and methods	22
3.1 Material	22
3.2 Material sectioning	22
3.3 Heat treatment	23
3.4 Sample preparation	24
3.5 3D laser-confocal microscopes	25
3.6 Average grain size (line intercept method)	26
3.7 Micro tensile test	27

3.8 Micro V-bending test	28
3.9 Software applied for numerical simulation and analytical solution	29
3.10 Research methodology	30
3.11 Summary	30
Chapter 4. Size effects on flow stress and surface roughness	31
4.1 Introduction	31
4.2 Micro tensile test	32
4.3 Effect of T/D on flow stress	33
4.4 Constitutive model	34
4.5 Verification	37
4.6 Effect of T/D on surface roughness	39
4.7 Summary	42
Chapter 5. Analytical and experimental determination of modified material intrinsic length of strain gradient hardening for micro V-bending test of pure copper	44
5.1 Introduction	44
5.2 Analytical determination of material intrinsic length (l)	45
5.3 Micro V-bending testing	48
5.4 A combined constitutive model incorporating microstructure and strain gradient effects	49
5.5 Calculation of springback	55
5.6 Prediction of springback angle	56
5.7 Summary	57
Chapter 6. Development of a compact and portable universal testing machine (UTM) for in-situ micro-observation of size effects in micro metal forming	58
6.1 Introduction	58

6.2 Specifications of the developed UTM	59
6.3 Design Concept	60
6.4 Performance and validation	65
6.5 Summary	70
Chapter 7. Conclusion and recommendations for future work	72
7.1 General conclusion	72
7.2 Future work	73
References	74
Appendix-A	81

List of Figures

Figure 1.1: The increase in micro parts from the industrial revolution onward	2
Figure 2.1: Issues related to size effect in micro forming system	5
Figure 2.2: Relation of surface grain to volume grains	6
Figure 2.3: Source of size effects	6
Figure 2.4: Schematic representations of the three main groups of size effects, F force, FA adhesion force, FF friction force, Fc gravity Variation of flow stress with T/D	8
Figure 2.5: Variation of flow stress with T/D	10
Figure 2.6: The microstructure of workpieces at different temperature	10
Figure 2.7: The microstructure of compresses specimen annealed at different temperature	11
Figure 2.8: Variation in yield stress with T/D	11
Figure 2.9: Different size scaled central headed parts	13
Figure 2.10: Variation of fracture strain with T/D	13
Figure 2.11: Fracture of the tested tensile samples	14
Figure 2.12: Formed geometry in different size scaled achieved in double cup extrusion	15
Figure 2.13: (a) Strip drawing test (b) Change of friction coefficient	16
Figure 2.14: Three-point bending test	18
Figure 2.15: Springback angle vs grain size	18
Figure 2.16: Most common adopted techniques for researching springback	19
Figure 2.17: (a) Springback vs thickness and (b) springback vs T/D	19
Figure 3.1: The microstructure of pure copper	22
Figure 3.2: (a) Tensile test specimen (b) Schematic of micro tensile samples, (c) Schematic of micro V-bending samples	23
Figure 3.3: Dog-bone samples preparation method	24
Figure 3.4: Vacuum tube annealing furnace	24

Figure 3.5: Polished sample	25
Figure 3.6: Grinder and polish machine	25
Figure 3.7: 3D laser-confocal microscope	25
Figure 3.8: Sample under microscope	26
Figure 3.9: Microstructure analysis	26
Figure 3.10: Micrograph with random line segments	26
Figure 3.11: Optimization of average grain size in ‘ImageJ’ software	27
Figure 3.12: METEX universal testing machine	27
Figure 3.13: (a) Schematic of micro V-bending punch and die (unit: mm), (b) Real photos of micro V-bending punch and die.	28
Figure 4.1: Real copper specimen	32
Figure 4.2: Micro tensile testing	33
Figure 4.3: The stress-strain curve of copper samples annealed at 700°C	34
Figure 4.4: (a) Rectangular gage section, (b) Gage section geometry	35
Figure 4.5: FEM analysis	37
Figure 4.6: (a) Calculated stress ($T/D > 2.6$) from FEM analysis, (b) Experimental and calculated stress	38
Figure 4.7: Simulation vs experimental comparison of stress-strain curve	38
Figure 4.8: Real copper samples	40
Figure 4.9: Surface roughness testing	40
Figure 4.10: Roughness and waviness profiles of (a) $T/D = 0.78$, (b) $T/D = 1.04$, (c) $T/D = 2.38$	41
Figure 4.11: 3D surface texture of (a) $T/D = 0.78$, (b) $T/D = 1.04$, (c) $T/D = 2.38$	42
Figure 4.12: Surface roughness vs T/D	42
Figure 5.1: Geometrically necessary dislocation morphology in plastic bending of metal	47
Figure 5.2: Stress-strain curves	48

Figure 5.3: V-bending configuration	49
Figure 5.4: (a-b) Actual V-bending test	49
Figure 5.5: Geometric model	52
Figure 5.6: Coordinate diagram defining the spatial quantities	52
Figure 5.7: Stress distribution along the sheet thickness direction	54
Figure 5.8: Schematic diagram of sheet curvature before and after springback	56
Figure 5.9: Springback angle of analysis equations and experimental data	56
Figure 6.1: Overall Structure of the testing machine: (1) stepper motor, (2) coupling, (3) lead screw, (4) supported columns (5) Tensile test fixtures, (6) LVDT, (7) Load-cell	60
Figure 6.2: (a) Original CNC table, (b) Original specifications of CNC linear sliding table (unit: mm)	61
Figure 6.3: Modified specifications of CNC linear sliding table (unit: mm)	61
Figure 6.4: (a) Drawing of specimen holder (unit: mm) (b) Actual specimen holder	62
Figure 6.5: (a) Drawing of specimen holder (unit: mm) (b) Actual specimen holder	62
Figure 6.6: (a) Drawing of specimen holder (unit: mm), (b) Actual specimen holder	62
Figure 6.7: (a) Drawing of V-bending punch (unit: mm), (b) Actual V-bending punch	62
Figure 6.8: (a) High-speed 3-axis vertical CNC machine, (b) Machined fixture	63
Figure 6.9: The overall electronic system	64
Figure 6.10: NEMA Stepper motor	64
Figure 6.11: (a) Circuit diagram of the stepper motor, (b) Circuit of the stepper motor	64
Figure 6.12: (a) Load cell with an amplifier, (b) Load cell interface Arduino	64
Figure 6.13: (a) Load cell interface Arduino, (b) LVDT interface Arduino	65
Figure 6.14: Static calibration curve for the load cell	66
Figure 6.15: Load vs displacement graph	66
Figure 6.16: Displacement vs time graph	66

Figure 6.17: Actual tensile testing on newly developed testing device	67
Figure 6.18: Stress-strain curves obtained from commercial Instron and newly developed testing apparatus	67
Figure 6.19: Stress-strain curve obtained from new testing apparatus	68
Figure 6.20: Stress-strain curve obtained from commercial UTM	68
Figure 6.21: The testing apparatus under the laser microscope	69
Figure 6.22: Schematic illustration of testing setup	69
Figure 6.23: 3D surface profile of copper foil obtained from laser microscope	70

List of Tables

Table 1.1: Typical micro-manufacturing process	1
Table 2.1: Size effects in micro metal forming	20
Table 3.1: Chemical composition of pure copper (Cu), wt%	22
Table 3.2: Sample preparation procedure for microstructural analysis	25
Table 4.1: Microstructure and grain size of the specimen before the tensile test	33
Table 4.2: The values of the parameters used in simulations	37
Table 4.3: Heat treatment and average grain size for surface roughness analysis	39
Table 5.1: Material and experimental set-up parameters	55
Table 6.1: Specifications of the developed apparatus	60
Table 6.2: Average values of a tensile test obtained from home-made machine	68
Table 6.3: Average values of a tensile test obtained from commercial UTM	68
Table 6.4: Calculated mechanical properties	69

List of Abbreviations and symbols

1. Abbreviations

LVDT	-	Linear variable differential transformers
DCE	-	Double cup extrusion
ASTM	-	American society for testing and materials
MEMS	-	Micro-electromechanical systems
FEA	-	Finite element analysis
CAE	-	Computer aided engineering
AGI	-	Average grain intercept
SSD	-	Statistically stored dislocations
GND	-	Geometrically necessary dislocations
UTM	-	Universal testing machine
3D	-	Three-dimensional

2. Symbols

T	-	Thickness
D	-	Grain size
E	-	Young's modulus
ϵ	-	Plastic strain
λ	-	Scaling factor
V	-	Punch velocity
ϵ	-	Logarithmic strain
σ_c	-	Flow stress in the cell interior
σ_w	-	Flow stress in the cell wall
ρ	-	Density

l	-	Material intrinsic length
l_m	-	Modified material intrinsic length
P	-	Conventional effective plastic strain
\acute{r}	-	Nye factor
Z	-	Taylor factor
M_P	-	Plastic bending moment
M_E	-	Elastic bending moment
θ_s	-	Springback angle
$\sqrt{\epsilon}$	-	Strain gradient effect
R_a	-	Arithmetic average of the roughness profile
V	-	Voltage

Abstract

The continuing trend of micro metallic devices and product miniaturization has motivated studies on micro metal forming technologies. A better understanding of material deformation behaviours with size effects is important for the design and operations of micro metal forming processes. In this dissertation, uniaxial micro tensile testing was conducted on copper specimens with characteristic dimensions to micro scales. The experimental results disclose the existence of size effects and reveal the inadequacies of the existing material models. Micro tensile experiments were carried out on copper specimens with varying grain sizes. The size effects on plastic deformation were demonstrated and were further elucidated by comparison between experimental results and the output of finite element simulations. The surface roughness assessment on tensile tested copper specimen showed the significant influences of size effects in micro metal forming process. Micro V-bending was conducted on copper foils with varying thicknesses and grain sizes. The material intrinsic length was observed and modified according to the average number of grains along the characteristic scale direction of specimen. The analytical model of springback with modified material intrinsic length was established and evaluated by employing MATLAB. This study also presents a research work aiming at the design and manufacturing of a compact UTM compatible with a 3D laser-confocal microscope for observing the deformation behaviour of materials in real-time.

Chapter 1. Introduction

1.1 Research Background

Miniaturization is a trend to manufacture ever-smaller mechanical and electrical products. Today in this modern world of miniaturization, the demands of high-performance micro-scale parts are increasing day by day. A micro-scale part is concerned as a small part with typical part-dimensions in the range of sub-millimetres up to a few millimetres [1]. The standard positional precision for such parts is expected to be in the range of 0.1 μm to 10 μm . Micro-manufacturing is a correct and significant approach for manufacturing the micro-scale parts [1, 2]. Both conventional and non-conventional methods have been used in micro-manufacturing to fabricate micro-products [2]. During the past few years, various advanced micro-manufacturing methods have been invented and they all have been continuously used to manufacture micro parts such as (i) mechanical parts – connectors pins, micro screw and spring (ii) electronics parts – cell phones, MEMS (ii) medical micro-components – therapy devices (iv) micro-aerial vehicles – micro-robots (v) sensors and actuators. The typical micro-manufacturing processes are shown in Table 1.1.

Table 1.1: Typical micro-manufacturing processes [2].

Subtractive processes	Micro-mechanical cutting, micro-EDM, laser beam machining, electron beam machining.
Additive processes	Surface coating, micro-casting, and micro-injection molding, sintering, photo-electron-forming.
Deforming processes	Micro-forming (stamping, extrusion, forging, bending, deep drawing, hydroforming) and micro-imprinting.
Hybrid processes	Micro-laser-ECM, laser assisted micro-forming, combined micro-machining and casting.
Joining processes	Micro-mechanical assembly, vacuum soldering, laser welding.

The market demands of the modern world about the microelements are dramatically increased due to which the state-of-the-art in micro-manufacturing processes for fabrication of micro parts thus becomes critical.

A micro forming process is a promising approach [3, 4] for producing micro-scale devices (miniature screw, micro-gear, micro-shaft, and IC-socket) using less manufacturing facilities such as a small space, less energy and resources. Razali et al. [4] studied all the micro-manufacturing methods as an alternative of micro forming, but in the last, they determined it

as a leading method due to the potential capabilities to produce a large volume of micro components cost-effectively. The machines used in micro forming have high accuracy in positioning in the range of several micrometres, which leads to producing a highly precise micro part [4, 5].

Micro forming, in the context of *metal forming*, is defined as the technology of production of micro metallic parts with at least two dimensions in the submillimeter range by using mechanically based processing technologies [5]. In other words, micro metal forming is a manufacturing process of permanent deformation, in which a solid body is preserving by both mass and cohesion [6]. Micro metal forming can be considered as an excellent micro forming process due to the well-known advantages, such as high production rate, near-net-shapes, minimized material wastage and close tolerance [7]. Engel [8] introduced the micro metal forming as a superlative micro-scale deformation process to fabricate the submillimeter range metallic parts with multi facilitation. These advanced features make micro metal forming suitable for the high-volume-low-cost production of metallic parts within the desire durability and strength [7].

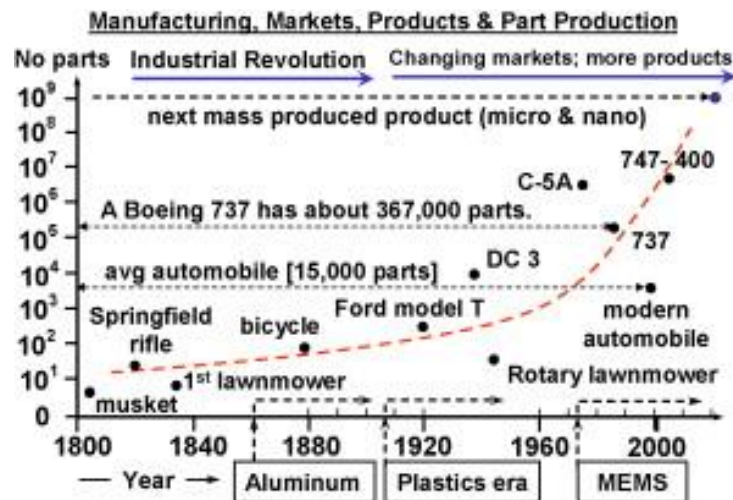


Figure 1.1: The increase in micro parts from the industrial revolution onward [1].

From the trend and previous studies [1-9], it is clear that the micro metallic parts have been achieved more attention due to their wide applications and superior characteristics. Additionally, the development of micro metal forming was driven by the need of mechanical property data on thin films and micro-electromechanical systems (MEMS) structures [9].

In micro forming technology, size effects occur when the dimensions of a specimen are changed, and the ratio among all the certain features cannot be kept constant [10]. Micro metal forming is a prominent field where size effects play a leading role. In micro metal forming, all

the process problems and material behaviour problems that become complicated with further steps in miniaturization are only highlighted with concerning the size effects [10]. For examples, the material deformation and surface roughness issues are directly affected by size effects [11]. All these issues need to be concerned continuously with micro metal forming operations to reach the required dimensions in final products. In micro forming, the optimization of process parameters with the interaction of size effects is very complicated. The size effects in tensile and bending testing of thin films have been studied extensively in the prior studies [11-14], but the size effects investigations for thin films are typically at least, when the T/D ratio is limited in a certain range and average grain numbers are existing along the characteristic scale direction of specimen. Therefore, the size effects related material deformation behaviours (flow stress, surface roughness) and springback mechanism are presented and studied. A boundless deal of research on material deformation behaviours and improvement of the micro metal forming system has been discussed.

1.2 Significance of research

Size effects in micro metal forming is greatly important to fabricate high-quality micro metallic components [15]. The primary feature of micro metal forming is the capacity of fabricating micro metal parts within the dimensions of less than 100 μm [15]. Due to size effects, the experimental and numerical results in micro metal forming are uncertain and cannot be accurately predicted and compensated. It is essential to find out the influence of size effects on a variety of processing in micro metal forming and the deep reasons behind their surface phenomena. For example, the study on size effects in micro metal forming is necessary for investigating the, stress distribution and formation of wrinkles in the material surface.

Only a little knowledge is gained on the influence of the polycrystalline structure of a workpiece on flow stress. Owing to the influences of workpiece thickness and grain size is a complicated process. The deep study of an advanced material model of flow stress is essential to bring superior performance in terms of precise output. Modifying the calculation of dislocations within a grain is a superior approach to evaluate the correct results.

In micro bending, the decrease or increase of foil thickness or the variation in grain size can result in a big springback. Therefore, the springback that is caused by size effects should be identified specifically. The development of a semi-empirical expression to determine the material intrinsic length according to number of grains in the thickness direction of workpiece is a new approach to analyse the size effects in micro bending. Determine the modified material intrinsic length and add it in the mixed constitutive model of springback calculation is an

inventive way to evaluate the more accurate results. The developed models will also help to increase the efficiency of selected deformation processes.

This study is also focused on the evolution of surface roughness in the form of the coupled effect of workpiece thickness and grain size. For the significant investigation of size effects, the material deformation behaviours need to be determined directly from the material characterization. A novel small-scale engineering testing instrument for micro sized specimens that allows in-situ observations of the surface roughness and fracture mechanism by a 3D laser-confocal microscope is newly developed. Micro scale experiments under 3D laser-confocal microscope provide not only a method to observe the microstructure but also the novel way to observe the early stage of fracture mechanism.

1.3 Outline of the thesis

This thesis has seven chapters.

Chapter 1 introduces research background, research significances and the main meaning of this study.

Chapter 2 reviews previous studies and findings that are correlated with the current research work. It includes a variety of researches involving most of the related works that can reflect the relationship between grain size effect and various material properties.

In Chapter 3, all experimental instruments and software adopted in this research are illustrated. The adopted research methodologies are also introduced.

Chapter 4 presents the specimen materials and devices used for micro tensile tests. The experiments comprise annealing, micro tensile tests and microstructural observation. This chapter primarily discusses the relationship between the ratio of T/D and deformation behaviour and surface roughness.

Chapter 5 delivers the analytical and experimental determination of springback angle in the micro V-bending tests of pure copper foils by using the modified material intrinsic length.

Chapter 6, a newly developed miniature universal testing machine (UTM) compatible with a 3D laser-confocal microscope is introduced to perform tensile, compression and micro V-bending tests. All the methods and techniques used to manufacture this machine are discussed and explained in detail.

Chapter 7 provides the conclusions of the current study and cover the recommendations for future research.

Chapter 2. Literature review

With the miniaturization of parts, size effects occur and increase in micro forming processes. Scaling down some specific process parameters of conventional forming is a technique to investigate the size effects in micro forming [11, 15]. In micro forming, there are mainly four factors that affect the quality and efficiency of manufactured parts and micro forming system, respectively, as shown in the following Figure 2.1.

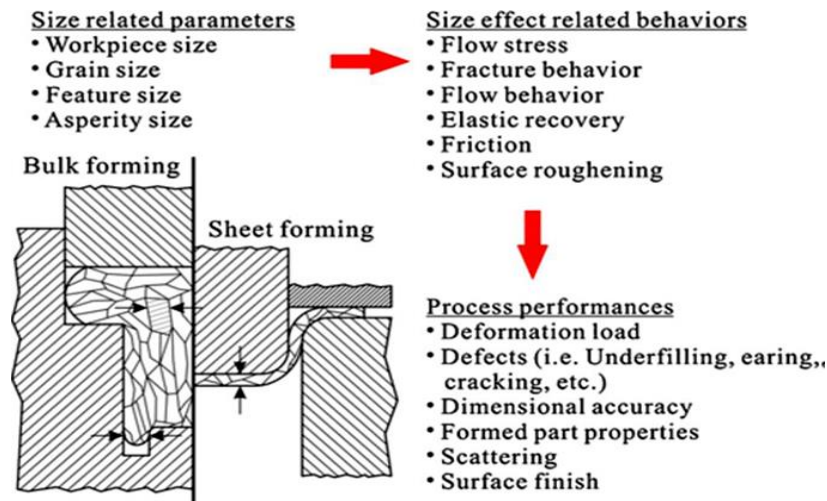


Figure 2.1: Issues related to size effect in the micro forming system [11].

This chapter is mainly focused on the size effects and their influences in micro metal forming. Various research articles and book chapters were reviewed for this research work. In this chapter, the detailed information of the analysis of selected aspects of intensive literature concerned with size effects in micro metal forming are discussed and presented to evaluate the possible mechanisms. This chapter begins with the brief introduction of size effects and then their influences in micro metal forming processes. The next part reviews the springback phenomenon, which is inevitable after bending. The last part concludes the literature review.

2.1 Size effects

2.1.1 Definition of size effects

The term 'size effect' is used when experiments with samples of a distinct size, present non-uniform behavior [16]. To establish the base of this thesis, the first work is to define the size effects. The different definitions of size effects are proposed as follows.

- Size effects are deviations from intensive or extensive values of a process, which occurs when scaling the geometrical dimensions [5].

- The fluctuations in the mechanical behaviour of a material are happened due to the reduction of size from macro to microscale, and that is called as the size effects [11].
- Size effects occur since the ratio between the dimension of the part and parameters of the microstructure is changed according to the process requirements [16].

The above definitions look more sophisticated than ‘size effects’ two words, size effects in this thesis are mainly observed as specimen size (T) and grain size (D). Figure 2.2 illustrates how size effects work when the size of the specimen is scaling down.

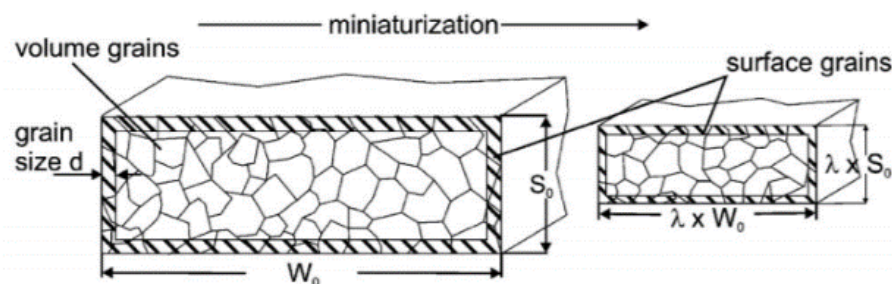


Figure 2.2: Relation of surface grains to volume grains [17].

From the above figure, it can be observed that even if average grain size remains constant, the miniaturisation of specimen dimension leads to the change of the ratio of volume grains and surface grains, which results a strong impact on the specimen mechanical properties.

2.1.2 Sources of size effects

Sources of size effects generation can be divided into two groups [18] physical source and structural source, as shown in Figure 2.3. Physical sources are those, which related to the workpiece size and forces affecting the process; structural sources are those which induced by the microstructure of the material [19].

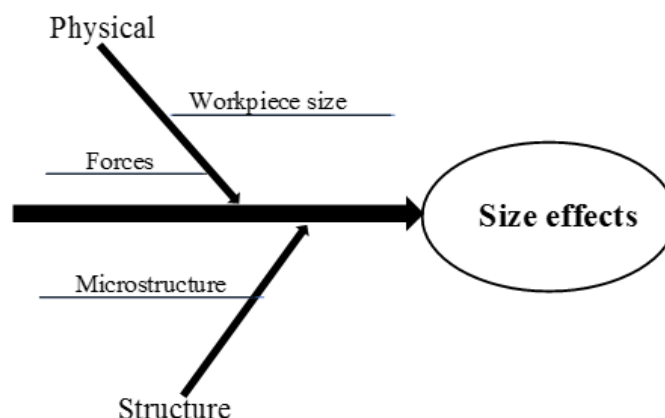


Figure 2.3: Sources of size effects.

2.1.3 Scaling law

To understand and optimize the size effects, it is necessary to review some basic scientific facts first. It is found that due to the size effects, it is impossible to scale down all the theories and technologies of macro to the micro world. To understand the knowledge of scaling the theory of similarity was introduced. According to the theory of similarity during the scaling, all the relevant features like size, weight and velocity must be altered in a fixed relation, e.g. by a constant factor known as scaling factor (λ) [17]. For better understanding, just take an example of a simple upsetting test with the plastic compression of a cylinder of initial height (h_0) to the final height (h). No friction considered to keep this example simple.

The punch velocity (V)

$$V = \Delta h / \Delta t = (h_0 - h) / \Delta t \quad (2.1)$$

The deformation velocity

$$\dot{\epsilon} = \Delta \epsilon / \Delta t \quad (2.2)$$

(where ϵ is logarithmic strain)

$$\epsilon = \ln (h / h_0) \quad (2.3)$$

When the initial height (h_0) is varied from the size a to size b , a similar material behaviour (K_f) is expected for similar deformation speeds, for example.

$$K_{fa} = K_{fb} \quad (2.4)$$

for

$$\dot{\epsilon}_a = \dot{\epsilon}_b \quad (2.5)$$

For identical strain equation (2.5) yield when using equation (2.2)

$$\Delta t_a = \Delta t_b \quad (2.6)$$

as $\Delta h_a \neq \Delta h_b$ and $v_a \neq v_b$

$$h_{0,a} = \lambda h_{0,b} \quad (2.7)$$

$$h_a = \lambda h_b \quad (2.8)$$

the relation of punch velocity (V), equation (2.1)

$$V_a / V_b = (h_{0,a} - h_a) / \Delta t_a / (h_{0,b} - h_b) / \Delta t_b$$

will together with equations (2.6), (2.7) and (2.8) yield

$$V_a / V_b = (\lambda h_{0,b} - \lambda h_b) / (h_{0,b} - h_b) = \lambda$$

Therefore, according to the theory of similarity if the height of $h_{o,a}$ is $\lambda = 10$ times to the height $h_{o,b}$ the punch velocity has also be increased by a factor of 10 to obtain similar material behaviour.

2.1.4 Types of size effects

Vollertsen et al. [5] suggested that size effects could be categorised into three main parts in a systematic order, density size effects, shape size effects, and microstructure size effects, as illustrated in Figure 2.4. Density size effect normally occurs when the absolute value or internal value of a certain feature (i.e. the density) is a constant and independent on the size of the objective [9]. Besides, if the shape of an objective is unchanged while the size of it does, the value of interest can happen to change [15]. Shape size effect is applicable to describe this phenomenon and relationship. The last microstructure size effect contains two conditions: one is the fact that the microstructural features are not scaled down with the macroscopic size of the objective, and the other is that the macroscopic size of the objective remains while the characters of microstructure (i.e. grain size) experience changes.

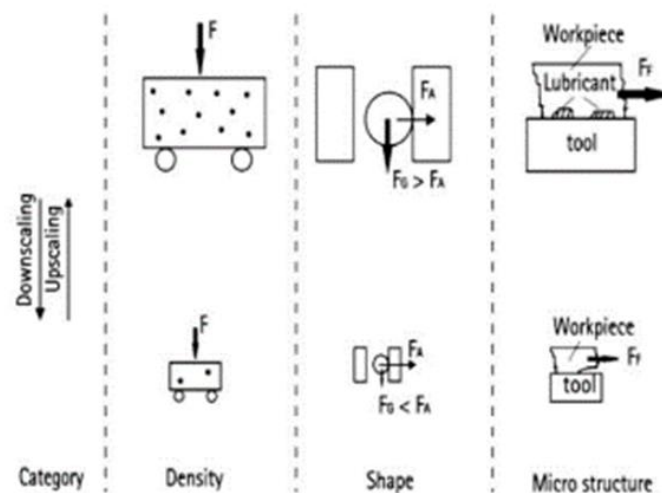


Figure 2.4: Schematic representations of the three main groups of size effects, F force, F_A adhesion force, F_F friction force, F_c gravity [9].

This study concentrates on the third microstructure size effect, to be more exact it mainly focused on the research about the specimen geometry and microscopic grain size and their influences on flow stress, surface roughness and springback through micro tensile and micro V-bending tests.

The size effects for flow stress and surface roughness are investigated in terms of the ratio of the thickness (T) to average grain size (D). The relation of the thickness of the sheet and average grain size can be explained in three different ratios ($T/D > 1$, $T/D = 1$ and $T/D < 1$).

- $T/D > 1$ (more than one grain in thickness direction)
- $T/D = 1$ (only one grain in thickness direction)
- $T/D < 1$ (incomplete grain in thickness direction)

2.2 Size effects in micro forming processes

2.2.1 Size effects on flow stress

In micro metal forming process, it is important to know the required force and power to achieve the necessary deformation. From the stress-strain graph, the required stress to change the workpiece into plastically in nature can be calculated. The instantaneous value of force, which is necessary to continue the yielding and the flow of the work material at any point during the process, is called 'flow stress' [20]. In other words, flow stress is the stress applied to cause a material to deform at a constant strain rate in its plastic range. Guo et al. [21] analysed that the flow stress and other factors such as forming limit, anisotropy, and the ductility all are influenced by size effects. Then, to observe and quantify the flow stress and all other factors the material properties test need to perform. Suzuki et al. [22] introduced the tensile and compression test as the essential experiments to study the size effects on flow stress and material properties.

In metal forming, the material behaviour describes in the form of flow stress and flow curves. To observe the 'specimen size effect' (t_o) on the material behaviour, the measuring of flow stress in various tensile test conditions of different material was performed. From these tests, it is concluded that instead of specimen size the grain size has a substantial effect on flow stress and material behaviour, when the length scale change from macro-to-micro level, especially when the T/D value is more than 10-15, shown in Figure 2.5 (c) [23]. Generally, it is analysed that with the decreasing of specimen size the flow stress is also declined, which is happened due to the inclination share of surface grains [24]. To analyse the effect of T/D on flow stress, results of numerous studies were investigated and, it was concluded that the flow stress shows a decreasing trend with decreasing T/D value, as shown in Figure 2.5 (a) and (b). Related results were observed in the compression test of CuZn15 and copper and bulging test of CuZn36 [23, 24]. However, Anand et al. [23] discussed that in some material tests, when T/D condensed to range 2~4, an increase in flow stress had reported. For example, in the tensile test of 99.999% Al and bulge test of CuZn36 an increase in flow stress is found as T/D value decrease from 3.9 to 3.2, as shown in Figure.2.5 (a). Further, the inclination in flow stress is also observed as T/D

is reduced to 1 (single crystal deformation) in bending test of CuZn15 [25], as shown in Figure 2.5 (c).

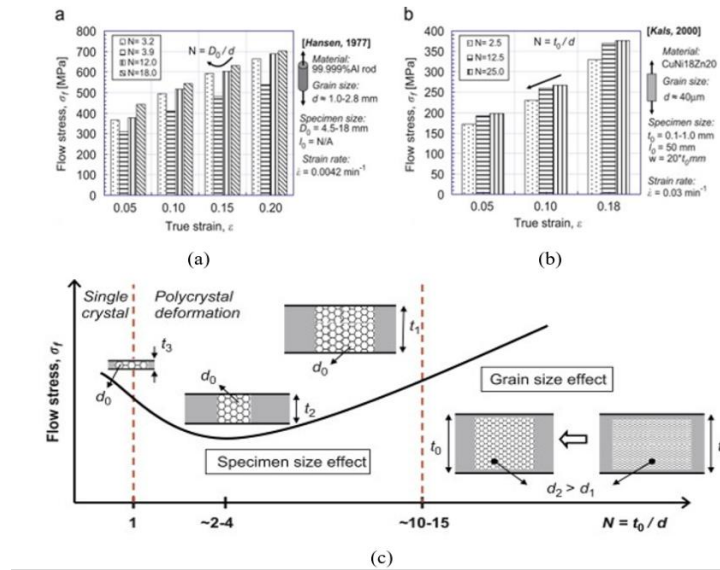


Figure 2.5: Variation of flow stress with T/D [23].

Sutou et al. [26] applied tensile tests on Cu sheets of a different scale to investigate the size effects of sheet material behaviour and found the same trend in flow stress as T/D vary. The grain size effect on flow stress occurs in both the macro and micro-sized specimens, while the specimen geometry size effect is only significant when there are less than 10 grains in the cross-section of specimen [27]. The dwindling of grain boundary strengthening effect causes this phenomenon.

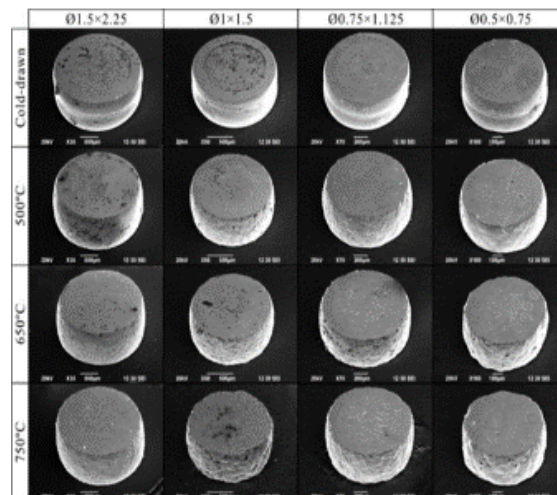


Figure 2.6: The microstructure of workpieces at different temperatures [15].

Wang et al. [28] performed upset forging experiments using cold drawn and annealed copper billets of different sizes from macro to micro scale. It was observed that the cross-section of

compressed specimens changing in shape from circular to irregular with the reduction in workpiece diameter and increase grain size, as shown in Figure 2.6.

It has resulted that the irregular material flow firstly has been found at the end of the material surface, not at the midsection. A similar observation was found by [29] in a micro-compression test of Al6061 with different sizes. Inhomogeneous and anisotropic material behaviour is observed in coarse-grained samples and it to be more accurate, with an increasing ratio of sample size to grain diameter. The non-uniform shapes and deformation process of deformed samples are prompt by the fluctuation in grain size, shape and orientation, as shown in Figure 2.7, which leads to the inhomogeneous billet deformation.

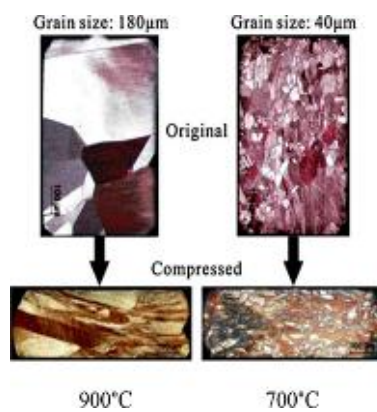


Figure 2.7: The microstructure of compresses specimen annealed at different temperature [29].

Ike et al. [30] also investigated the relationship between the blank thickness and grain size by introducing the new stress-strain constitute equation contained by the Nelder-Mead method. They applied the uniaxial test when the grain size was constant, and thickness was different and on the other side, bending test was performed when the thickness was constant, and grain size was different.

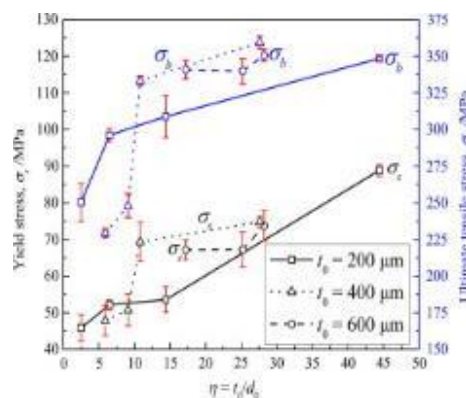


Figure 2.8: Variation in yield stress with T/D [29].

One possible consequence of Lai and Peng [37] work was that the yield stress reduces when grain size was less than thickness and when the grain size is larger than thickness the yield stress and tensile stress increases, as shown in Figure 2.8.

According to the Schmid law, shear stress is at its peak level when it occurs in slip plane and direction [31]. Crystal slip or slipping is the main reason behind the grain deformation. The slip system is defined by the combination of slip plane with normal and slip direction, and it is determined by the combination of grain orientation and applied stress. This deformation mechanism leads to the anisotropic properties of a single grain. Since the macro-scaled polycrystalline material is composed of many grains, the grains can be evenly and randomly distributed with different properties. If a micro workpiece with coarse grain size then there will be, only a few grains constituting the sample and the distribution of different grains will no longer exist. Therefore, if every grain has an anisotropic property, then it should affect the flow behaviour and leads the inhomogeneous deformation.

Fu et al. [32] performed a micro-tensile test to investigate the results of grain size effects on deformation behaviour and fracture in phosphor foil while in experimental study, to obtain the different grain sizes the various heat treatments has performed on the specimen. It successfully examined that the material plastic deformation increases with the increase of T/D ratio. Wang et al. [33] performed the same experimental work on the copper sheet to study out the changes in volume fraction with the alteration in the ratio of thickness to average grain size (T/D). It is found that the accuracy and flow behaviour of copper sheet could be improved by introducing the additional thickness [33, 34]. It is essential to check the quality of the micro-formed part. In a microscale deformation, process the focus concern on the geometrical accuracy, high durability and accuracy of micro-formed parts, because a micro part with few microns is required for many industrial applications.

2.2.2 Size effects on fracture

Fracture is caused by the progressive degradation of material stiffness when plastic deformation reaches a certain limit [34]. No doubt, that in micro forming the fracture behaviour is much different from macro-forming [35]. Researchers performed different experimental and simulation studies to investigate the size effects on fracture behaviour in micro metal forming. Furushima et al. [36] observed the fracture behaviour in the compression test of brass, and concluded that the formability increases with the reduction of specimen size for given grain size, as illustrated in Figure 2.9. In other words, it could be explained that it needs larger deformation or strain to initiate the fracture in micro metal forming.

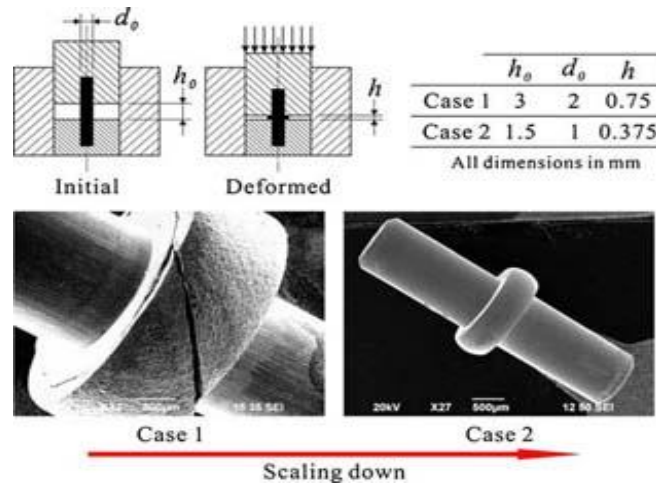


Figure 2.9: Different size scaled central headed parts [37].

Similarly, to flow stress, the fracture strain decreases with the decrease of specimen size [37] such as in compression of metal where a larger strain is needed to achieve the critical damage energy. Furthermore, the variation in fracture strain with the change of T/D in the tensile test is shown in Figure 2.10.

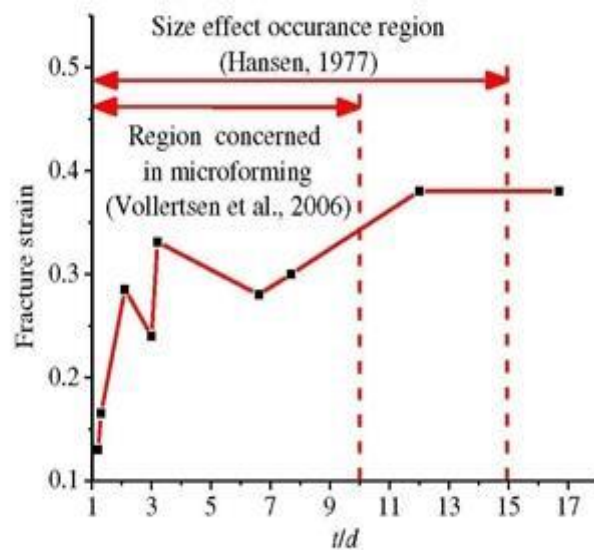


Figure 2.10: Variation of fracture strain with T/D [38].

Figure 2.11 shows the fractography of tensile tested sample with two separation thickness (600 and 100 μm) and different T/D values. It is notable that different ratio of thickness to average grain size has different fractography images. Figure 2.11 (a-b), clears that fracture strain and micro-voids on fracture surface decrease with decreasing T/D [36]. The fracture behaviour in a micro metal forming process mostly occurs due to the small number of grain in thickness of the metal sheet. When there are only few grains across the thickness direction, the grain boundary shares reduced, which caused the void formation of grains in micro forming [36].

Therefore, the number of micro-dimples or micro-voids decreases with the decreasing of T/D. In the extreme case with only about one grain ($T/D = 1.2$) in the thickness direction, there is no micro-void found [40], as shown in Figure 2.11 (c).

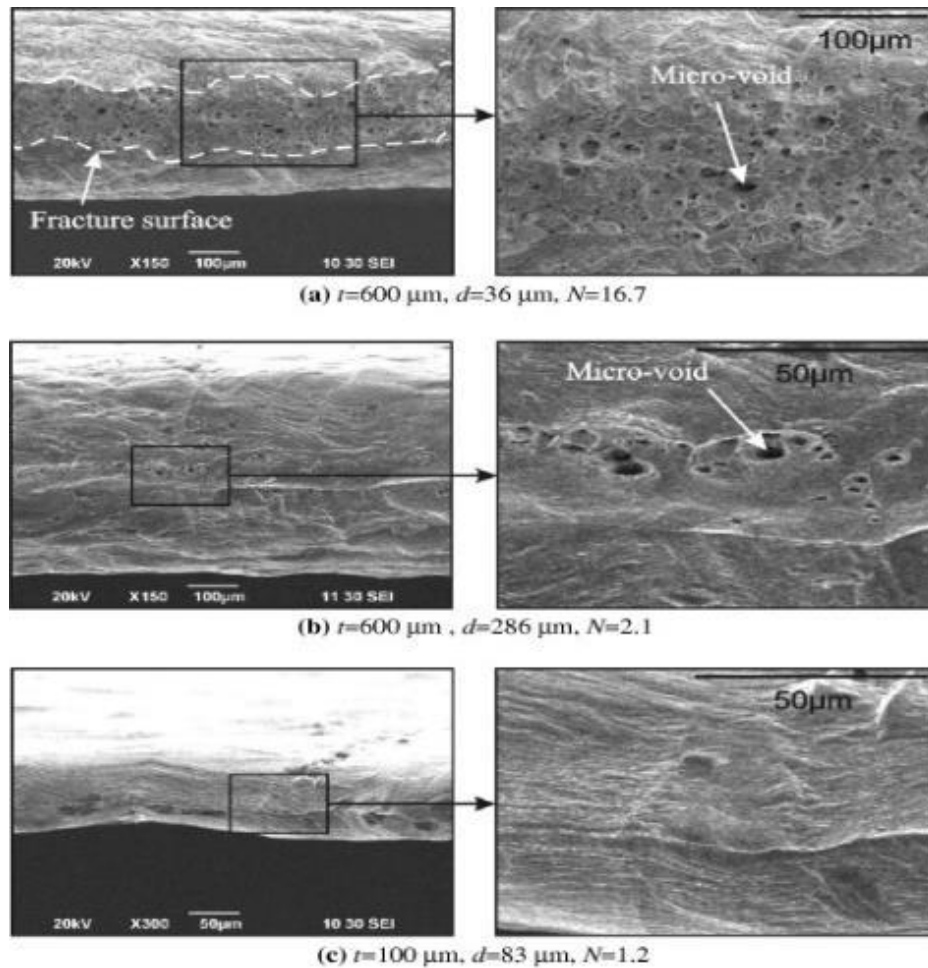


Figure 2.11: Fracture of the tested tensile samples [40].

It is also found that the fractographs reflects unique features in the three-different T/D values, which show that material can have the mixture of ductile fracture mode and brittle fracture mode [43]. Fu et al. [32] highlighted that the materials tend to fracture in ductile mode when $T/D > 1$ because then the micro-voids averagely distributed along fracture direction, while when $T/D < 1$ only a few micro-voids can be found which caused the brittle fracture nature and only a few micro-dimples focused in a certain limited area when $T/D \approx 1$.

2.2.3 Size effects on friction and surface roughness

On the micro level, the tribology is a phenomenon by which we can get more knowledge about the process feasibility and quality. In micro metal forming, the tribology has a significance influence on the quality of manufactured parts, the tool lifetime and process stability [41]. The

tribological behaviour depends on the various parameters such as contact pressure between tool and material and the lubrication conditions [42].

Friction is a phenomena in which the two surfaces get interlock with each other due to the surface asperities. Friction is an undesirable property that leads to non-homogeneous deformation of the material, causes tool wear and residual stress in the product [42]. Whereas, in micro metal forming when surfaces tend to slide against each other the shear stress induced at the interface, is called as sliding friction. In micro metal forming the friction effect has much considerable as compare to in traditional macro metal forming [43]. It is important to investigate both theoretical and experimental studies for better friction modelling because it is one of the key inputs in the finite element analysis method.

According to Jiang et al. [44], the friction could be observed by measuring the change in the shape and dimension of the deformed sample. Klusemann et al. [45] explained size effect on friction in metal forming by categorizing them into two groups (i) bulk-forming and (ii) sheet metal forming and revealed that the friction in the micro forming process increases with decreasing the specimen size.

Friction behaviour in micro bulk-forming -

The variation in interfacial friction with the reduction of specimen size or micro-scale deformation can be observed by the size-scaled ring compression test and double-cup extrusion test [46]. These both tests involve higher surface expansion and force per unit area and thus represents more nearly the practical situation encountered in micro-scale deformation.

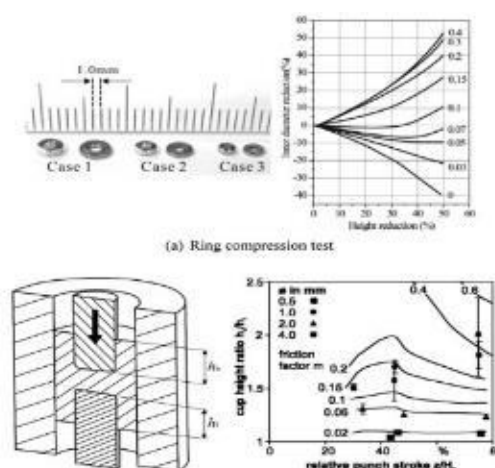


Figure 2.12: Formed geometry in different size scaled achieved in double cup extrusion [46].

The ring-compression test, which uses the friction-dependent change of the inner diameter when upsetting a ring-like sample, is one of the most frequently used tests in micro metal

forming operations. In-ring compression test, the inner diameter of the deformed ring decreases with the increasing friction, whereas in double cup extrusion (DCE) the ratio of upper cup height h_u to lower cup height h_i increases with the increase in friction [47], as illustrated in Figure 2.12.

The double cup extrusion (DCE) can be conducted using workpiece with scaled-down diameters in the range of 4.8-5.0 mm [48]. In double cup extrusion process if the height of two cups is same, then the friction will be very low. Furthermore, it is observed that in double cup extrusion, process the highest friction occurs at the beginning of the operation and then it decreases, but it increases again at the end of the process.

Friction behaviour in micro sheet forming -

Eckstein et al. [48] defined the micro sheet forming as more sensitive to the coefficient of friction than in micro bulk forming. Figure 2.13 shows the strip drawing method that is the simplest method to determine the friction coefficient.

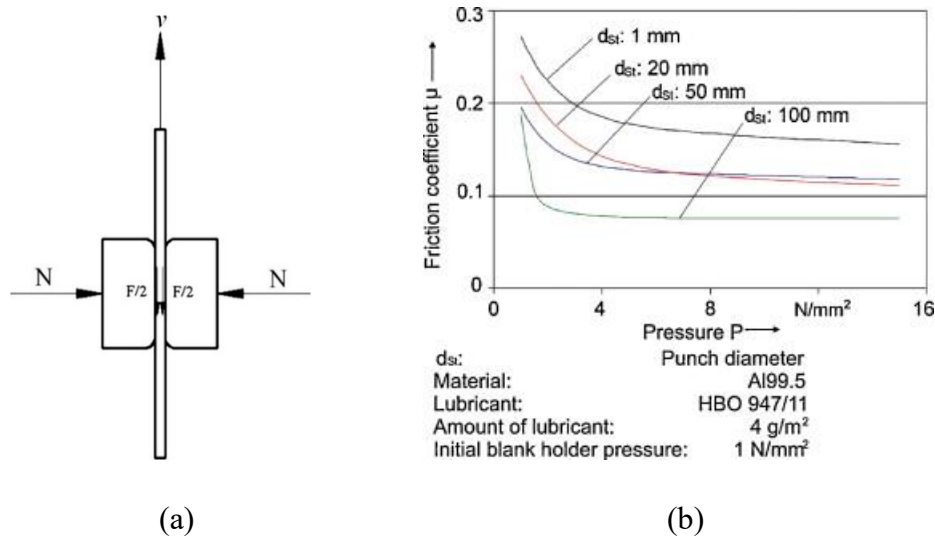


Figure 2.13: (a) Strip drawing test (b) Change of friction coefficient [48].

Vollertsen et al. [47] studied both micro and macro deep drawing and made a new friction test model and observed that the friction factor m is high in micro forming than in macro-forming.

$$\mu = \frac{F}{2N} \quad (2.9)$$

Where is μ coefficient of friction F and N are the friction force and normal force respectively. From the most of the experimental studies [9, 34], it is concluded that the friction coefficient increases (with lubrication) clearly with the reduction in specimen size, as illustrated in Figure 2.13 (b). Instead of the deep drawing process, a researcher [42] used another method to discover

the tribological size effects with considering the tangential forces, which exists when blank is drawn into die. Furthermore, another modification method is required to make many nanoscale crystals on the sample surface so that the lubricant oil is trapped into them to reduce friction [43]. During the miniaturization, the friction and deviation of punch forces increases. Thus, the friction law developed by Kim et al. [12] is the best way to study the scaling effects in the micro forming process.

Surface roughness behaviour - The ratio of tool asperity size to the formed element size increases with the decrease of workpiece size and increase of grain size [39]. The interface effects between die and workpiece become significant in micro metal forming. Geiger et al. [48] examined and found that the friction factor can lead to wrong results in micro metal forming. Some researchers have been studied impact of degree of tool/die roughness on the workpiece/material deformation by numerical analysis. Surface roughness is a non-intrinsic property of the micro forming process; the micro-scale parts should be less rough for better product quality. The arithmetic average (R_a) has been used to express the surface roughness of the material.

In micro forming, the surface roughening easily occurs on the free surface of the specimen because the deformation sample contains several grains [48]. In the micro metal forming processes, the surface roughness is mostly occurred due to the crystal orientation between the grains. The variation of thickness and surface irregularity can be attributed to the difference of schmid factor of individual grain, which specify the slip system for the occurrence of surface roughness [48]. The grain with high schmid factor stretched easily without any interruptions, but the opposite scenario occurs for the grain with lower schmid factor. As a result, the variation in the schmid factor of neighbouring grains leads high surface roughness. The surface roughness of the deformed sample increases significantly with the decrease of T/D; this is because the surface grains are less constrained and easier to deform on the free surface with a small ratio of T/D.

2.2.4 Size effects on springback

2.2.4.1 Mechanism

In a forming process, when the load is applied on the workpiece, it produced stress within the workpiece, which leads to both elastic and plastic strain [49]. For example, in a sheet metal forming process, the elastic strain tries to recover the part of deformation after the removal of external load and this phenomenon is known as springback [50, 51]. The workpiece material elasto-plastic characteristic directly affects springback behaviour.

The variation in grain orientation in the material surface resulted as the main reason for springback [50]. The springback behaviour has been investigated in various forming experiments. The springback effect is also considered in an L-bending process, and it is found that springback decreases with die radius, die angle and the clearance between the punch and die [52]. Moreover, in a rolling process, it is found that the springback angle along the rolling direction is bigger than that in the transverse direction. Gau et al. [51] performed the three-point-bending experiments on pure copper foils to investigate the impact of size effect on springback. All the bending experiments are performed on a MST, shown in Figure 2.14.

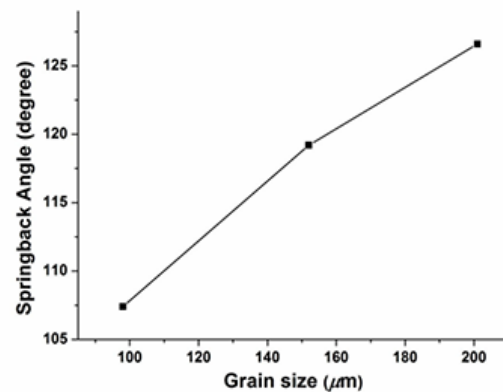
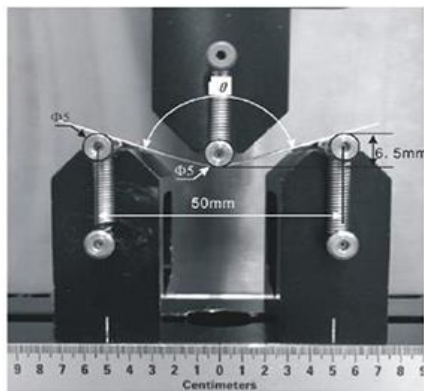


Figure 2.14: Three-point bending test [51]. **Figure 2.15:** Springback angle vs grain size [50].

It was found, as shown in Figure 2.15 that in a micro-bending process the reduction of sheet foil thickness (T) or inclination in grain size (D) caused a big springback. The inclination in surface grains resulting a reduction in the springback angle, which exerts an influence that is normally countered by strain gradient effect ($\nabla \epsilon$) [54]. However, to investigate the impact of size effects on springback the micro bending process of pure titanium foils has been performed. It is observed that the springback angle increases with the decreases of foil thickness at room temperature, but while performing the micro-bending test at elevated temperature the springback angle decreases with decreasing the foil thickness [50]. A reduction in springback angle with the rising of temperature indicates a better accuracy of the parts formed at elevated temperature.

2.2.4.2 Experimental research on springback

Springback of sheet metals has been studied and characterised by developing various experimental techniques and procedures. The most popular and commonly used techniques are cylindrical bending, U bending, and V bending as illustrated in Figure 2.16. The sensitivity of springback to basic parameters, such as R/T ratio (tool radius to sheet thickness), geometric

parameters of the tools, mechanical properties of sheet material and friction parameters are usually investigated by using these methodologies and related equipment's.

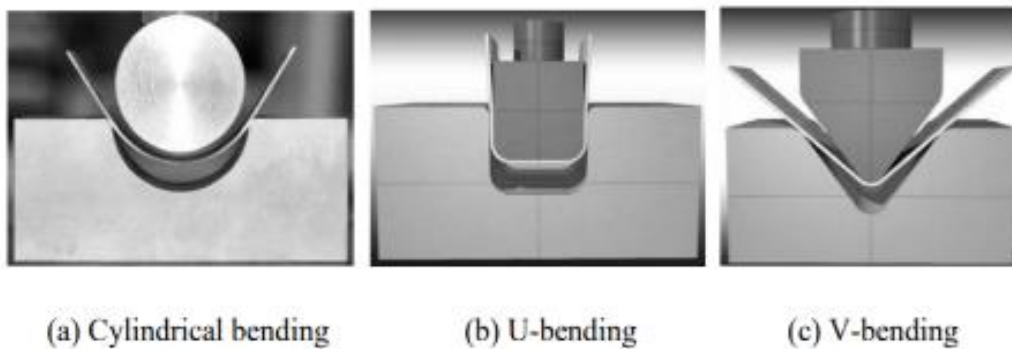


Figure 2.16: Most commonly adopted experimental techniques for springback analysis.

There is sufficient experimental findings dealing with understanding and characterising the springback phenomenon of sheet metals. However, the experimental methods that are capable of controlling the sliding over the tools, surfaces and that allow careful control of experiment parameters are less common. Gau et al. [51] conducted the micro three-point bending with different sample thicknesses and different grain sizes, more importantly, different T/D (thickness/average grain size) ratios. The focus of that research was to analyse the relationship between springback amount and T/D ratios for brass material only, and a conclusion was made based on the results shown in Figure 2.17.

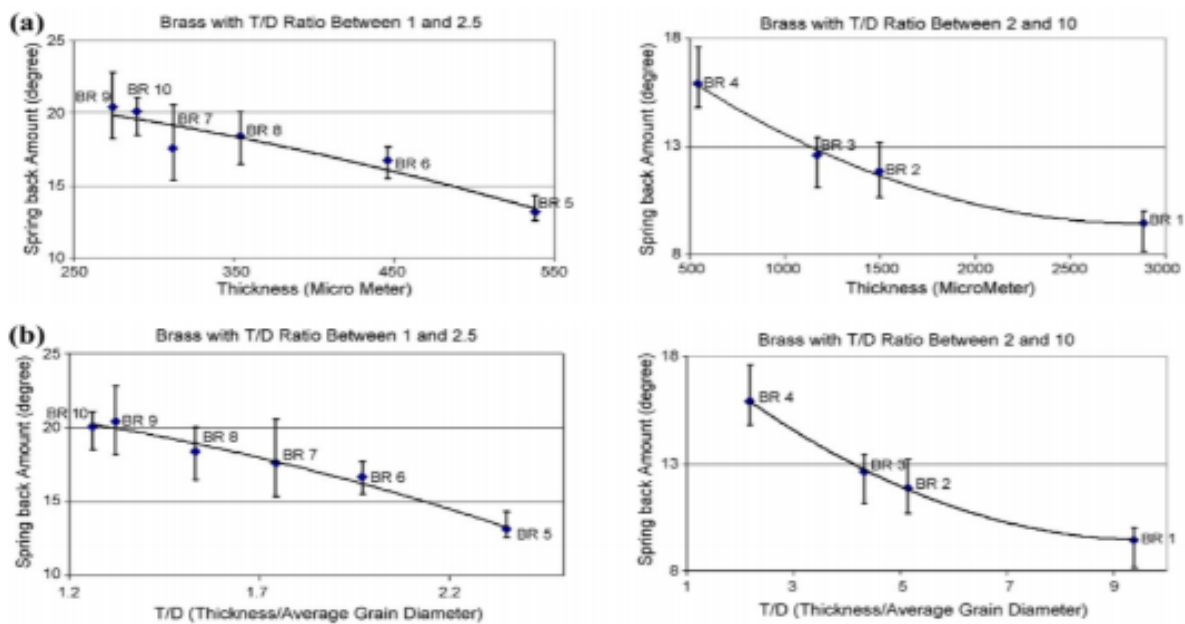


Figure 2.17: (a) Springback vs thickness and (b) springback vs T/D [51].

2.3 Summary and objectives of this research

In this chapter, a brief introduction to a special phenomenon in micro metal forming processing called size effects was given. Further, the experimental investigations and numerical studies on material deformation behaviours were reviewed in detail. All the researchers conducted parametric research and concluded that the advancement of the micro metal forming process could be characterized by the measurement of their properties accurately. All the identified critical issues in the micro metal forming system are explained in the following Table 2.1.

Table 2.1: Size effects in micro metal forming.

Flow stress	Decline with the decrease of specimen size and an increase in grain size [23]. Non-uniform material flow occurs with the decrease and increase of workpiece size and grain size respectively [21].
Fracture strain	Fracture strain decrease with the decrease of workpiece size and an increase in grain size [14].
Frictional behaviour	The interfacial friction of tool-workpiece occurs due to the fraction of open lubricant pockets, which increase with the decrease of workpiece size [34].
Surface roughness	The ratio of roughness size to formed part size (asperity) increase with the decrease of workpiece size and the increase in grain size [38].
Springback	Elastic recovery increases with the reduction of T/D (specimen size to grain size) [51].

After reviewing the previous studies it is found that in micro metal forming processes, the ‘grain size’ size effect plays a significant role as compared to other, and the function of T/D is a critical condition to distinguish the micro-scale from macro-scale. Due to the important role of grains in the micro-scale processes, the strength of the material can be observed by measuring the changes in average grain size. This statement is based upon the observations that grain boundaries obstruct dislocation movement and that the number of dislocations within a grain. Therefore, by changing the grain size one can influence dislocation movement and improve the material properties. For example, heat treatment after plastic deformation and changing the rate of solidification are the two different ways to alter grain size.

There are some blanks in the research of micro metal forming, for instance, the relationship between grain size effect ratio and deformation behaviour, especially when the ratio is limited in a certain range. A more accurate modelling technique for FE simulation is required with the consideration that current modelling cannot display. No significant research has been done on the plasticity model of micro bending with characteristic length to capture size effects. The method of in-situ observation of surface roughening during plastic deformation is required for the better understanding of the influences of size effects.

Based on the above summary and analysis, in this thesis, the following objectives will be tackled to obtain a clear and unambiguous understanding of size effects in micro metal forming:

- i. To determine how the size effects affect the flow stress in terms of specimen's thickness (T) / average grain size (D) in polycrystalline structure.
- ii. To propose some modifications in material model, in order to explain the size effects in polycrystalline structure and deliver reliable calculations.
- iii. To determine how the T/D ratios affect the evolution of surface roughness.
- iv. To comprehend the effect of modified intrinsic length according to average grain numbers along the thickness direction of specimen for micro V-bending test and use it in the proposed constitutive model to study the springback angle.
- v. To develop a new micro testing machine (UTM) compatible with 3D laser-confocal microscope for in-situ micro-observations.

Chapter 3. Material and methods

In this chapter, the experimental instruments numerical software and methodologies adopted in this study are briefly introduced. The corresponding results are described in detail in the following chapters.

3.1 Material

Nonferrous metals are widely used in electronic components, medical devices in terms of micro parts due to their high electrical and thermal conductivity, good ductility and excellent wear resistance, fatigue strength and bearing properties. The most commonly used wrought forms are a strip, rod, wire and tube. Pure copper (99.9%) foils are selected as the experimental material in this study. The typical microstructure of pure copper (99.9%) is shown in Figure 3.1. The supplier of this material was K.T. Global Incorporation, Kanagawa, Japan. The supplied form was 0.05mm × 200mm × 1000mm, 0.1mm × 200mm × 1000mm, 0.3mm × 200mm × 1000 mm and 0.5mm × 200mm × 1000 mm rolled coil. The chemical composition of the selected pure copper is displayed in Table 3.1.

Table 3.1: Chemical composition of pure copper (Cu), wt%.

Element	Zn	Sn	Fe	P	Ni	Co	Pb	Cu
Contents	0.01	< 0.01	0.02	< 0.003	0.02	0.03	0.02	> 99.5



Figure 3.1: The microstructure of pure copper.

3.2 Material sectioning

The sectioning of pure copper foil includes two conditions. One is sectioning for micro tensile test, and its schematic is shown in Figure 3.2. The dimensions of the tensile sample are designed

according to ASTM E8/E8M. The other is cutting for micro V-bending test, and its dimensions are $0.1\text{mm} \times 5\text{mm} \times 10\text{mm}$, $0.3\text{mm} \times 5\text{mm} \times 10\text{mm}$ and $0.5\text{mm} \times 5\text{mm} \times 10\text{mm}$. All dimensions are given in the form of (thickness \times width \times length). Both sets of sectioning were conducted on a laser-cutting machine.

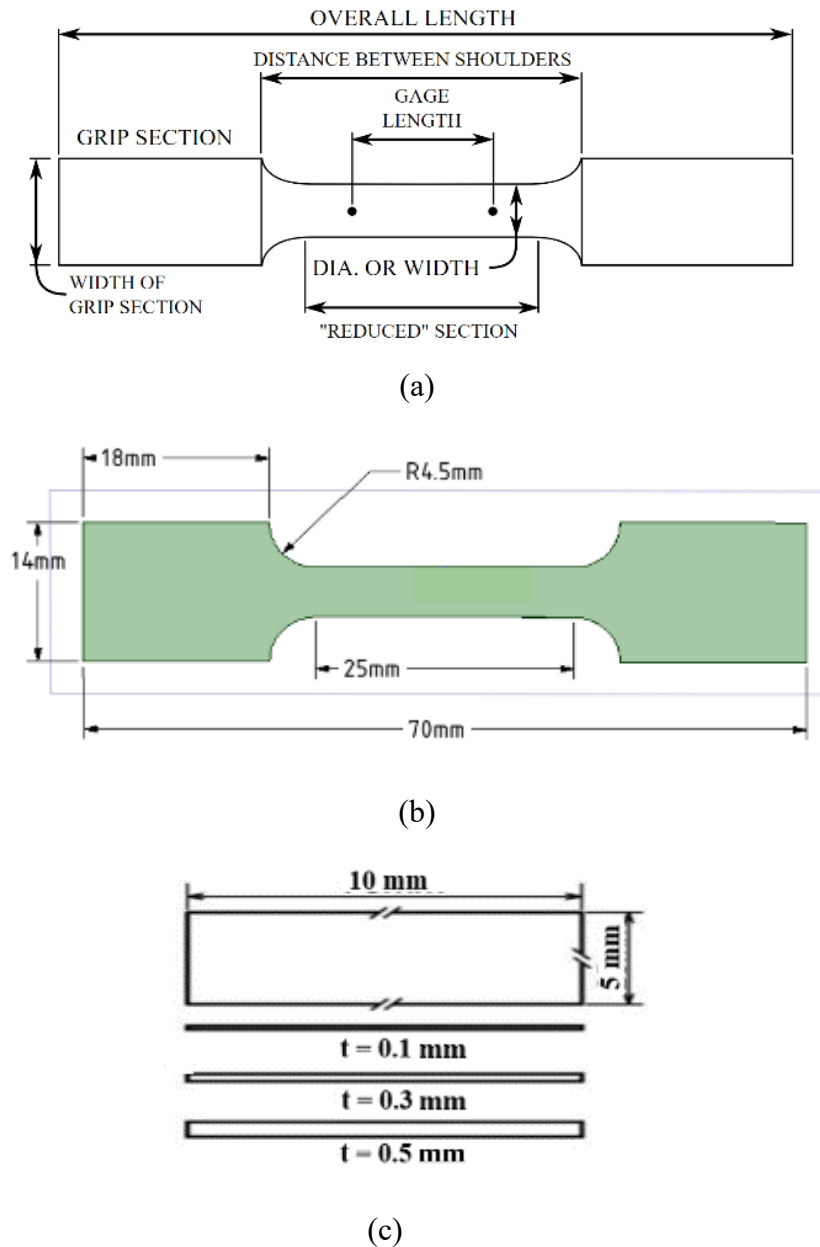


Figure 3.2: (a) Tensile test specimen (b) Schematic of micro tensile samples
(c) Schematic of micro V-bending samples.

3.3 Heat treatment

In order to obtain different average grain sizes in copper samples to achieve different grain size annealing heat treatment was carried out, as defined in Figure 3.3. The micro tensile and micro V-bending samples were annealed in a NBD-O1200 vacuum tube annealing furnace, as shown

in Figure 3.4. Because the samples were very small, besides vacuum condition during heat treatment, the Ar air protection was also adopted to avoid oxidation.

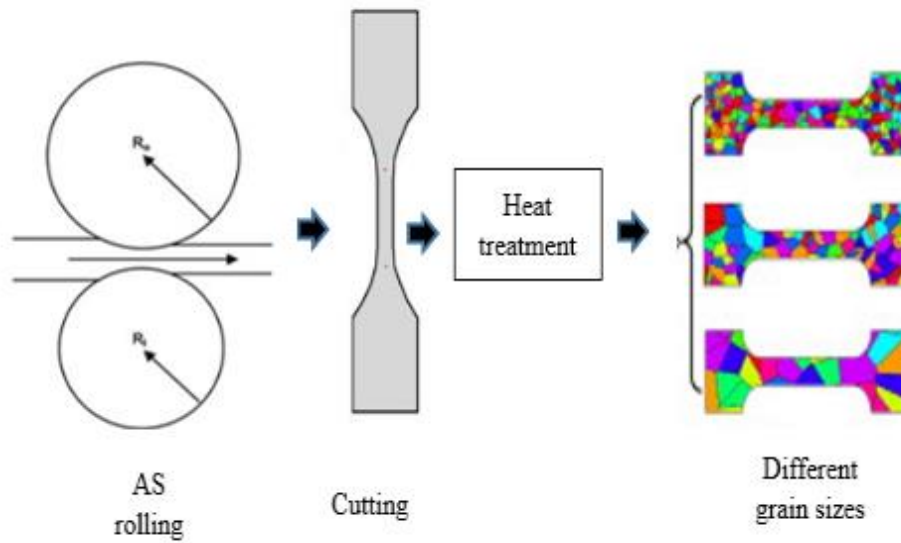


Figure 3.3: Dog-bone samples preparation method.



Figure 3.4: Vacuum tube annealing furnace.

3.4 Sample preparation

After annealing, the most difficult job was to get a high diamond finish on copper samples for determining the average grain size. The normal size fine Alpha aluminium powder (0.3 and 0.5 microns) was used to polish the copper samples. To achieve the good shine in soft copper material, the Alpha aluminium powder was constantly rubbed on samples during polishing. To ensure the fine level of flatness during polishing, all the copper samples were mounted on smooth round pieces of hard plastic (Polyfast powder), as shown in Figure 3.5. The both grinding and polishing were performed on the Struers automatic Tegrapol 21, as shown in Figure 3.6. The grinding and polishing procedures for metallography are presented in Table 3.2. After it, for the microstructure analysis, the samples were treated further. The samples for micro tensile test and micro V-bending were etched using a solution of 5ml saturated aqueous

sodium thiosulfate, 45mL water, 20g potassium metabisulfite for 10 seconds. The image of one of the polished sample is shown in Figure 3.5.

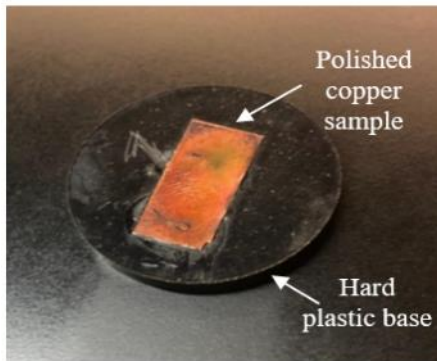


Figure 3.5: Polished sample.



Figure 3.6: Grinder and polish machine.

Table 3.2: Sample preparation procedure for microstructural analysis.

Procedure	Surface	Time	Solution
Grinding	9 μm Largo cloth	2 min	Water
Polishing	3 μm Mol cloth	1 min	Alpha or Gamma aluminium powder (0.5 microns)
Polishing	OP-chem	20 second	Alpha aluminium powder (0.3 microns)

3.5 3D laser-confocal microscope

In this study, a 3D laser-confocal microscope was used to examine the microstructure of the materials and measures the surface roughness at the submicron level. The laser-based confocal microscope used in this study was Olympus OLS5000 and the real photo of this microscope is shown in Figure 3.7.

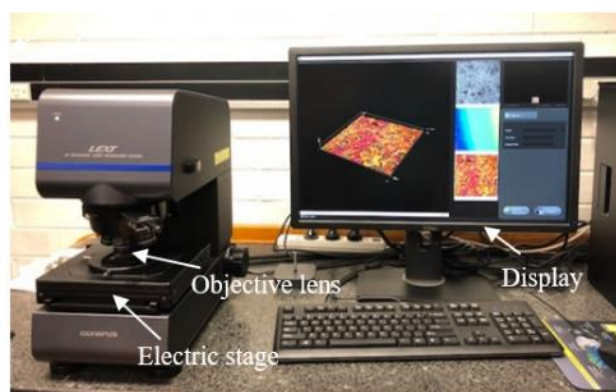


Figure 3.7: 3D laser-confocal microscope.

This microscope has an electric stage, and a large region of the stretched blank surface can be observed by using different lens (e.g. 5X: 0.45μm). For microstructural analysis, the prepared samples were placed on the microscope stage, as shown in Figure 3.8, where the visible light and a series of lenses to magnify images of specimens were used to examine the microstructure, as shown in Figure 3.9. This feature was also used to measure the springback angles after magnifying the bended samples.

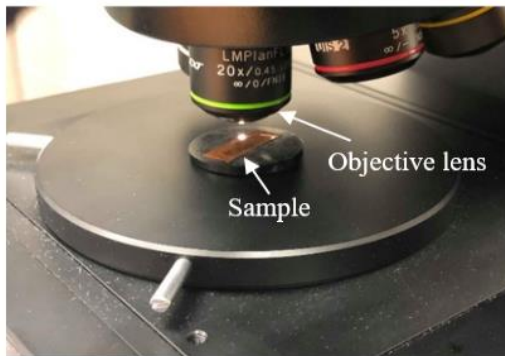


Figure 3.8: Sample under the microscope. **Figure 3.9:** Microstructure analysis.

3.6 Average grain size (Line intercept method)

To measure the average grain size, the line intercept method was used. The average grain intercept (AGI) method is a technique to quantify the grain size in a given material by drawing a set of randomly positioned line segments on the micrograph, counting the number of times each line segment intersects a grain boundary, and finding the ratio of intercepts to line length, as illustrated in equation 3.1.

$$\text{Average grain size} = \frac{\text{Line length}}{\text{Number of grains}} \quad (3.1)$$

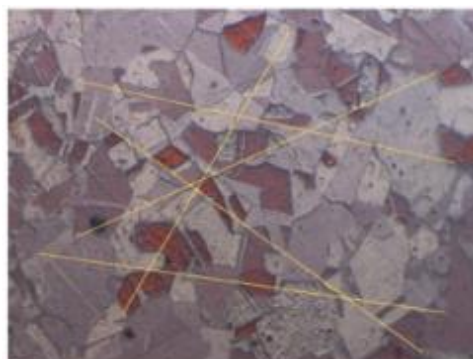


Figure 3.10: Micrograph with random line segments.

Figure 3.10 shows a micrograph (microscopic photograph) of one copper sample that has been used to observe the average grain size. The microstructure image of the copper sample was

moved to 'ImageJ' software to measure the actual grain size. In Figure 3.10, the line segments (yellow lines) that are randomly placed over on the micrograph show the first step in determining the average grain size. In 'ImageJ' software, the detected microstructure picture was changed to a grayscale image, as shown in Figure 3.11. The reason that the grain boundaries are darker than the grains themselves that make it easy to count the grain boundaries, which are, intersected by the line segment.

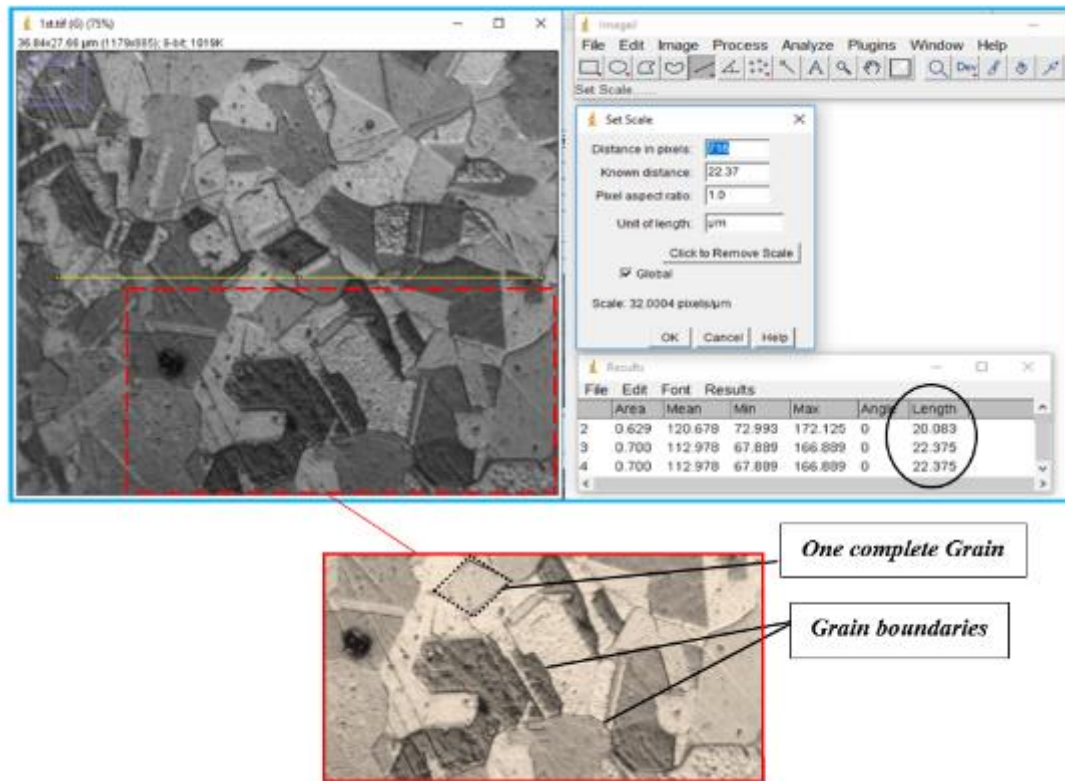


Figure 3.11: Optimization of average grain size in 'ImageJ' software.

3.7 Micro tensile test

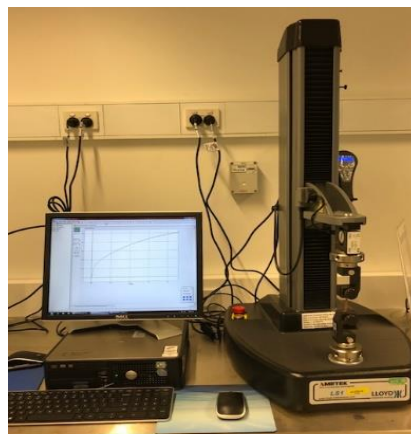
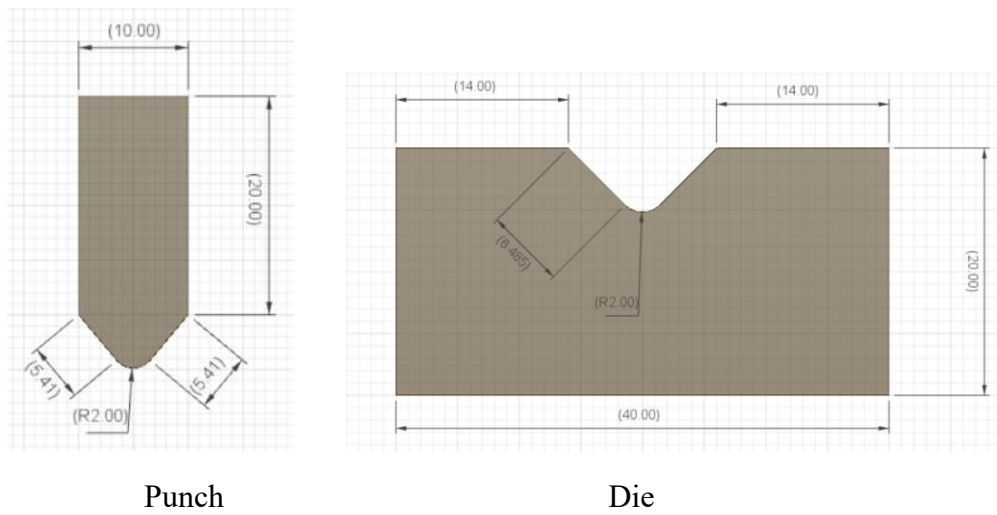


Figure 3.12: METEX universal testing machine.

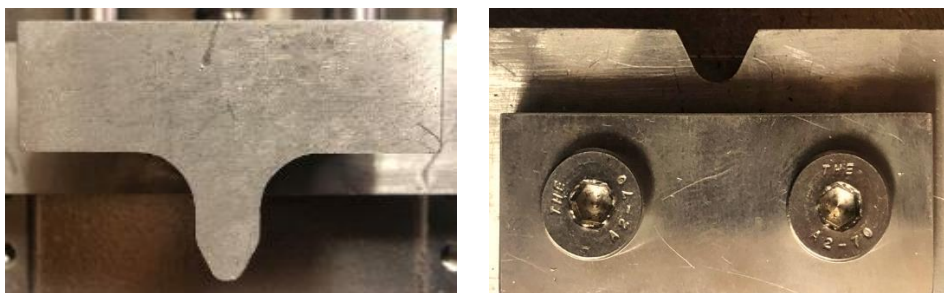
To carry out the uniaxial micro tensile test on pure copper samples with different grain size effect ratios, a set of METEX universal tensile testing machine with a maximum capacity of 1kN, as shown in Figure 3.12 was selected. This equipment can offer ultra-precise displacement control: 20 nm and can accommodate odd-shaped components. This instrument provides very accurate stress-strain measurements, so, it was very suitable to use to investigate the microscale level deformation behaviour.

3.8 Micro V-bending

Micro V-bending test conducted on the same universal testing machine, after making some modifications in the system. Figure 3.13 (a-b) shows the drawings and real images of punch and die used to conduct the micro V-bending tests. Both punch and die were made of aluminium alloy. For the design of micro V-bending punch and die, ASTM D790-17 standard was followed.



(a)



(b)

Figure 3.13: (a) Schematic of micro V-bending punch and die (unit: mm), (b) Real photos of micro V-bending punch and die.

3.9 Software applied for numerical simulation and analytical solution

To obtain a better understanding of micro forming, numerical simulation was also carried out besides the physical experiments. However, it is not easy to conduct because the most obvious difference between conventional models and micro forming models is that the materials involved cannot be recognised as homogenous ones. This requires an innovative approach to be adopted in the modelling to realise the inhomogeneity of micro forming samples. In this study, two kinds of software: MATLAB and ABAQUS were used to achieve this goal.

3.9.1 MATLAB

MATLAB (matrix laboratory) is a multi-paradigm numerical computing environment and fourth-generation programming language. Developed by MathWorks which is an American privately held corporation that specialises in mathematical computing software, MATLAB allows matrix manipulations, plotting of functions and data, implementation of algorithms, the creation of user interfaces, and interfacing with programs written in other languages, including C, C++, Java, Fortran and Python. In this research, the analytical calculation of material intrinsic length is performed by MATLAB.

3.9.2 ABAQUS

Abaqus software suites for finite element analysis (FEA) and computer-aided engineering (CAE). In this study, the ABAQUS 6.13 version was used. It consists of five core software products:

- ABAQUS/CAE, a software application used for both the modelling and analysis of mechanical components and assemblies (pre-processing) and visualising the FEA results.
- ABAQUS/Standard, a general-purpose FE analyser that employs an implicit integration scheme.
- ABAQUS/Explicit, a special-purpose FE analyser that employs an explicit integration scheme to solve highly nonlinear systems with many complex contacts under transient loads.
- ABAQUS/CFD, a computational fluid dynamics software application that provides advanced computational fluid dynamics capabilities with extensive support for pre-processing and post-processing provided in ABAQUS/CAE.
- ABAQUS/Electromagnetic, a computational electromagnetic software application that solves advanced computational electromagnetic problems.

3.10 Research methodology

The research methods, which are involved in this dissertation, can be categorised as physical experiments and numerical modelling. For physical experiments, micro tensile and micro V-bending tests have been chosen as the processing method to investigate the research objectives. The grain size effect is expressed by the ratio of the specimen's thickness (T) / average grain size (D). In this study, annealing is chosen to obtain different average grain sizes with fixed and different specimen's thickness. The flow stress and surface roughness experimental results are discussed and analysed from a size effects (T/D) centred perspective. The normal numbers of grains across the foil thickness are considered to express the size effects in micro V-bending. To analyse the surface roughness and springback angle after experiments a 3D laser-confocal microscope is used. For numerical analysis of flow stress the numerical modelling with some modifications is carried out on commercial and prestige finite element (FE) software ABAQUS. MATLAB programming is used for springback analysis by using the improved material intrinsic length equation. Finally, a new compact and portable UTM compatible with a 3D laser-confocal microscope is designed and developed to understand the influence of size effects in micro metal forming.

3.11 Summary

The experimental facilities, simulation software and methodologies used for the current study were introduced in this chapter. The detailed experimental and modelling procedures employed to study the particular condition as well as corresponding results are presented and discussed in the following chapters.

Chapter 4. Size effects on flow stress and surface roughness

4.1 Introduction

These days all the compact size devices require a significant number of micro-scale components, e.g. miniature screws. The fabrication of these micro-level connecting elements can be done by micro metal forming processes of a thin ($5\mu\text{m}$ - $100\mu\text{m}$) sheets [44]. The traditional micro forming techniques are not applicable to this thickness range. Because in micro forming the mechanical behaviours are changed due to the scale down the sample dimensions, results in so-called size effects [47].

After review the previous studies, it is found that the in micro forming the material behaviour is not only influenced by overall dimension but also by the microstructural topographies, notably the grain size [47]. Therefore, in this study, both factors (workpiece thickness and grain size) are considered together for deep understanding. The relation of the thickness of the sheet and average grain size can be explained in three different ratios ($T/D < 1$, $T/D = 1$ and $T/D > 1$), which are briefly explained as follows.

In the case of $T/D < 1$ states that the average grain size is larger than sample thickness, which means most grains involved in the specimens are incomplete. Consequently, due to the lack of grain boundaries and grain boundary corners, concentrated plastic deformation is very difficult to be initiated [52].

When $T/D \approx 1$, there is only one grain in the thickness direction, and grain deformation and grain boundary sliding can be dominant simultaneously during tests [54]. Plastic deformation is relatively easy to happen because there are grain boundary corners gathering near two sides of thickness direction. However, due to the limitation from thickness direction, grain orientation and coordination cannot occur as easily as they are comparing to materials with $T/D > 1$ [53, 54].

In the last group of $T/D > 1$, the specimen materials can be considered as polycrystalline aggregate. Moreover, in $T/D > 1$ the number of grain boundaries and grain boundary corners increase largely, which lead to the appearance of work-hardened grain boundary layers. In micro forming processes, the deformation normally, take place within the most favourable grain sliding systems. At the same time, due to the large number of dislocations pile up at grain boundaries and their corners, there is great tendency to activate the plastic deformation, so materials with the ratio $T/D > 1$ have the best plasticity comparing to the other two.

In this study for the flow stress analysis, only the $T/D > 1$ is selected. Mahabunphachai [6] discussed that in some material tests when the T/D is reduced to 2~4, a decrease in flow stress had reported, which is totally opposite to reported results obtained from numerous studies [52, 54]. Hence, to investigate the significance of T/D on flow stress the selected range of T/D is less than 3. The researchers explained the influences of size effects on different material deformation behaviours in micro forming with their models. All the models [55, 56] directly added dimensions factors like T and D to conventional constitutive model to fit their experimental data. Wang et al. [53] proposed the surface layer model to explain the variation in flow stress in micro forming by dividing the sample into inner portion and a surface layer. In this chapter, some modifications have been proposed in a material model in order to predict the correct trend of flow stress.

4.2 Micro tensile test

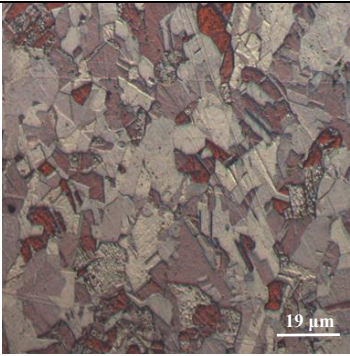
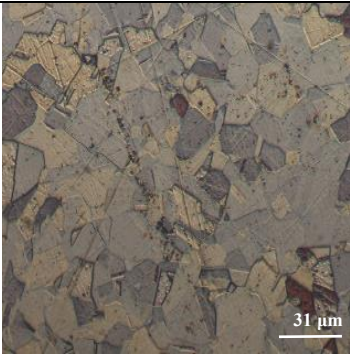
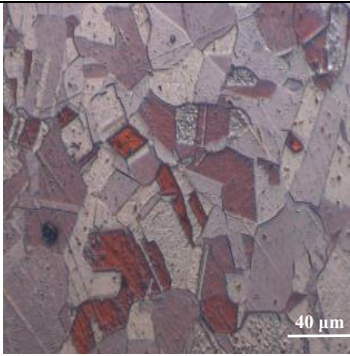
To investigate the size effects on the flow stress and surface roughness micro tensile tests of pure copper foil were conducted. A pure copper foil with the thickness of 50 μm used for this research due to its wide applications. After cutting all the samples in dogbone shape for the micro tensile test, all the samples were annealed at the temperature of 700°C for different times in order to gain different grain sizes. The annealing conditions are presented in Table 4.1. After etching, the microstructures of the prepared samples were observed using a 3D laser-confocal microscope, as shown in Table 4.1. From Table 4.1 it is clear that the grain size increases by increasing the holding time under the same temperature range (700°C) of annealing.

The micro tensile tests were performed to investigate the mechanical properties of the prepared specimens. The actual copper tensile sample is shown in Figure 4.1. All tensile tests were conducted on the universal testing machine, as shown in Figure 4.2 with a maximum capacity of 1 kN, and the 0.05 mm/s crosshead velocity was selected for all the experiments. All the tensile tests were repeated three times.



Figure 4.1: Real copper specimen.

Table 4.1: Microstructure and grain size of the specimen before the tensile test.

	Sample 1	Sample 2	Sample 3
Material	Copper	Copper	Copper
Thickness (μm)	50	50	50
Temperature (°C)	700	700	700
Time (min)	5	10	20
Average grain size (μm)	19	31	40
Micro-structure			
T/D	<i>2.6</i>	<i>1.6</i>	<i>1.3</i>

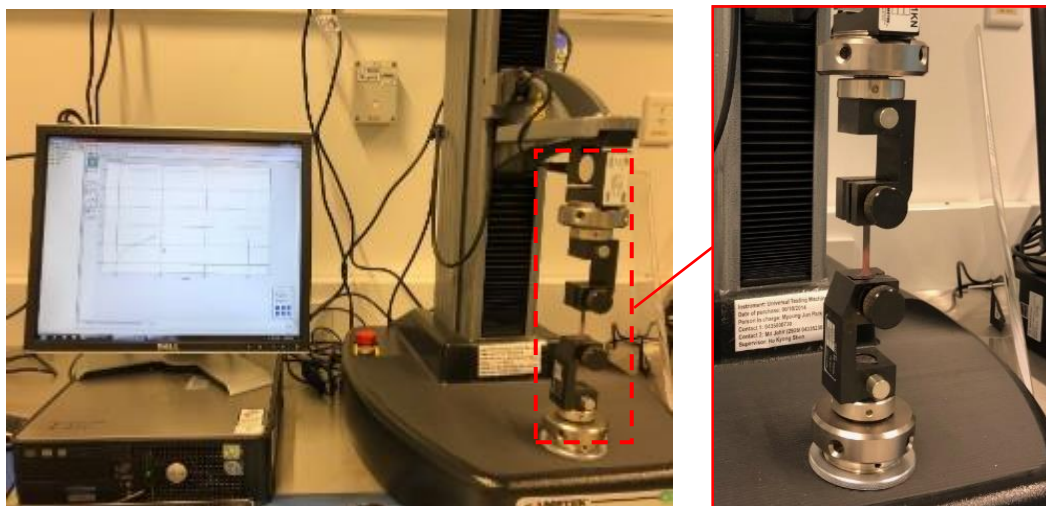


Figure 4.2: Micro tensile testing.

4.3 Effect of T/D on flow stress

The impact of grain size (D) comparative to the sample thickness becomes very important, specifically when the sample is actually thin. The stress-strain curves of the copper samples with different grain sizes are shown in Figure 4.3. The stress-strain graphs represent the required stress to origin the further plastic flow in the material. Therefore, it is clear that the

strain is directly linked to the flow stress. When $T/D > 1$ the amount of grain boundaries and grain corner increases essentially, which leads the strain-hardening ability. In other words, due to the increase of T/D ratio, the grain boundary strengthening effect is enhanced, which further leads the fluctuation in flow stress.

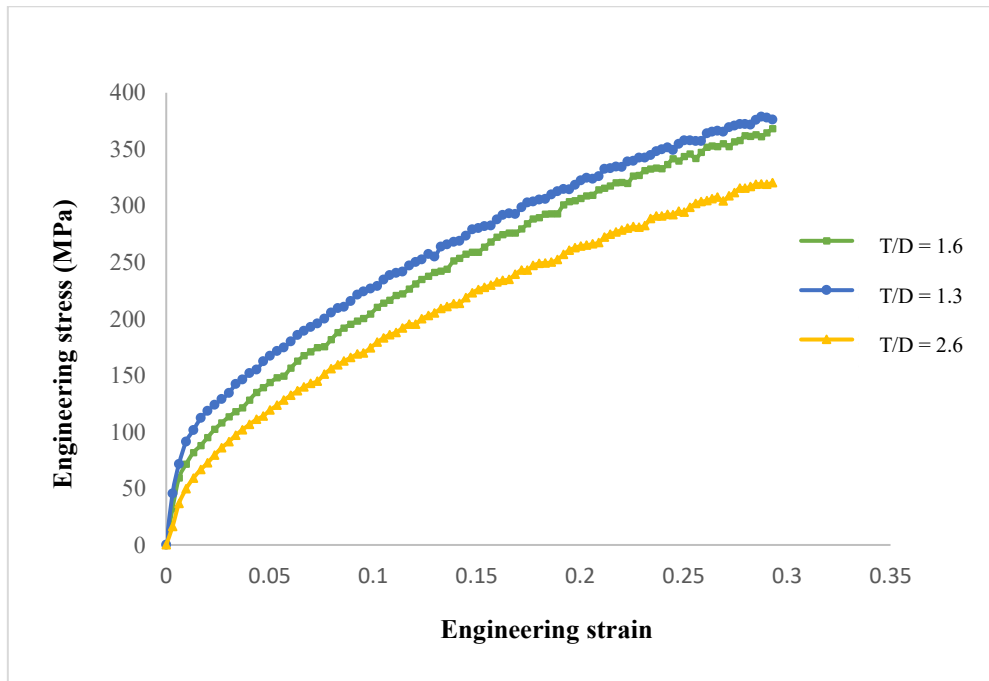


Figure 4.3: The stress-strain curve of copper samples annealed at 700°C.

Anand et al. [23] investigated that for higher values of T/D flow stresses at different strain levels increased with an increase in T/D ratio. It is also explained that flow stress declines with the increasing of T/D ratio, especially when T/D is between 2~4. The same fluctuation can be observed here when T/D varies from 1.6 to 2.6. The usage of traditional constitutive equations for thin samples to calculate the flow stress without taking the impact of grain size relative to the thickness possibly can activate major errors in the flow stress values. A modification in the existing constitutive equations has been proposed. The model is based on the assumption that dislocations within a grain are organized in a dislocation cell structure, the dislocations density of the cell interiors.

4.4 Constitutive model

The model presented in this study is based on the Levy–von Mises formulation and establishes a relation between scalar equivalent von Mises quantities. The equivalent stress σ is assumed to dependent on an internal variable $\bar{\sigma}$ and the equivalent plastic strain rate [58].

$$\sigma = \bar{\sigma} \left(\frac{E^p}{E_0} \right)^{\frac{1}{m}} \quad (4.1)$$

where E_0 is a reference strain rate and $\frac{1}{m}$ is the strain rate sensitivity of stress. In the surface layer model, when $T/D > 1$ the sample cross-sectional area can be divided into interior grains and surface layer, and the flow stress is calculated for each region, as shown in Figure 4.4. The surface layer model can be applied only when T/D is larger or equal to one ($T/D \geq 1$) [56]. Surface layer model is represented by the weighted average of stresses in the inside portion and the outer layer of the sample. The internal variable $\bar{\sigma}$ represents the microstructural state of the material and is regarded as a weighted average of stresses acting in the interior of the sheet and in the surface layers, as following equation (4.2).

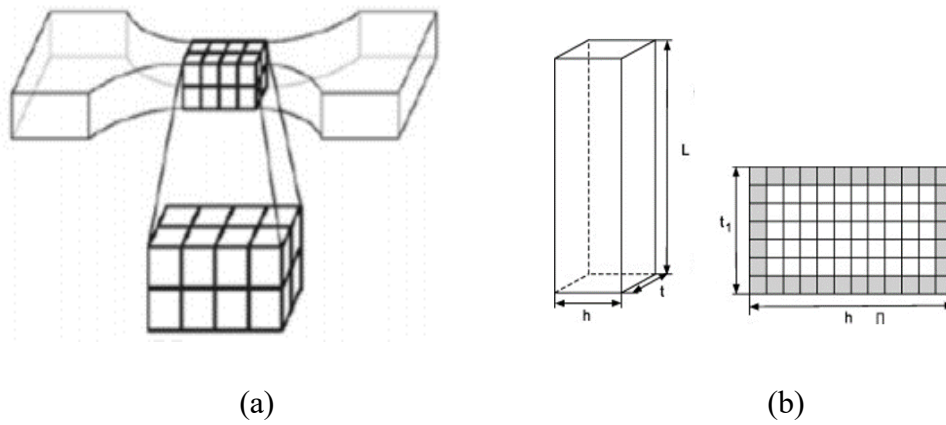


Figure 4.4: (a) Rectangular gage section, (b) Gage section geometry.

$$\bar{\sigma} = \eta \sigma_{inner} + (1 - \eta) \sigma_{surf} \quad (4.2)$$

where σ_{inner} is inside stress and σ_{surf} is the surface layer stress of the material. To express the fraction of inner portion to the complete material area the size factor η is employed. To calculate the η for the sheet sample with rectangular cross-section the following equation (4.2) can be used.

$$\eta = \frac{T-D}{T} \quad (4.3)$$

As surface layer model is only applicable for $T/D \geq 1$, not for $T/D < 1$ because of no complete grain existing in the thickness direction. Molotnikov et al. [58] explained that the Hall-Petch relation is applicable for $T/D < 1$. The flow stress of the inner grains can be explained by polycrystalline aggregate ($\sigma_{inner} = \sigma_s$), so the flow stress of inner grains is determined by dislocation cell structure. Grains located at the free surface of material have less hardening effect than the inner grains, so the strengthening effect in surface layer can be neglected [58].

Then it is assumed that the flow stress of the surface layer portion is equal to grain interior ($\sigma_{surf} = \sigma_c$). From the viewpoint of dislocation accumulation strengthening or dislocation density, the inner grains are treated as a two-phase composite structure. In terms of cell walls and cell interior, the two-phase composite model can be represented as following equation (4.4).

$$\sigma_s = (1 - f) \sigma_c + f \sigma_w \quad (4.4)$$

where f is the volume fraction of cell walls or grain boundary equation (4.5). σ_c and σ_w are the flow stresses of grain interior (cell interior) and boundary (cell wall) respectively.

$$f = f_\infty + (f_0 - f_\infty) \exp(-\gamma_r/\tilde{\gamma}_r) \quad (4.5)$$

here f_0 and f_∞ are the initial value and saturation value of f , at large strains. $\tilde{\gamma}_r$ describes the rate of decrease of f , the value of these parameters are selected from [59, 60]. The shear strengths of the wall and inner phase are as follows according to the Taylor relation.

$$\tau_w = \alpha G b \sqrt{\rho_w} \quad (4.6)$$

and

$$\tau_c = \alpha G b \sqrt{\rho_c} \quad (4.7)$$

where G and b are the shear modulus and the magnitude of the dislocation burgers vector respectively, and α is a numerical constant, $\alpha = 0.25$. ρ_w and ρ_c are the dislocation densities in the cell walls and cell interiors, respectively. The stresses σ_c and σ_w are related to the respective dislocation densities, and explained in equations (4.9) and (4.10), respectively. To include this effect into flow-rule, the shear stress has to relate to the tensile stress.

$$\sigma = M \tau \quad (4.8)$$

where M is taken as an average Taylor factor ($M = 3.06$) in polycrystalline material.

$$\sigma_c = M \alpha G b \sqrt{\rho_c} \quad (4.9)$$

and

$$\sigma_w = M \alpha G b \sqrt{\rho_w} \quad (4.10)$$

The dislocation density of cell interiors and cell walls are;

$$\rho_c = \alpha^* \left(\frac{1}{\sqrt{3}} \right) \left(\frac{\sqrt{\rho_w}}{b} \right) \gamma_w - \beta^* \left(\frac{6\gamma_c}{bd(1-f)^{\frac{1}{3}}} \right) - k_0 \left(\frac{\gamma_c}{\gamma_0} \right)^{\frac{1}{n}} \gamma_c \rho_c \quad (4.11)$$

$$\rho_w = \left(\frac{6\beta^* \gamma_c (1-f)^{\frac{2}{3}}}{bdf} \right) + \left(\frac{(\sqrt{3})\beta^* \gamma_c (1-f) \sqrt{\rho_w}}{fb} \right) - k_0 \left(\frac{\gamma_w}{\gamma_0} \right)^{-\frac{1}{n}} \gamma_w \rho_w \quad (4.12)$$

In both equations (4.11 and 4.12), d is the average dislocation cell size, which can be explained and linked to the dislocation densities by the following relation [60];

$$d = \left(\frac{K}{\sqrt{(1-f)\rho_c + f\rho_w}} \right) \quad (4.13)$$

where K is constant. The parameters α^* , β^* , k_0 , and n were executed from the previous studies [58]. By using these equations the new rule of mixtures is developed and the flow stress in micro forming can be expressed:

$$\bar{\sigma} = (1 - \eta f) \sigma_c + f \eta \sigma_w \quad (4.14)$$

4.5 Verification

Finite element software ABAQUS was implemented to comprised the above set of equations via UMAT user subroutine. The thickness of the specimen and the grain size and other material parameters were input quantities, in the subroutine. For simulation, some of the material parameters are taken from previous studies. The appropriately chosen parameter values of Cu used in simulation are presented in Table.4.2.

Table 4.2: The values of the parameters used in simulations.

α^*	β^*	b	f_0	f_∞	p_w	p_c	M	K	m	n
0.00654	0.012	2.5610×10^{-10}	0.25	0.06	10^{14} m^{-2}	10^{13} m^{-2}	3.06	10	40	50

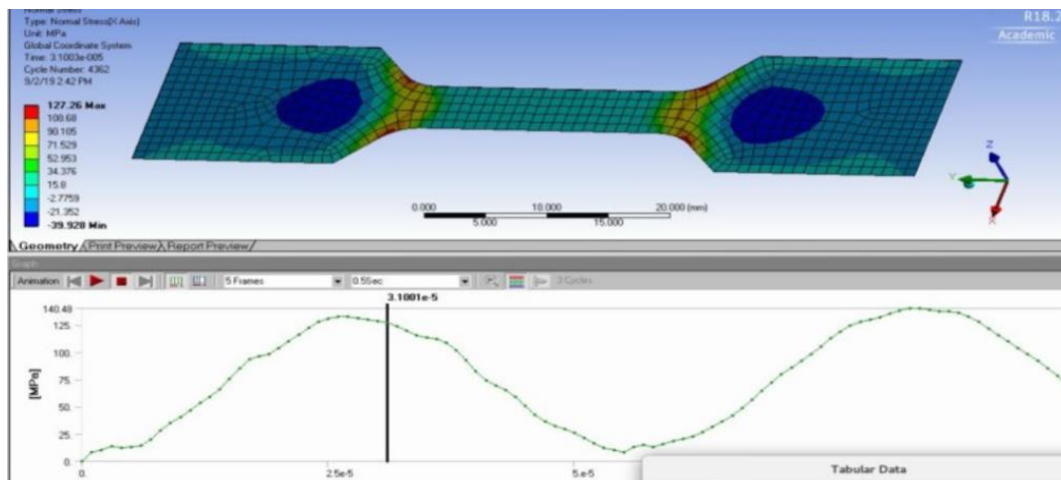


Figure 4.5: FEM analysis.

Time [s]	Minimum [MPa]	Maximum [MPa]	Experiment (MPa)	FEM (MPa)
1.1755e-038	0.	0.	10.535	8.324
1.0039e-006	-6.5741	8.3246	14.3954	10.026
2.0004e-006	-12.124	10.026	21.151	13.227
3.0041e-006	-16.045	13.618	24.816	13.618
4.0006e-006	-22.743	12.568	29.223	14.600
5.0042e-006	-21.129	13.227	34.568	19.974
6.0005e-006	-14.876	14.6	39.123	28.065
7.0041e-006	-10.157	19.974	46.348	34.898
8.0005e-006	-13.07	28.065	53.402	40.686
9.0039e-006	-14.444	34.898	58.194	46.593
1.e-005	-16.599	40.686	65.436	53.587
1.1003e-005	-20.806	46.593	71.043	59.546
1.2006e-005	-19.076	53.587	77.627	66.326
1.3002e-005	-19.56	59.546	83.587	75.661
1.4005e-005	-18.413	66.326	88.504	85.401
1.5001e-005	-20.091	75.669	93.635	93.597
1.6003e-005	-27.796	85.401	98.100	96.223
1.7006e-005	-36.641	93.597	102.236	98.491
1.8002e-005	-43.886	96.223	106.2289	103.81
1.9005e-005	-41.388	98.491	108.709	110.03
2.0007e-005	-34.786	103.81	11.98	116.39
2.1002e-005	-33.115	110.03	118.11	122.69
2.2005e-005	-34.017	116.39	124.25	127.85
2.3007e-005	-40.945	122.69		
2.4002e-005	-49.897	127.85		
2.5004e-005	-55.208	130.97		
2.6006e-005	-55.706	133.11		
2.7001e-005	-55.943	133.13		
2.8003e-005	-49.515	131.65		
2.9006e-005	-41.387	129.98		
3.0001e-005	-36.559	128.88		

(a)

(b)

Figure 4.6: (a) Calculated stress ($T/D > 2.6$) from FEM analysis, (b) Experimental and calculated stress

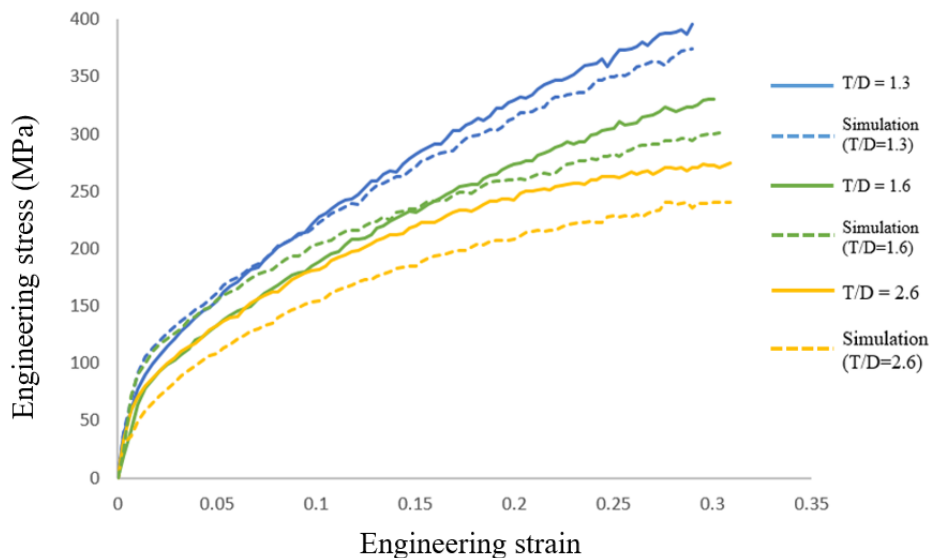


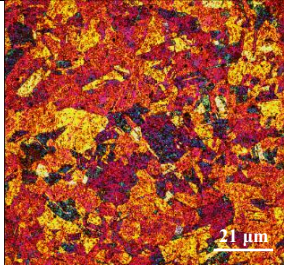
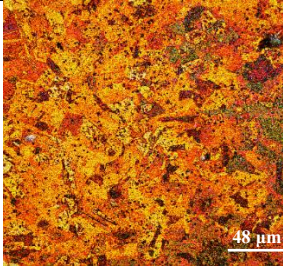
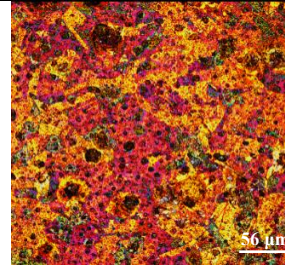
Figure 4.7: Simulation vs experimental comparison of stress-strain curve.

Figure 4.7 represents the evaluation of the calculated and the experimental stress-strain curves for $T/D > 1$. With the selected parameter values, the model is capable of analysing the deformation behaviour of Cu under uniaxial tension, at least up the first 15% plastic deformation. Because, adequately recovering of the strain-hardening behaviour of Cu with proposed technique is only suitable up to few points before necking.

4.6 Effect of T/D on surface roughness

The increase in surface roughness of the metal foils occurs during plastic deformation, and it is one of the main factors affecting the ductile fracture behaviour of metal foils. As the deformation process scales down to micro scale, the characteristics of single grain involved in the deformed region start playing a significant role. Three different ratios $T/D > 1$, $T/D = 1$ and $T/D < 1$ are used to investigate the surface roughness phenomena. The objective of considering all three ratios of T/D was to improve the understanding of the evolution of surface asperity during micro tensile test of copper samples. The annealing conditions are presented in Table 4.3.

Table 4.3: Heat treatment and average grain size for surface roughness analysis.

	Sample 1	Sample 2	Sample 3
Material	Copper	Copper	Copper
Temperature (°C)	600	600	600
Time (min)	10	20	30
Thickness (µm)	50	50	50
Average grain size (µm)	21	48	56
Micro-structure			
T/D	2.38	1.04	0.89

The dog bone-shape copper specimens before and after the micro tensile test can be seen in Figure 4.8. The edge thicknesses of the tested samples were smaller than the thicknesses of the inner areas. Therefore, the observation of the surface roughness was obtained from the inner areas of the tested samples. The surface roughness was measured in the selected region (black area) using a 3D laser-confocal microscope, as shown in Figure 4.9.

The roughness profile, waviness profile and 3D surface texture of the tensile-tested samples are shown in the following Figures 4.10 and Figure 4.11, respectively. Different surface texture

images were obtained with different ratios of thickness to average grain size. It is found that the surface roughness of deformed sample increases significantly with the decrease of T/D because the surface grains are less constrained and easier to deform on the free surface with a small ratio of T/D. When $T/D < 1$, the average grain size is larger than the thickness of the specimen, which means most grains involved in the tensile specimens are incomplete. Consequently, due to the lack of grain boundaries, it becomes very easy to initiate the surface irregularities. From Figure 4.12, it can be clearly observed that the surface roughness increases with the decrease of the T/D ratio. In this figure, the relative average surface roughness 'R_a' was evaluated.



Figure 4.8: Real copper samples.

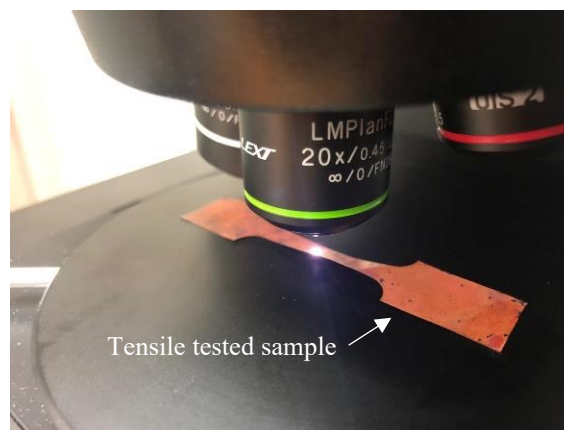
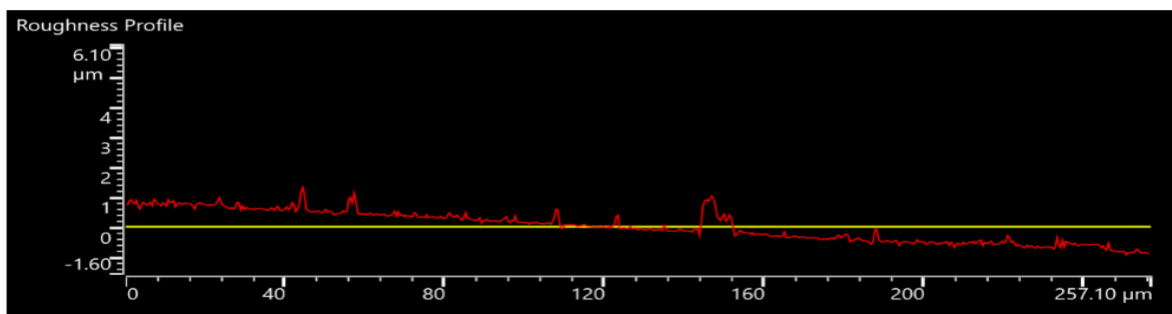
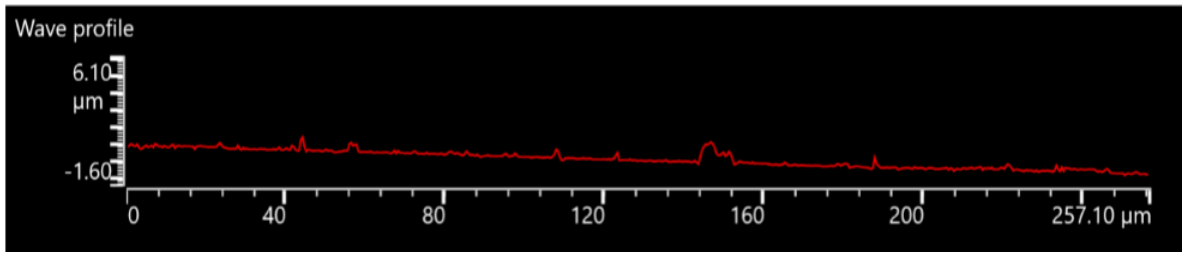
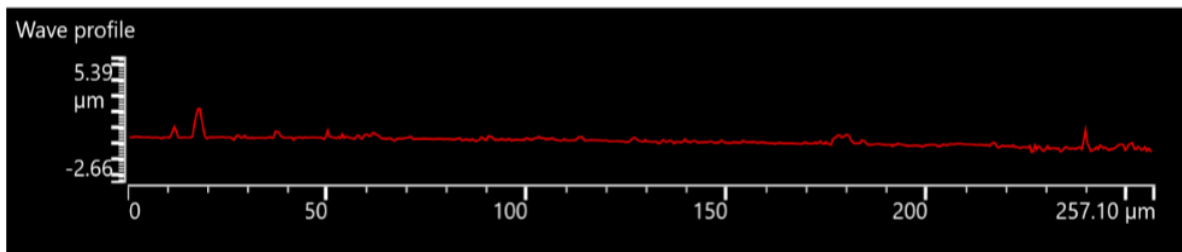
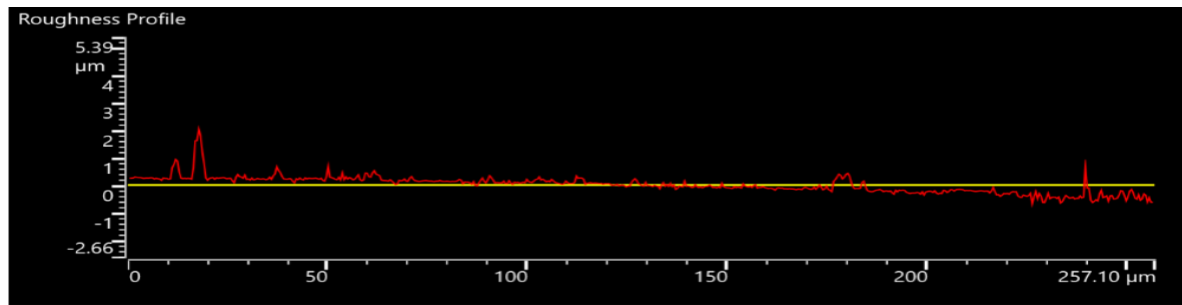


Figure 4.9: Surface roughness testing.

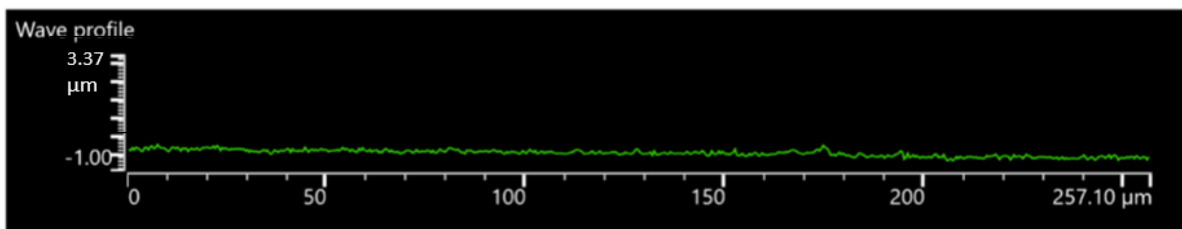
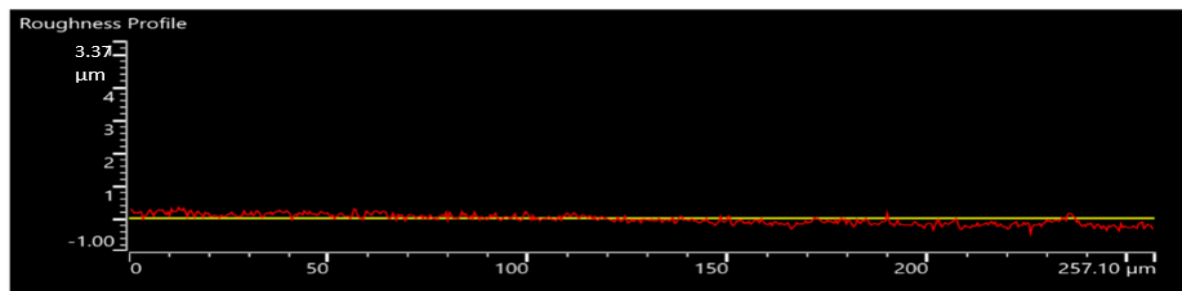




(a)



(b)



(c)

Figure 4.10: Roughness and waivness profiles of (a) $T/D = 0.78$, (b) $T/D = 1.04$, (c) $T/D = 2.38$.

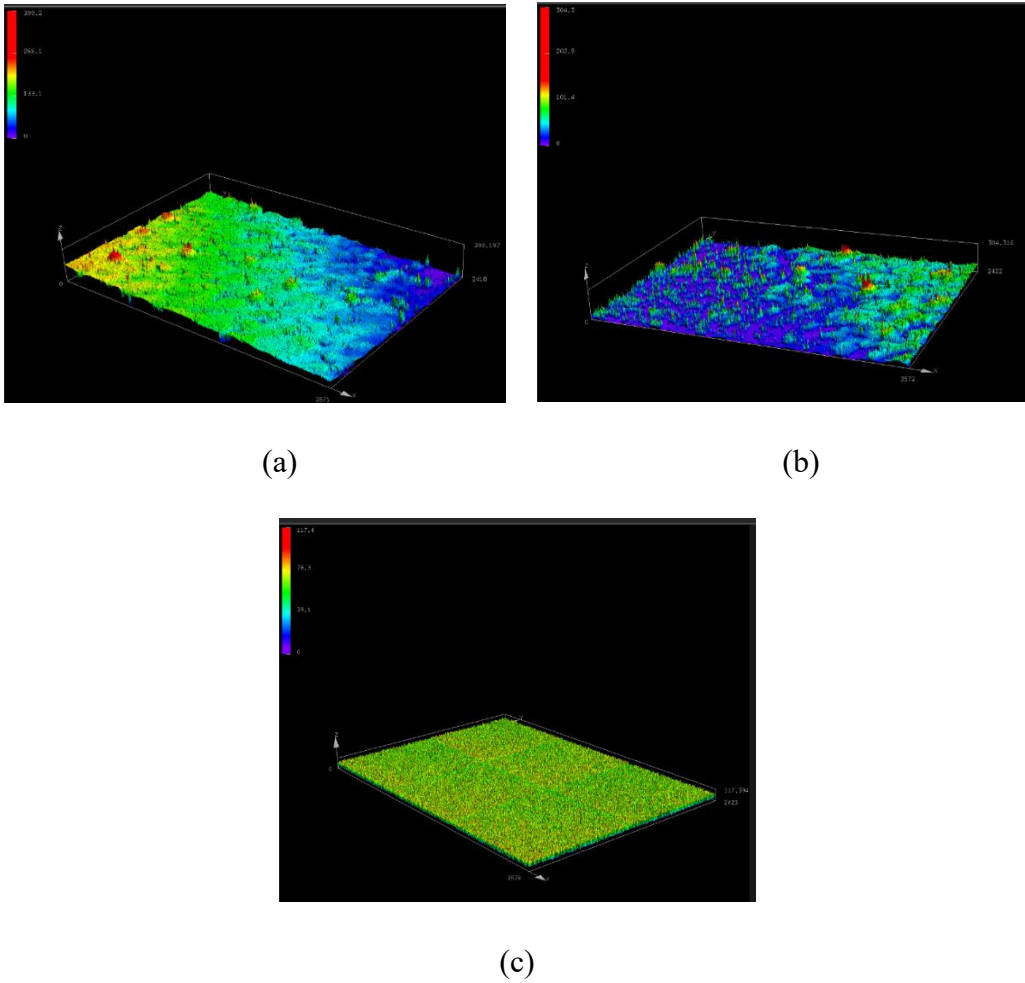


Figure 4.11: 3D surface texture of (a) $T/D = 0.78$, (b) $T/D = 1.04$, (c) $T/D = 2.38$.

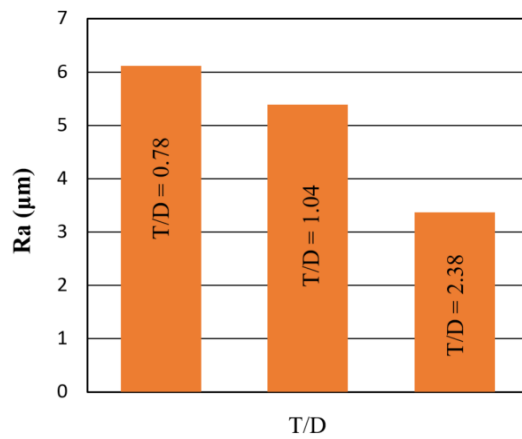


Figure 4.12: Surface roughness vs T/D .

4.7 Summary

For the flow stress analysis only the $T/D > 1$ was selected and the influences of all three T/D ratios on surface roughness were investigated. The following conclusions are obtained:

- i. Plastic deformation (flow stress) increase with the increase in T/D ratio, but the flow stress starts to decrease with the increase of T/D when the values of T/D are close to the critical value ($T/D = 2\sim 4$).
- ii. A material model was modified to describe the hardening behavior of grains in polycrystalline material, and the model is capable of analysing the deformation behaviour only up to a few points before necking.
- iii. It was found that the surface roughness of the deformed sample increases significantly with the decrease in T/D ratio.

Chapter 5. Analytical and experimental determination of the modified material intrinsic length of strain gradient hardening for micro V-bending test of pure copper

5.1 Introduction

Over the past few years, the experimental and theoretical research on micro bending of metal foils have been implemented and apparent size effects observed. It is well identified that at the micron scale, the strain gradient has a more dominant impact on the effective bending strength [61, 62]. Voyiadjis et al. [63] analysed the micro bending behaviour of metal foils and specified that strain gradient effects are significant on bending stiffness when the beam thickness becomes comparable to the material intrinsic length l . The gradient plasticity theories build a constitutive framework on a continuum level that can be used to bridge the gap between the micromechanical plasticity and the classical continuum plasticity [62]. With the help of these theories, it becomes easy to explain the size effects encountered in the micro forming due to the incorporation of material intrinsic length into constitutive modelling.

The material internal length can be defined as a length scale which can be determine from the strain and stress fields calculated from experimental data, which explicitly accounts for the selected microscopic features such as grain size. The material intrinsic length is one of the important factors in plastic strain gradient theory and originally proposed for dimensional consistency, which was provided with various values by different investigators. The material intrinsic length is related to the free slip distance of dislocations, which decreases with the increase in grain size. The mechanical properties of metallic materials, whether in simple tension, bending, or indentation testing are thus size dependent [61, 62]. In all of these cases, the characteristic length l of the deformation field sets the qualitative and quantitative behaviour of size effects. Hence, it becomes essential to consider the intrinsic length in strain gradient hardening for size effects analysis.

In previous studies [64, 65], all researchers determined the intrinsic length by fitting the experimental data of micro-indentation, micro-bending or micro-torsion tests, but no expression of intrinsic length scale is commonly accepted, and different authors estimated different values even based on the same experimental data. Such as, Voyiadjis et al. [63] have summarized the material length scale between 0.010 mm and 0.025 mm, and the average fitting value of length scale was about 0.06 mm for an annealed metal, such as soft aluminum, copper and iron.

If the actual values of intrinsic length are taken in strain gradient hardening for micro-bending analyses, the predicted values can agree better with the experimental data. Therefore, in this chapter, a modified material intrinsic length related to average grain numbers along the thickness direction of the sample is calculated. To investigate size effects encountered with material intrinsic length, micro V-bending test is adopted. The modified material intrinsic length is included in mixed constitutive model to calculate the springback angle after micro V-bending tests.

5.2 Analytical determination of material intrinsic length (l)

Material deformation in metals enhances the dislocation formation, dislocation motion, and dislocation storage. Dislocation storage causes material hardening. The stored dislocations generated by trapping each other in a random way are referred to as statistically stored dislocations (SSDs), while the stored dislocations that relieve the plastic deformation incompatibilities within the polycrystals caused by non-uniform dislocation slip are called geometrically-necessary dislocations (GNDs) [61].

To describe the dislocation interaction processes at the microscale, the mechanism-based strain gradient plasticity theory is used. The tensile flow stress σ_f is related to the shear flow strength through the Taylor factor Z , can be explained as:

$$\sigma_f = Z \tau_f = Z \alpha_S G b_S \sqrt{\rho_T} \quad (5.1)$$

where σ_f is equivalent to the effective stress, and the Taylor Z acts as an isotropic interpretation of the crystalline anisotropy at the continuum level, $Z = \sqrt{3}$ for an isotropic solid and $Z = 3.08$ for FCC polycrystalline metals [87]. The non-local conventional effective plastic strain (P), the conjugate variable of the plasticity isotropic hardening, in terms of its local counterpart (p) and corresponding high-order gradients (η). However, the coupling between p and η was presented in many different mathematical forms, such as [64]:

$$P = [f(p)^{\gamma_1} + g(l\eta)^{\gamma_2}]^{\frac{1}{\gamma_3}} \quad (5.2)$$

where l is a material intrinsic length parameter that is required for dimensional consistency. For the simplicity, assumed that $f(p) = p$, $g(l\eta)$ and $\gamma_1 = \gamma_2 = \gamma_3 = \gamma$, and non-local conventional effective plastic strain (P) could be expressed as:

$$P = [(p)^\gamma + (l\eta)^\gamma]^{\frac{1}{\gamma}} \quad (5.3)$$

where γ is an interaction coefficient. Equation (5.3) ensures that $P \rightarrow p$ whenever $p \gg l\eta$ and that $P \rightarrow l\eta$ whenever $p \ll l\eta$. The homogenous flow stress without the effect of deformation gradients can be identified, in general, as follows:

$$\sigma_f = \sigma_o f(p) \quad (5.4)$$

where σ_o is a measure of the stress in uniaxial tension. For the majority of ductile material, the $f(p)$ can be written as a power-law relation, such as:

$$f(p) = p^{\frac{1}{m}} \quad (5.5)$$

where $m \geq 1$ is the hardening exponent, which can be determined from a simple uniaxial tension test. Here, the equation cannot predict the size dependence of material behaviour after normalization, which involves no material intrinsic length scales. Therefore, the equation needs to be modified to be able to incorporate the size effects, as follow:

$$\sigma_f = \sigma_o [p^\gamma + (l\eta)^\gamma]^{\frac{1}{m\gamma}} \quad (5.6)$$

In the plastic strain field, the gradients are accommodated by GND density, p_G , so that effective strain gradient η that appears in the equation.

$$\eta = \frac{p_G b_G p}{\acute{r}} \quad (5.7)$$

\acute{r} is the Nye factor introduced by [61] to reflect the scalar measure of GND density resultant from macroscopic plastic strain gradients. For FCC polycrystals, Arsenlis and Parks [61] have reported that the Nye factor has a value of $\acute{r} = 1.85$ in bending and a value of $\acute{r} = 1.93$ in torsion. The Nye factor is an important parameter in the predictions of the gradient plasticity theories as compared to the experimental results [62].

p as a function of SSDs:

$$p = b_S L_S p_S M \quad (5.8)$$

Substituting p_G and p_S from equations (5.7) and (5.8), respectively, into equation (5.1), yields the following expression for the flow stress σ_f :

$$\sigma_f = Z\alpha_S G \sqrt{\frac{b_S}{L_S M}} \left[p^{\beta/2} + \left(\frac{\alpha_S^2 b_G L_S M \acute{r} \eta}{\alpha_S^2 b_S} \right)^{\frac{\beta}{2}} \right]^{\frac{1}{\beta}} \quad (5.9)$$

Comparing equation (5.6) and (5.9)

$$\gamma = \frac{\beta}{2}, m = 2, \sigma_0 = Z\alpha SG \sqrt{\frac{b_S}{L_S M}} \quad (5.10)$$

With the intrinsic material length scale l expressed as follows:

$$l = \hbar L_S$$

$$\text{where } \hbar = \left(\frac{\alpha G}{\alpha S}\right)^2 \left(\frac{bG}{bS}\right) M \dot{\epsilon} \quad (5.11)$$

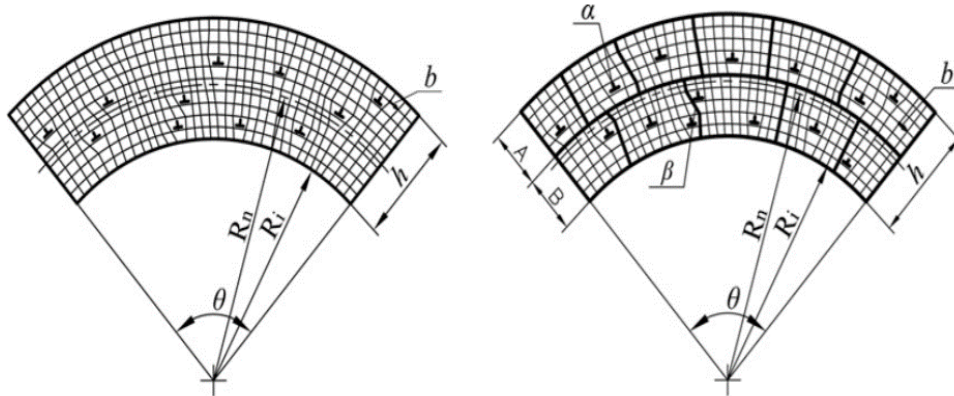
By substituting L_S, M from equation (5.10) into equation (5.11), one obtains a relation for l as a function of the sheet modulus and yield stress, such as:

$$l = Z^2 \alpha^2 G b_G \dot{\epsilon} \left(\frac{G}{\sigma_0}\right)^2 \quad (5.12)$$

after substituting the values of Z and $\dot{\epsilon}$ we get the final equation to calculate the intrinsic length.

$$l = 18\alpha^2 \left(\frac{G}{\sigma_0}\right)^2 b \quad (5.13)$$

The mechanism of plastic strain gradient hardening within the polycrystalline across foil thickness is different from a single crystal in the bending process. For simplification, the bending models are given in Figure 5.1 (a-b), Figure 5.1 (a) illustrates the case of a single crystal, and Figure 5.1 (b) illustrates the case with two layers of grains across the foil thickness.



(a) Single grain along thickness direction (b) Two grains along thickness direction

Figure 5.1: Geometrically necessary dislocation morphology in plastic bending of metal [63].

The bending conditions are identical in both cases, but the distribution and the effects of geometrically necessary dislocations on material hardening are different apparently. Considering the weakening effects of the boundary between multilayer grains across thickness on the geometrically necessary dislocations, equation (5.13) is modified as:

$$l_m = 18 \alpha^2 \left(\frac{G}{\sigma_0} \right)^2 \frac{b}{n_G} \quad (5.14)$$

where n_G is the numbers of grain layer across the foil thickness. In the case of single grain layer foils ($n_G = 1$), equation (5.14) is the same as equation (5.13). When there are multilayer grains across the foil thickness ($n_G > 1$), the material intrinsic length l will decrease by $\frac{1}{n_G}$ according to equation (5.14), that is, the relative contribution of strain gradient hardening caused by geometrically necessary dislocations will decrease by $\frac{1}{n_G}$. If the average grain number is less than 1.0, the material intrinsic length is calculated by equation (5.14) setting $n_G = 1$ because there are no grain boundaries through the thickness.

5.3 Micro V-bending testing

A pure copper sheet (99.9%) is used to assess the geometric and strain gradient size effects in micro V-bending. Young's modulus E of this metal varies from 70–100 GPa, poisson's ratio $\nu = 0.36$, the shear modulus G varies from 25 to 36 GPa, and burgers vector b for FCC crystals $= 2.608 \times 10^{-10}$ m. Three kinds of copper specimens were studied with the thickness of 0.1mm, 0.3mm and 0.5mm respectively. The grain size (D) and total no of grains (n_G) in the thickness direction of the selected specimens are provided in Table 5.1. No annealing treatment was carried out on copper specimens. The mechanical properties of the copper specimens were determined by the tensile tests conducted in a UTM. The engineering stress-strain curves for the three kinds of copper samples with different grain size and thicknesses were obtained, as shown in Figure 5.2.

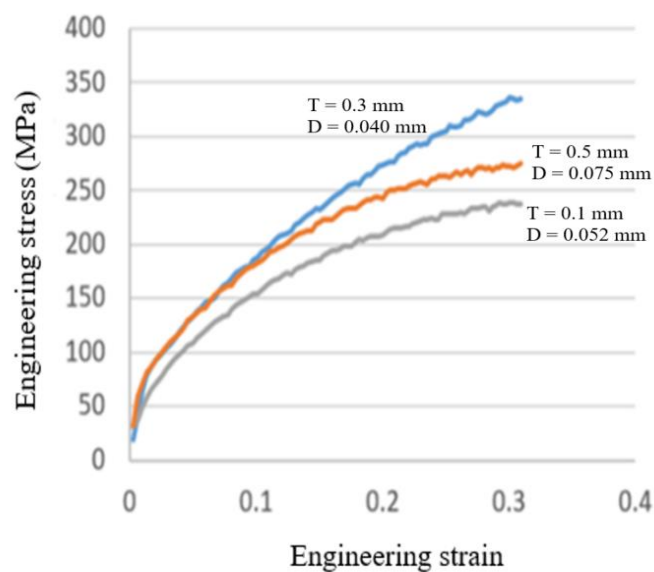


Figure 5.2: Stress-strain curves.

To explore the response of samples to pure bending deformation, free V-bending tooling was designed, as shown in Figure 5.3. The radius of the pressing bar (punch) was 2 mm as shown in Figure 5.4 (a-b). The velocity of the crosshead of the test machine was set to 0.15 mm/s in all micro bending experiments conducted using a UTM test machine.

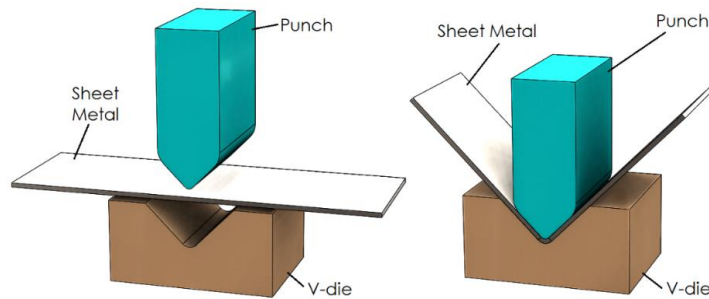
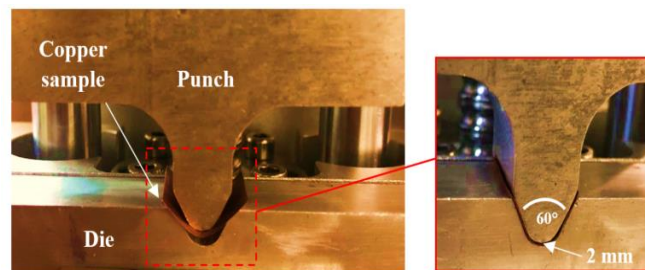
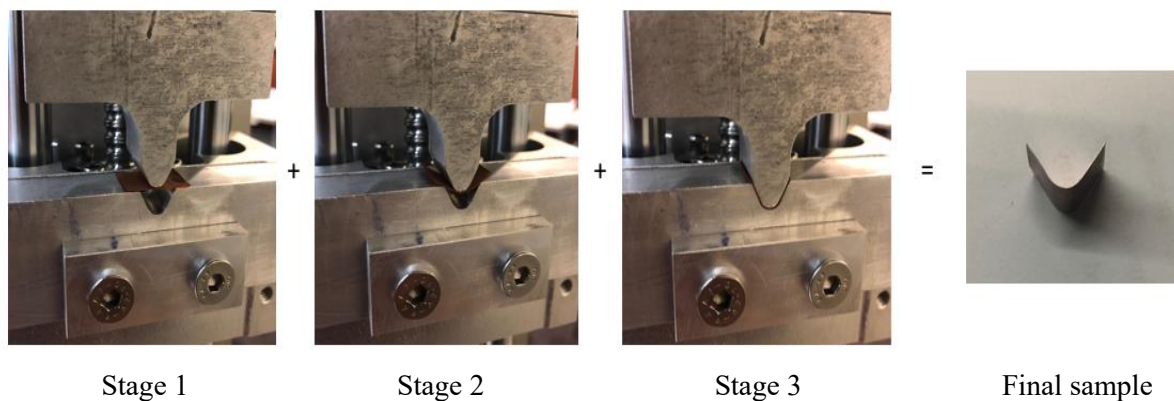


Figure 5.3: V-bending configuration.



(a)



(b)

Figure 5.4: (a-b) Actual micro V-bending test.

5.4 A combined constitutive model incorporating microstructure and strain gradient effects.

5.4.1 Size effect constitutive model

In order to explain the underlying mechanism of springback with modified material intrinsic length l_m , an appropriate constitutive model was required that considers simultaneously both

the geometric and strain gradient size effects. The constitutive model based on the traditional surface layer model was used to explain the grain-geometric size effect, while the strain gradient was taken into account via embedding the higher order of strain into the model. To describe the micro-scale flow stress of sheet metal, the surface layer model [17] was employed. The polycrystalline material was considered to be comprised of inner and surface portions. Hence, in this model, the flow stress of the material was determined by the contribution from two kinds of flow stresses: the flow stress of inner grains and that of surface grains.

$$\sigma = \eta\sigma_S + (1 - \eta)\sigma_i \quad (5.15)$$

$$\text{where } \eta = \frac{N_S}{N} = \frac{d}{t}$$

In equation (5.15), σ and N are the flow stress and the total grain number of the material, and σ_S and N_S are the flow stress and the number of surface grains, while σ_i is the flow stress of the inner grains, and η denotes the ratio between the number of surface grains to the number of the grains in the whole deformation body. In accordance with the crystal plasticity theory and Hall–Petch equation [64], the stresses in the surface and inner grains can be described as follows:

$$\sigma_S(\varepsilon) = m\tau_o(\varepsilon) \quad (5.16)$$

$$\sigma_i(\varepsilon) = M(\tau_o(\varepsilon) + K(\varepsilon)d^{-\frac{1}{2}}) \quad (5.17)$$

In equation (5.16) and (5.17), d is the grain size; m and M are the orientation factors of single crystal and polycrystals respectively; $\tau_o(\varepsilon)$ is the critical resolved shear stress of a single crystal, and $k(\varepsilon)$ is the local stress needed for general yield associated with the transmission of slip across polycrystals grain boundaries [66].

Based on the crystal plasticity theory [67], shear stress $\tau_o(\varepsilon)$ can be expressed in the following form:

$$\tau_o(\varepsilon) + \alpha Gb\sqrt{\rho_T} = \tau_o(\varepsilon) + \alpha Gb\sqrt{\rho_S + \rho_G} \quad (5.18)$$

where α is an empirical material constant ranging between 0.1 and 0.5. In the classical plasticity, only the statistically stored dislocation density $\rho_S(\varepsilon)$ is considered. However, due to the significant deformation gradients that exist between the sample surface and bulk, geometrically necessary dislocations described by density $\rho_G(\varepsilon) = \frac{C_G\varepsilon}{bd}$ may dominate in microscale plastic deformation, while the influence of statistically stored dislocations can be

neglected ($\rho_S(\varepsilon) \approx 0$). Based on Swift's hardening model $\tau(\varepsilon) = k(\varepsilon)^n$, the constitutive model for macro-scale deformation:

$$\begin{aligned}\sigma_i(\varepsilon) &= M(\tau_o(\varepsilon) + \alpha Gb\sqrt{\rho_T}) = M\left(\tau_o(\varepsilon) + \alpha Gb\sqrt{\frac{C_G\varepsilon}{bd}}\right) \\ &= Mk(\varepsilon)^n + M\alpha Gb\sqrt{\frac{C_G\varepsilon}{bd}}\end{aligned}\quad (5.19)$$

Combining equations (5.15) and (5.19), the flow stress of material in micro-deformation can be formulated as:

$$\sigma(\varepsilon) = \eta mk_1(\varepsilon)^{n_1} + (1 - \eta)\left(Mk_2(\varepsilon)^{n_2} + M\alpha Gb\sqrt{\frac{C_G\varepsilon}{bd}}\right) \quad (5.20)$$

where

$K_1=K_2$	$n_1=n_2$	C_G	α	m	M
150	0.48	0.18	0.34	2	3.06

5.4.2 Constitutive model with plastic strain gradient

Considering the plastic strain gradient hardening in the constitutive model, the following flow stress model is proposed:

$$\sigma(\varepsilon) = \eta mk_1(\varepsilon)^{n_1} + (1-\eta)\left(Mk_2(\varepsilon)^{n_2} + M\alpha Gb\sqrt{\frac{C_G\varepsilon}{bd}}\right) + k_3 l |\nabla\varepsilon| \quad (5.21)$$

The presence of the term $|\nabla\varepsilon|$ indicates the contribution of the plastic strain gradient to the flow stress, with l denoting the material intrinsic length, and $k_1 = k_2 = k_3$.

The variation of the plastic strain gradient in the thickness direction with longitudinal coordinate is given by:

$$\nabla\varepsilon = \frac{1}{R_n} = c \quad (5.22)$$

where c is the curvature of the neutral layer, R_n is the radius of the neutral layer. Using conventional effective plastic strain, equation (5.21) could be rewritten as: $\bar{\sigma}$

$$\bar{\sigma}(\varepsilon) = \eta mk_1(\bar{\varepsilon})^{n_1} + (1-\eta)\left(Mk_2(\bar{\varepsilon})^{n_2} + M\alpha Gb\sqrt{\frac{C_G\bar{\varepsilon}}{bd}}\right) + k_3 l |\nabla\bar{\varepsilon}| \quad (5.23)$$

The material intrinsic length (l) parameter is the multiplier of the strain gradient and determines the characteristic dimension of the size effect encountered in micro and nano-scale deformation, and the modified intrinsic length can be calculated based on equation (5.14).

5.4.3 The calculation of strain, strain gradient, stress, and bending moment

5.4.3.1. The calculation of strain and strain gradient

The geometric model of micro-bending deformation is illustrated in Figure 5.5 [50].

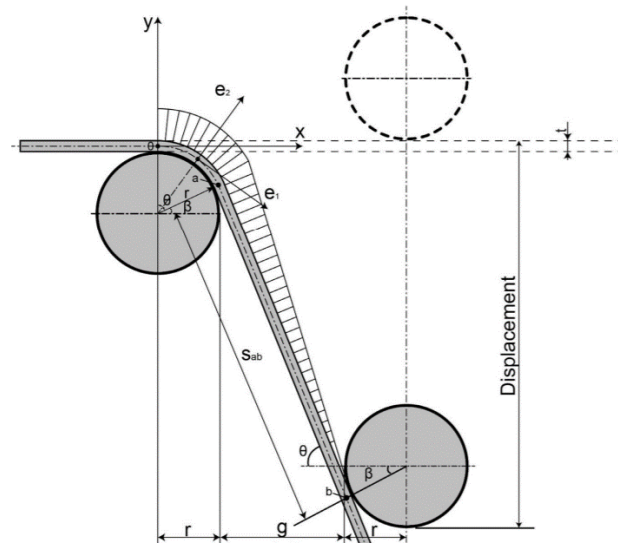


Figure 5.5: Geometric model.

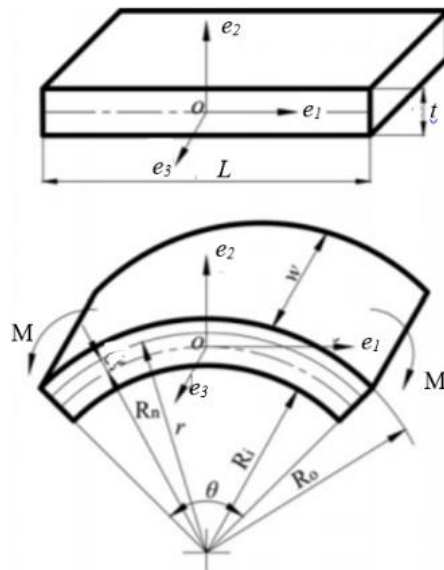


Figure 5.6: Coordinate diagram defining the spatial quantities for the pure moment bending.

The axes of the local coordinate system e_1 , e_2 and e_3 are along the length, thickness and width directions, respectively (as shown in Figure 5.6). Since the width w is much larger than the sheet thickness t , plane strain deformation is assumed. The displacement field is supposed as [64]:

$$u_1 = C e_1 e_2, \quad u_2 = \frac{-c(e_1^2 + e_2^2)}{2}, \quad u_3 = 0 \quad (5.24)$$

The strain tensor can be expressed as:

$$[\varepsilon_{ij}] = \begin{bmatrix} ce_2 & 0 & 0 \\ 0 & -ce_2 & 0 \\ 0 & 0 & 0 \end{bmatrix} \quad (5.25)$$

The conventional effective strain is:

$$\bar{\varepsilon} = \sqrt{\frac{2}{3} \varepsilon_{ij}' \varepsilon_{ij}'} = \frac{2}{\sqrt{3}} ce_2 \quad (5.26)$$

The gradient of effective strain is given by:

$$\nabla \bar{\varepsilon} = [0 \quad \frac{2}{\sqrt{3}} c \quad 0] \quad (5.27)$$

$$|\nabla \bar{\varepsilon}| = \frac{2}{\sqrt{3}} c \quad (5.28)$$

When equations. (5.27) and (5.28) are substituted into equation. (5.23), the constitutive relation used in the analytical model is obtained:

$$\bar{\sigma}(\varepsilon) = \eta m k_1 \left(\frac{2}{\sqrt{3}} ce_2 \right)^{n1} + (1-\eta) \left(M k_2 \left(\frac{2}{\sqrt{3}} ce_2 \right)^{n2} + M \sqrt{C_G \frac{2ce_2}{\sqrt{3} bd}} \right) + \frac{2}{\sqrt{3}} k_3 l \quad (5.29)$$

5.4.3.2. The calculation of stress

For foil micro bending, the radial stress normal to the foil is assumed to be zero (plane stress state), and only stresses along the longitudinal and width direction are considered;

$$\sigma_2 = 0, \sigma_3 = \frac{1}{2} \sigma_1 \quad (5.30)$$

Thus the effective stress is:

$$\bar{\sigma} = \sqrt{\frac{3}{2} \sigma_{ij} \sigma_{ij}} = \frac{\sqrt{3}}{2} \sigma_1 \quad (5.31)$$

In micro bending deformation, a sheet section may deform elastically or may contain an elastic core. In such an elastically deformed region, the stress is:

$$\sigma_1 = \frac{E}{1-\nu^2} \quad 0 < \varepsilon < \varepsilon_E \quad (5.32)$$

where ε_E is the elastic strain limit.

Substituting equation (5.31) into equation (5.29), the constitutive equation of the plastic deformation region is formulated as:

$$\sigma_1 = \frac{2}{\sqrt{3}} \left\{ \eta m k_1 \left(\frac{2}{\sqrt{3}} c e_2 \right)^{n_1} + (1 - \eta) \left(M k_2 \left(\frac{2}{\sqrt{3}} c e_2 \right)^{n_2} + M \alpha G b \sqrt{C_G \frac{2 c e_2}{\sqrt{3} b d}} \right) + \frac{2}{\sqrt{3}} k_3 l \right\} \quad (5.33)$$

5.4.3.3. The calculation of bending moment

The bending moment is calculated as:

$$M = \int_0^t \sigma_1 e_2 w. de_2 \quad (5.34)$$

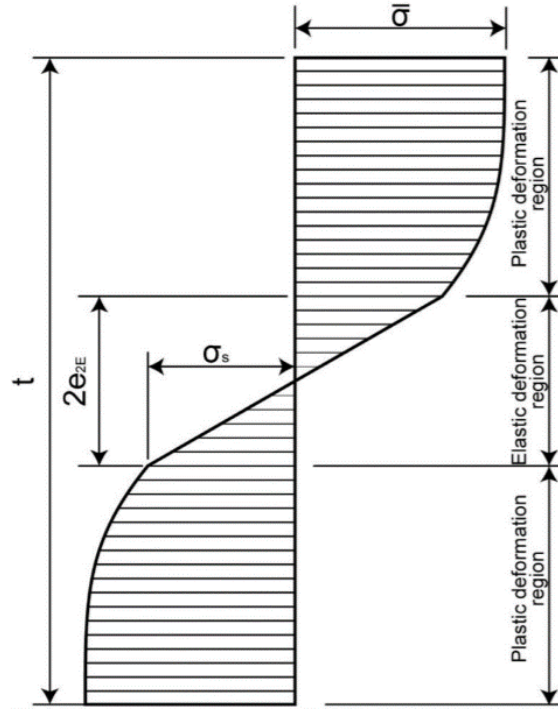


Figure 5.7: Stress distribution along the sheet thickness direction.

For the stress within the elastic region, as shown in Figure 5.7 [50], the elastic bending moment can be expressed based on equation (5.32) and (5.34) as follows:

$$M_E = \int_{-e_2E}^{e_2E} \sigma_1 e_2 w. de_2 = \frac{2wE}{3(1-\nu^2)} c (e_2E)^3 \quad (5.35)$$

As for the plastic deformation region illustrated Figure 5.9, the plastic bending moment can be obtained using equations (5.33) and (5.34):

$$\begin{aligned} M_P &= 2 \int_{e_2E}^{t/2} \sigma_1 e_2 w. de_2 \\ &= \frac{4w}{\sqrt{3}} \int_{e_2E}^{t/2} \left\{ \eta m k_1 \left(\frac{2}{\sqrt{3}} c e_2 \right)^{n_1} + (1 - \eta) \left(M k_2 \left(\frac{2}{\sqrt{3}} c e_2 \right)^{n_2} + M \alpha G b \sqrt{C_G \frac{2 c e_2}{\sqrt{3} b d}} \right) + \frac{2}{\sqrt{3}} k_3 l \right\} e_2. de_2 \end{aligned}$$

$$= \frac{4w}{\sqrt{3}} \left\{ \frac{\eta m k_1 \left(\frac{2}{\sqrt{3}c}\right)^{n_1}}{n_1+2} \left[\left(\frac{t}{2}\right)^{n_1+2} - e_{2E}^{n_1+2} \right] + \frac{(1-\eta) m k_2 \left(\frac{2}{\sqrt{3}c}\right)^{n_2}}{n_2+2} \left[\left(\frac{t}{2}\right)^{n_2+2} - e_{2E}^{n_2+2} \right] + (1 - \eta) M \alpha G b \sqrt{\frac{C_G}{bd}} \sqrt{\frac{2}{\sqrt{3}} c \frac{2}{5}} \left[\left(\frac{t}{2}\right)^{5/2} - e_{2E}^{5/2} \right] + \frac{1}{\sqrt{3}} k_3 l \left[\left(\frac{t}{2}\right)^2 - e_{2E}^2 \right] \right\} \quad (5.36)$$

For completely plastic bending ($e_{2E} = 0$), the plastic bending moment is represented by:

$$M_P = \frac{4w}{\sqrt{3}} \left\{ \frac{\eta m k_1 \left(\frac{2}{\sqrt{3}c}\right)^{n_1}}{n_1+2} \left(\frac{t}{2}\right)^{n_1+2} + \frac{(1-\eta) m k_2 \left(\frac{2}{\sqrt{3}c}\right)^{n_2}}{n_2+2} \left(\frac{t}{2}\right)^{n_2+2} + (1 - \eta) M \alpha G b \sqrt{\frac{C_G}{bd}} \sqrt{\frac{2}{\sqrt{3}} c \frac{2}{5}} \left(\frac{t}{2}\right)^{5/2} + \frac{1}{\sqrt{3}} k_3 l \left(\frac{t}{2}\right)^2 \right\} \quad (5.37)$$

All the material and experimental set-up parameters are given in Table 5.1.

Table 5.1: Material and experimental set-up parameters.

T (mm)	D (mm)	n_G	c	l (mm)	l_m (mm)	η
0.1	0.052	2	4	0.053	0.027	0.52
0.3	0.040	5.4	2	0.051	0.09	0.126
0.5	0.075	6.5	0.8	0.078	0.012	0.15

5.5 Calculation of springback

After micro bending, if the neutral radius of the bent sheet changes from R_n to R_n' the curvature changes before and after bending is, as shown in Figure 5.8 [50].

$$\Delta c = \frac{1}{R_n} - \frac{1}{R_n'} = \frac{M_b}{I} \cdot \frac{1-\nu^2}{E} \quad (5.38)$$

where, M_b is the bending moment at a section of the sheet, $I = \frac{wt^3}{12}$ is the second moment of area, c is the change of curvature of the neutral layer, R_n' is the radius of the neutral layer after springback.

The springback angle of an infinitesimal segment of the bended foil is obtained as:

$$d\theta_s = \Delta c \cdot ds = \frac{M_b}{I} \cdot \frac{1-\nu^2}{E} \cdot ds \quad (5.39)$$

where ds is the segment length. The total springback angle of the bent sheet can be calculated by integrating equation (5.39) across the total bending range:

$$\theta_s = \int_0^b \frac{M_p}{I} \cdot \frac{1-\nu^2}{E} \cdot ds = \int_0^a \frac{M_p}{I} \cdot \frac{1-\nu^2}{E} \cdot ds + \int_0^a \frac{M_p}{I} \cdot \frac{1-\nu^2}{E} \cdot \frac{S}{S_a} \cdot ds = \frac{M_p}{I} \cdot \frac{1-\nu^2}{E} (\hat{S}_{oa} + S_{ab}) \quad (5.40)$$

where \hat{S}_{oa} is the die-sheet contact arc length.

$$\hat{S}_{oa} = \left(r + \frac{t}{2}\right) \cdot \theta \quad (5.41)$$

Referring to the geometric relationship shown in Figure, the length from

$$S_{ab} = \left[i - 2 \left(r + \frac{t}{2}\right) \sin\theta \right] / \cos\theta \quad (5.42)$$

where θ is the bending angle, and $i = g+2r$.

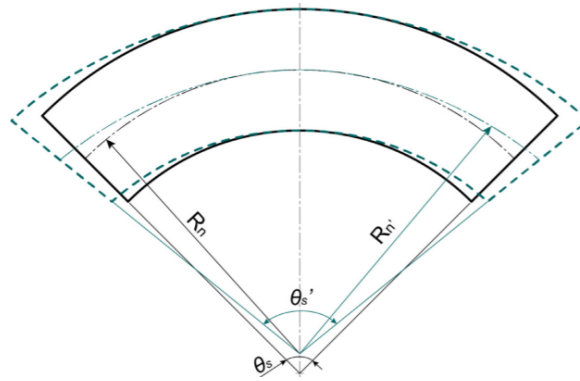


Figure 5.8: Schematic diagram of sheet curvature before and after springback.

5.6 Prediction of springback angle

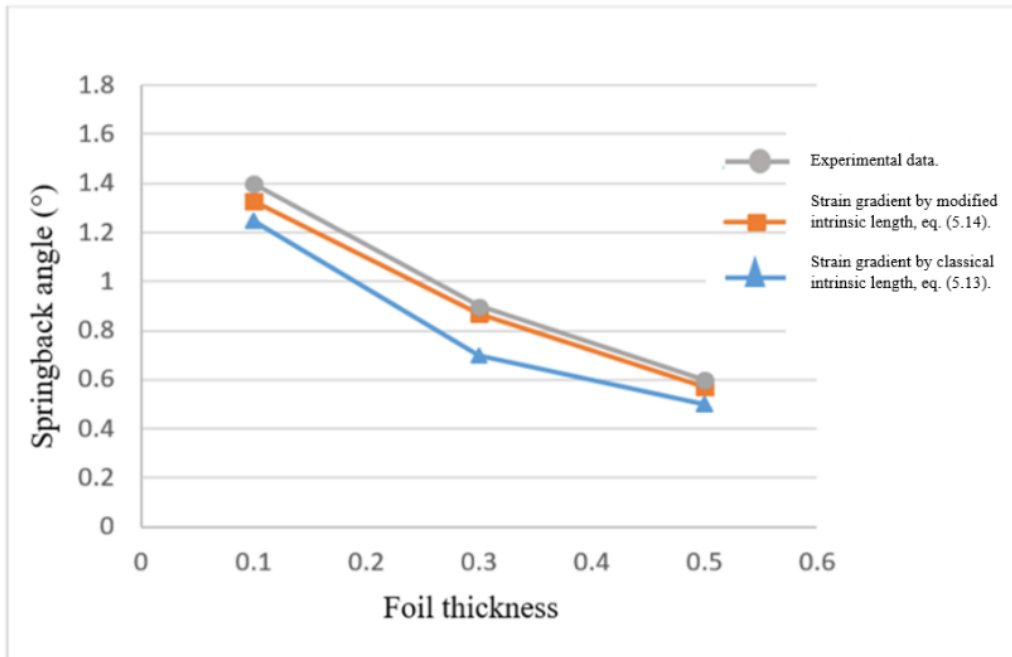


Figure 5.9: Springback angle of analysis equations and experimental data.

Equations (5.39) and (5.37) provide an estimate of the springback angle, from which the main influencing factors can be identified. M_p is the main factor leading to the change of springback angle that in turn depends on the material intrinsic length (l). For the calculations of the springback angle, according to the classical intrinsic length (l) and modified material intrinsic length (l_m) the MATLAB programming was employed. All the values of experimental parameters used in MATLAB program are specified in Table 5.1. The calculated springback angles with the analytical model are compared with the experimental data as shown in Figure 5.9. The data illustrates that the springback angle predicted by the mixed constitutive model with modified intrinsic length is close to the experimental data that means the conventional material intrinsic length is not valid any longer.

5.7 Summary

The modified material intrinsic length related to average grain numbers along the thickness direction of the specimen was determined and implemented in the analytical model to analyse the size effects. The following conclusions are obtained:

- i. In the micro bending process analysis of metal foils, the strain gradient can be simply calculated by the modulus of the gradient of conventional effective plastic strain instead of strain gradient tensor operating.
- ii. The average grain numbers across the foil thickness were considered into the modified material intrinsic length equation. It is more accurate to predict the springback angle using the modified material intrinsic length equation.
- iii. The quantitative expression of contribution of each effect on springback can be obtained based on the proposed mixed constitutive model.

Chapter 6. Development of a compact and portable universal testing machine (UTM) for in-situ micro-observation of size effects in micro metal forming

6.1 Introduction

Micro metal forming is a correct and relevant approach to manufacture the micro-scale metallic parts [7, 44]. With the fabrication of micro-scale parts, it is essential to do the engineering design and analysis for which the stress-strain relationship is essential [22, 71]. The study of the stress-strain relationship in small-scale samples is very important to understand the various mechanical properties of the selected material, such as the ultimate tensile and yield strengths, young's modulus, and the poisson's ratio [72]. The tensile test is the most significant method to study out the stress-strain relationship of material and it is broadly used due to its high degree of flexibility and economic advantages. The universal testing machine (UTM) is one of the most common equipment used for tensile testing [73]. This type of traditional testing machine is relatively heavy and typically installed in a laboratory. For evaluating the mechanical properties, this machine requires relatively large material samples. In the traditional testing machines, two crossheads are used; one is to adjust the length of the sample, and other is driven to apply the force to the test sample. The traditional testing machines are unable to apply the slow force on small test samples to properly replicate the actual force application. It is not easy to evaluate the tensile properties of the small (micro-scale) samples on the traditional UTM. The relationships between the dimensions and surface geometry in treated workpieces as well as in tools are different in macro and micro-scale, which directly affect the stress-strain relationship [73, 74].

Furthermore, the surface roughness is one of the core problems in the micro metal forming, which is mainly caused by non-uniform deformation of metal foils [74]. The increase in surface roughness of the metal foils occurs during plastic deformation, as investigated in chapter 4. Then, it becomes significant to investigate the mechanism of surface roughness in micro metal forming process in real-time for better analysis. Finally, it was concluded that the in-situ observations of the deformation behaviour and the surface roughness phenomena of different materials foils are very important to understand the influence of size effects in micro metal forming. For this persistence, the testing system should have the ability to perform the mechanical test of miniature and extremely small and thin specimens. In the past few years, the concern about the development of miniature testing apparatus inclined the interest of

researchers. The established systems [73, 75] are very complicated. Apart from this, only a few innovative small test machines are currently available in the market, but the typical budgetary limitation is another challenge to acquire those laboratory apparatus [76]. Therefore, it is necessary to develop a new highly precise compact testing apparatus.

This chapter presents research work aiming at the design and manufacturing of a compact test device. In this chapter, a new compact and portable UTM is developed with an ultrahigh precision drive system and high accuracy load and displacement measurement to perform the different mechanical tests with utmost control and data collection performance. The main objective was to develop a novel compact UTM compatible with a 3D laser-confocal microscope for in-situ micro-observation of size effects. The developed instrument can also be used for compression and bending analysis with appropriate fixtures and samples, but to validate the developed apparatus, these challenges are not be addressed. After developing this machine, metallic test samples made of thin copper sheet are used to perform the actual tensile test. To verify the performance of the developed machine the reported results of thin copper samples are compared with the results of similar samples tested in a commercial UTM machine (METEX – 1kN) using the same crosshead speed.

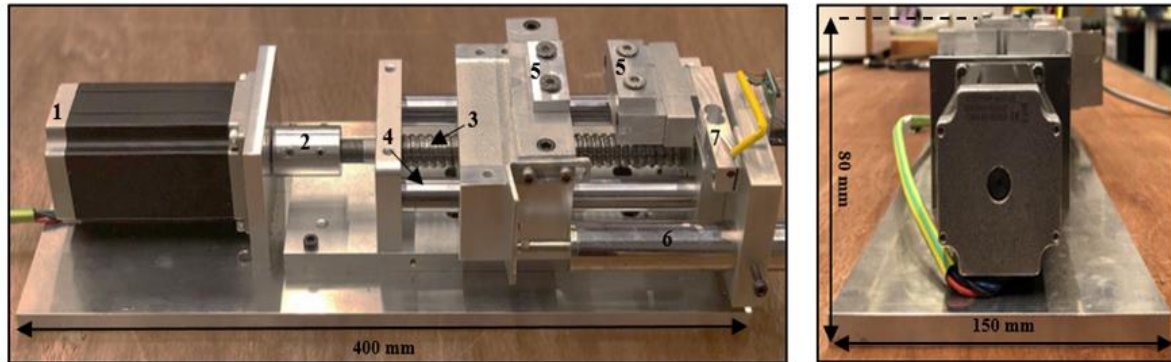
6.2 Specifications of the developed UTM

The developed UTM is designed to test small and thin specimen made of metals, polymers and metallic alloys, in the selected load range. In terms of the loading capacity of the developed apparatus, the specimen preparation and handling processes, only the thin miniaturised specimens are suitable for testing. This apparatus is capable of analysing tensile samples up to 8 cm of length. The following Figure 6.1 shows the overall structure of the established testing machine and all the specifications of the developed apparatus are listed in the Table 6.1. The general features of the developed UTM are described as following.

6.2.1. Features

- Oil and grease-free device for clean conditions.
- Easy to operate and control the system (e.g. emergency stop).
- Able to test miniaturised components (e.g. strain gauges).
- No hydraulic or pneumatic air supplies.
- Compatible with 3D laser-confocal microscope.
- Easy to carry or move (portable).
- Stable design.

- Compact instrument – apparatus requires less than 0.06 m² of floor space.
- Able to perform micro compression and bending tests.
- Machine table, which moves forward and backward with leadscrew-nut mechanism.



(a) Front view.

(b) Side view.

Figure 6.1: Overall Structure of the testing machine: (1) stepper motor, (2) coupling, (3) lead screw, (4) supported columns (5) Tensile test fixtures, (6) LVDT, (7) Load-cell.

Table 6.1: Specifications of the developed apparatus.

Maximum stroke	30 mm
Configuration	Twin column support
Mounting	Table/ground: Horizontal
Load cell	3kg, 5kg and 10 kg (as required)
Electrical supply	240v single-phase main supply
Strain-rate	0.01 mm/s, 0.02mm/s and 0.05mm/s (as required)
Column diameter	15 mm
Distance between columns	50 mm
Weight	5.5 kg (12 lbs)
Operating temperature	Room temperature

6.3 Design concept

6.3.1 Mechanical design

This instrument was mechanically designed to minimize the effects of load introduction in the mainframe, ball screw, and the relative movement between the movable crossheads. The testing machine is mainly made of Aluminium alloy, excepting some frictional elements like the bearing and ball screw, which were made of steel. After examining the previous studies [74, 75] and conventional standard testing methods [77-80] it was found that the screw-driven

mechanism is a leading technique to construct an ideal small testing apparatus. Therefore, a small CNC linear table, as shown in Figure 6.2 (a-b), driven by a ball screw was selected, which further attached to a stepper motor. In order to pull the tensile samples without torsion the ball screw converts the stepping motor rotation into linear motion. To develop this small testing device, some modifications have done in the original specifications, such as the height of the CNC table, as shown in Figure 6.3.

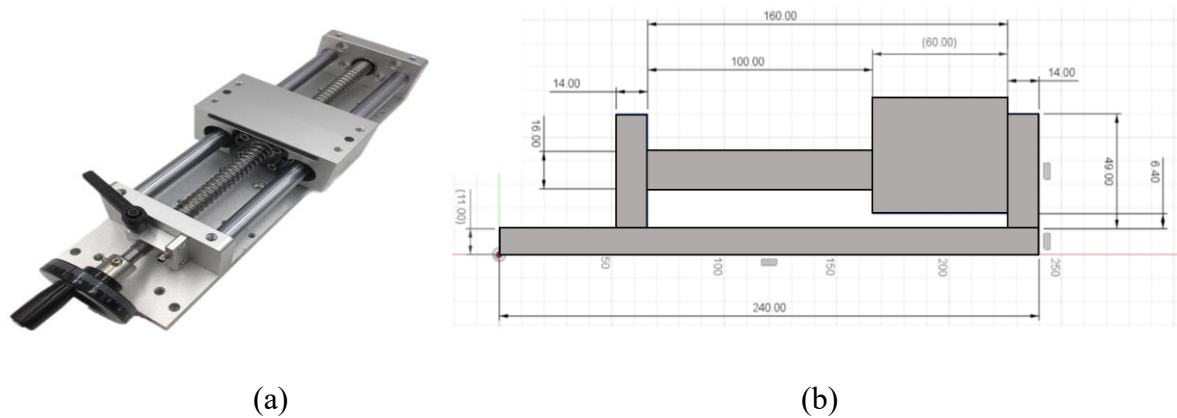


Figure 6.2: (a) Original CNC table, (b) Original specifications of CNC linear sliding table (unit: mm).

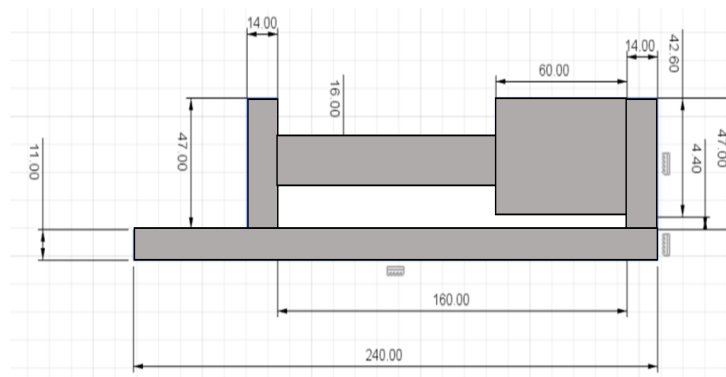
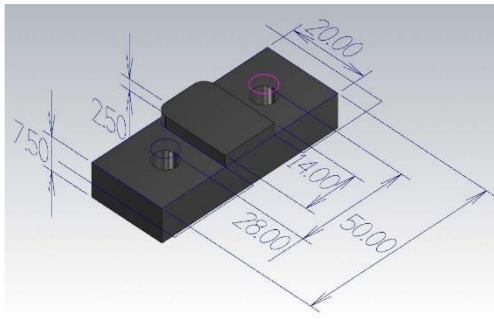


Figure 6.3: Modified specifications of CNC linear sliding table (unit: mm).

In the next design stage, the clamps or grippers were designed to hold the dog-bone shape test samples without slippage to carry out the actual testing. The specimen holder consists of two fixtures made of aluminium. The tensile test fixtures were provided in the form of male and female part, as shown in Figure 6.4 (a-b) and Figure 6.5 (a-b), respectively. Each fixture was composed by a fixed part and a movable plate joined with two screws to uniformly press the samples. A special specimen holder was designed to carry out both the tensile test and bending test, as shown in Figure 6.6.

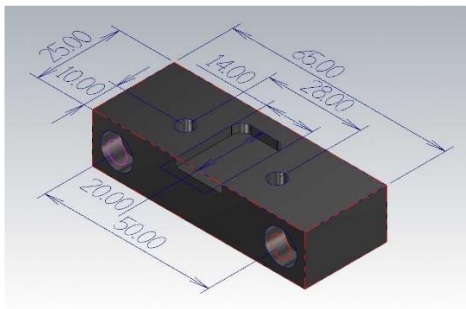


(a)

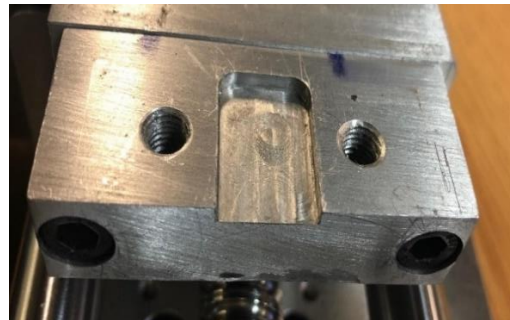


(b)

Figure 6.4: (a) Male part of tensile fixture (unit: mm), (b) Actual specimen holder.

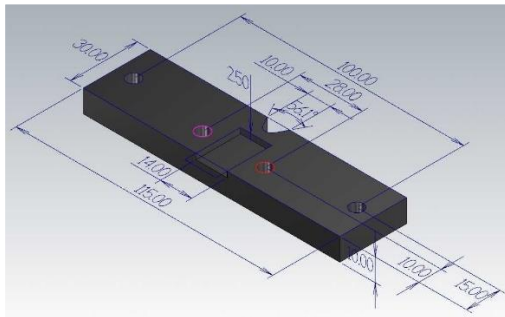


(a)

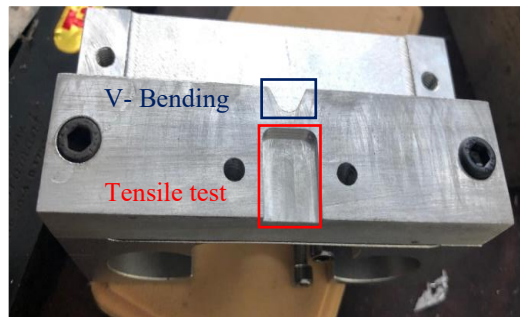


(b)

Figure 6.5: (a) Female part of tensile fixture (unit: mm), (b) Actual specimen holder.

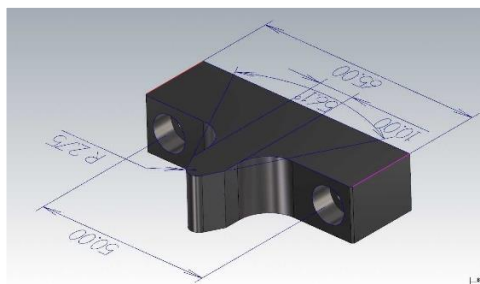


(a)

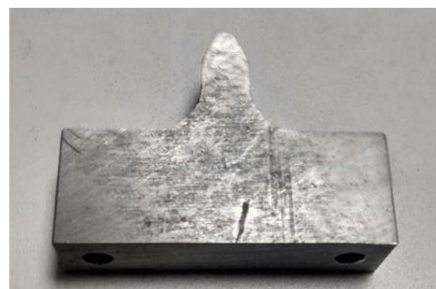


(b)

Figure 6.6: (a) Drawing of specimen holder (unit: mm), (b) Actual specimen holder.



(a)



(b)

Figure 6.7: (a) Drawing of V-bending punch (unit: mm), (b) Actual V-bending punch.

At the same time, a small punch, as shown in Figure 6.7 (a-b) was developed, to perform the micro V-bending test. The specimen is attached at both ends by fixing the specimen holders. After it, one of the specimen holders was attached to the load cell in order to record the load intervals, while the second clamp was moved forward and backward by a leadscrew-nut mechanism to provide enough pressure.



Figure 6.8: (a) High-speed 3-axis vertical CNC machine, (b) Machined fixture.

All the special design holders and fixtures were machined and manufactured on a high-speed 3-axis vertical CNC machine, as shown in Figure 6.8 (a-b).

6.3.2 Electronic Design

The overall electronic system of the devices and signals is shown in Figure 6.9. In this small UTM, a stepper motor (NEMA 23 Stepper Motor 3Nm) as shown in Figure 6.10 was used to drive the linear table with ball-screw guide-way. For different test routines, it was necessary to control both speed and position of the movable clamp, and therefore a stepper motor is used. The Control of the stepper motor was done by analogue signal generator device. With the signal generator, the speed, and rotation of the stepper motor were easily controlled, the circuit diagram and actual circuit of the stepper motor are shown in Figure 6.11 (a-b). A miniature straight bar load cell of 10Kg capacity was employed on the developed machine to acquire the required resolution from the measurements. This miniature UTM was designed according to the different ranges of miniature straight bar load cell, for measuring the different load intervals. The selected 10Kg load cell was connected to the Arduino board through an HX711 load cell amplifier, as shown in Figure 6.12 (a). No programming was applied for the internal registers because all the controls to HX711 were prepared through the pins. Load cell connections to the Arduino board are shown in Figure 6.12 (b). The material strain was measured by the movement of the crosshead displacement of the machine with a precision

digital displacement gage (LVDT), as shown in Figure 6.13 (a) with 0.01 mm resolution and 20 mm maximum displacement. Encoder signals were required to determine the actual position of LVDT therefore, the LVDT was attached to an Arduino board. LVDT connections to the Arduino board are shown in Figure 6.13 (b).

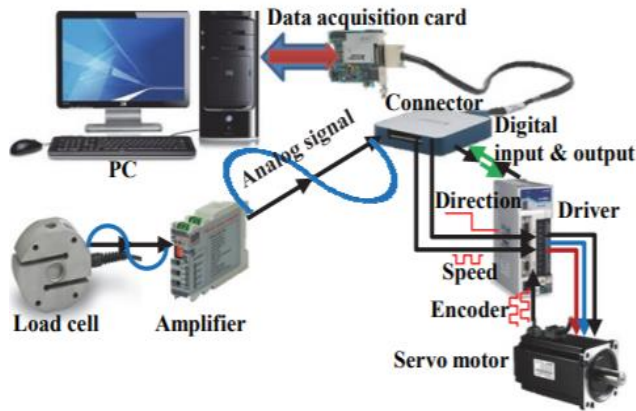
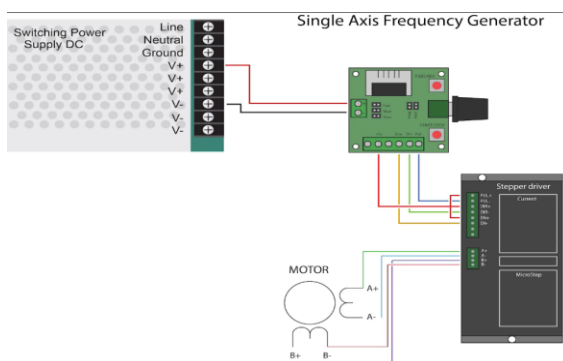


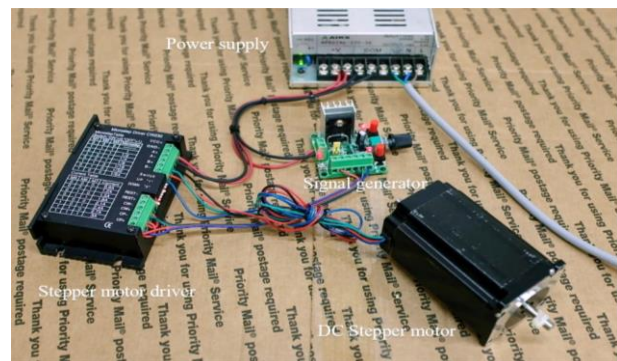
Figure 6.9: The overall electronic system.



Figure 6.10: NEMA Stepper motor.

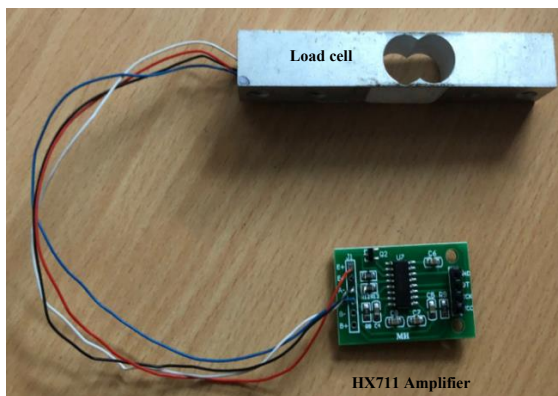


(a)

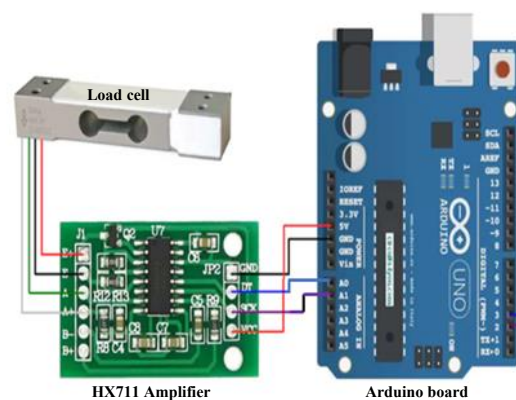


(b)

Figure 6.11: (a) Circuit diagram of the stepper motor, (b) Actual circuit of the stepper motor.



(a)



(b)

Figure 6.12: (a) Load cell with an amplifier, (b) Load cell interface Arduino.

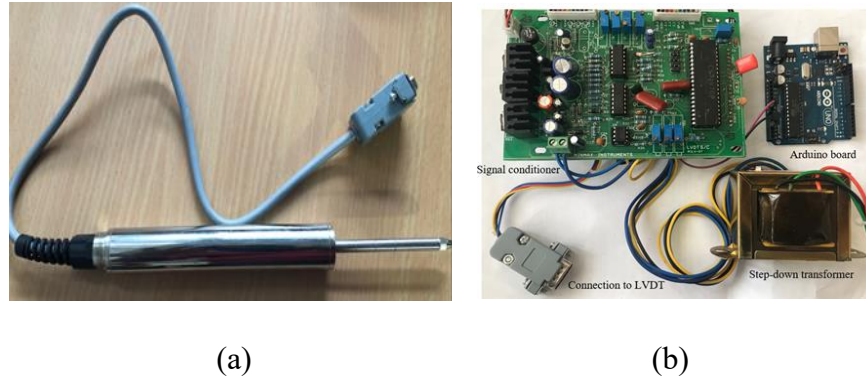


Figure 6.13: (a) Load cell interface Arduino, (b) LVDT interface Arduino.

6.3.3 Software

Arduino contains a microcontroller, which is able to be programmed to sense and control objects in the physical world. Once all the circuits have been prepared and completed, the sketches (Arduino coding) were uploaded to Arduino. The Arduino coding is a set of instructions that tells the board what functions it needs to perform and it can only hold and perform one coding at a time. After the connections, the Arduino sketching of the load cell to measure the load was prepared, presented in Appendix A-1. The coding to measure the elongation with LVDT is presented in Appendix A-2. However, to achieve high-resolution load-displacement curves for the analysed sample, it was necessary to measure the load intervals and strain-rates simultaneously. Therefore, a new sketch was prepared and uploaded to the data acquisition card (Arduino) to measure the loads and elongations at the same time, presented in Appendix A-3. After it, by responding to the sensors and inputs, the Arduino board was able to interact with a large array of outputs. In the end, the Tera-Term software was used to transfer the Arduino sensor data to excel sheet. Using this method, parameters as data acquisition time, displacement, and applied force were captured and saved in real-time for subsequent analysis.

6.4 Performance and validation

Before using this instrument for commercial purpose, the performance of the new testing device was required to evaluate. Most importantly, the calibration of the selected load cell, 10Kg was required before attaching it to the testing instrument for conducting the actual experiment. Therefore, the calibration of the load cell was conducted by collecting data of different known applied loads and measuring its corresponding output voltage. Figure 6.14 shows the obtained linear behavior between the applied load and the output voltage as obtained from the load cell. The following equation (6.1) was used to describe the relationship between the applied load (P) and the output voltage (V) [76].

$$P = 12.8366V - 0.06574 \quad (6.1)$$

where the applied load P is given in Newtons and the output voltage (V) in millivolts.

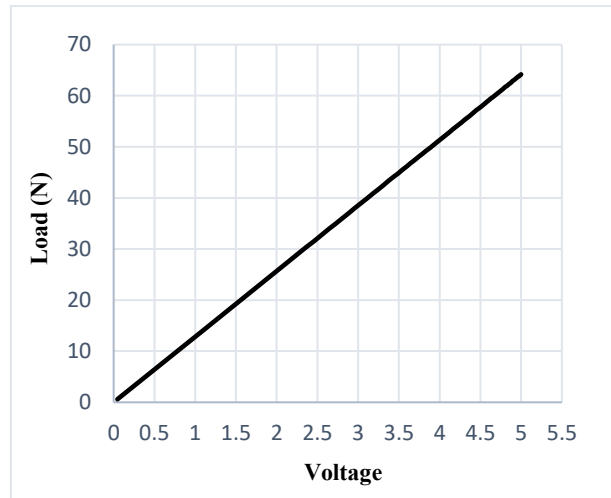


Figure 6.14: Static calibration curve for the load cell.

In order to validate the developed testing machine, a pure copper foil with the thickness of 50 μm was selected for actual tensile tests. The similar copper samples with the same thickness were used in chapter 4 to investigate the size effects with the micro tensile test. All the tensile tests on the new UTM have been performed with the same crosshead velocity (0.05 mm/s), so that the results of the newly developed machine can be compared with the reported test results derived from a standard testing machine to examine the performance.

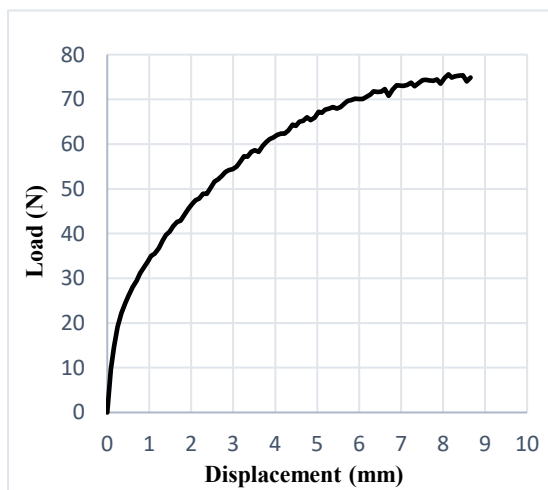


Figure 6.15: Load vs displacement graph.

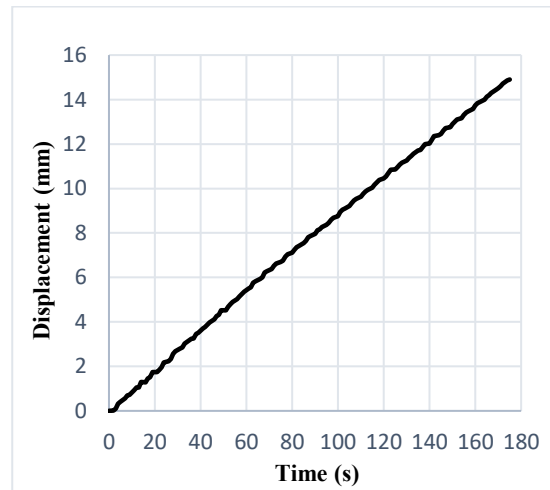


Figure 6.16: Displacement vs time graph.

Figure 6.15 shows load-displacement curve for the analyzed sample measured by the machine-crosshead and strain gage (simultaneously). Figure 6.16 shows a plot of the displacement of the movable crosshead vs. time, where high stability can be observed when it moves along the

drive screw with the sample gripped. This figure shows the very low mechanical noise during the crosshead displacement, which means that the machine does not have additional effects, such as vibrations or speed changes that could affect the performance. Figure 6.17 shows the real photograph of actual tensile tests conducted on the newly developed testing instrument.

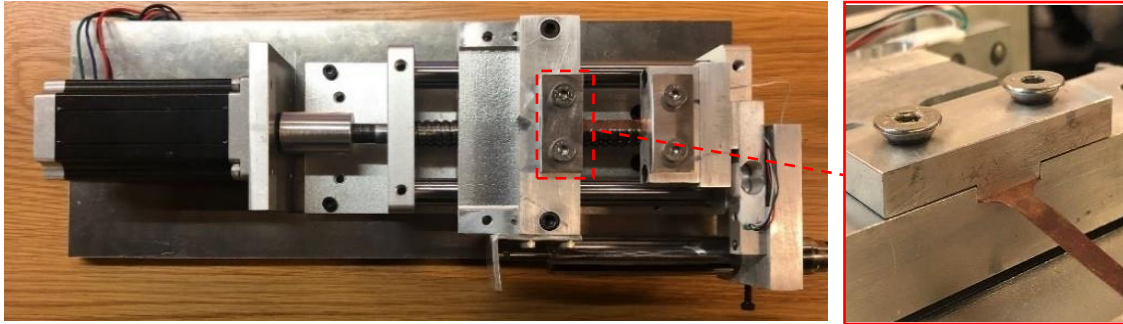


Figure 6.17: Actual tensile testing on newly developed testing device.

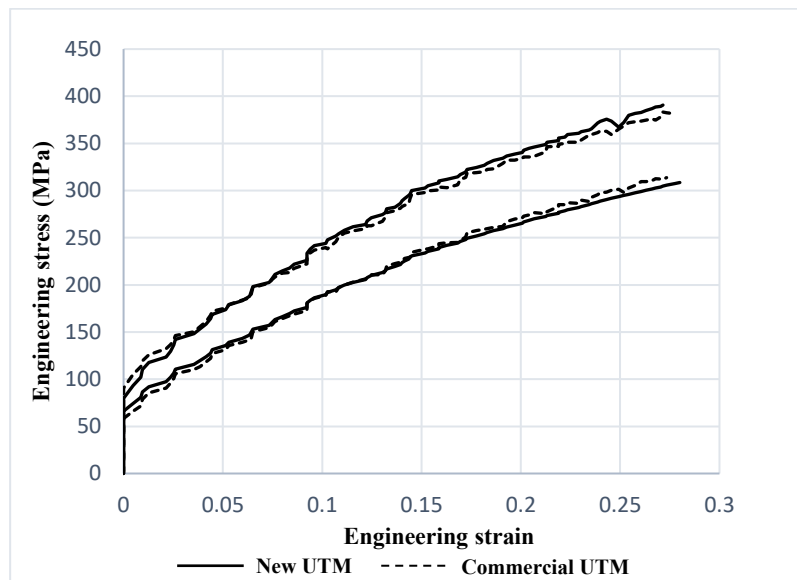


Figure 6.18: Stress-strain curves obtained from commercial Instron and newly developed testing apparatus.

Figure 6.18 shows the stress-strain curves of the similar copper samples as obtained from a standard Instron machine and home-made testing apparatus under similar conditions. From this figure, it can be observed the calculated values or results are quite similar, which indicate that the developed testing instrument is suitable to obtain reliable mechanical properties. The reported results obtained from the fabricated machine and standard machine were further used to determine the absolute errors in calculated mechanical properties values. Table 6.2 and Table 6.3 shows the average values of tested copper sample achieved from fabricated machine and standard machine, respectively.

Table 6.2: Average values of a tensile test obtained from home-made machine.

Load (N)	Extensions (mm)	Stress (MPa)	Strain
0	0	0	0
3.168634	0.08	12.674536	0.003194891
13.392514	0.26	53.53701	0.0104
19.582752	0.44	78.331008	0.017446914
29.781906	1	119.127624	0.036910354
39.517814	1.66	158.071256	0.065038396
49.211778	2.72	196.847112	0.101834306
60.073902	4.44	240.295608	0.161438346
65.550142	5.64	262.200568	0.206688913
70.518154	7.48	282.072616	0.2758119
69.860574	8.3	279.442296	0.287281992

Table 6.3: Average values of a tensile test obtained from commercial UTM.

Load (N)	Extensions (mm)	Stress (MPa)	Strain
0	0	0	0
9.77408312	0.06	39.09633248	0.002553994
16.82906108	0.150	67.31624431	0.005976785
22.42374233	0.23	89.69496931	0.009512599
29.27552539	0.51	117.1021016	0.020363291
39.91247333	1.32	159.6498933	0.05278862
49.47612521	2.46	197.9045008	0.098480559
60.30650191	4.14	241.2260076	0.165771358
65.4403902	5.56	261.7615608	0.222681854
70.00886894	7.43	280.0354758	0.297200355
68.88791484	7.60	275.5516593	0.304312552

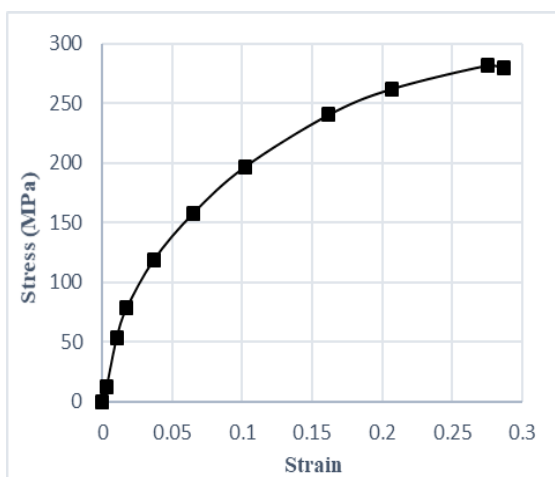


Figure 6.19: Stress-strain curve obtained from new testing apparatus.

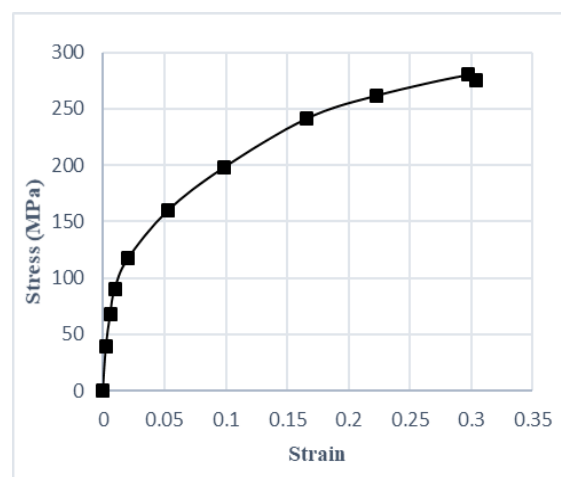


Figure 6.20: Stress-strain curve obtained from commercial UTM.

From these average stress strain values, the following mechanical properties were determined, as shown in Table 6.4. These results also reveal the absolute errors of measurement of 0.72%, 4.07%, 8%, and 5.61% for ultimate tensile strength, yield strength, yield strain, and ductility respectively.

Table 6.4: Calculated mechanical properties.

Mechanical properties	UTS (MPa)	Yield strength (MPa)	Yield strain	Ductility (%El)
New device	282.072	78.6	0.0232	28.72
Commercial UTM	280.035	81.94	0.0258	30.43
Abs. error (%)	0.72%	4.07%	8%	5.61%

The apparatus is very compact in size to put under the 3D laser-confocal microscope, as shown in Figure 6.21. To calculate the relative surface roughness behaviour of pure copper foil, the micro tensile test was performed on the newly developed machine under a 3D laser-confocal microscope. Where, the arithmetic average of the roughness profile ‘ R_a ’ was evaluated. Figure 6.22 shows the schematic illustration of testing setup.

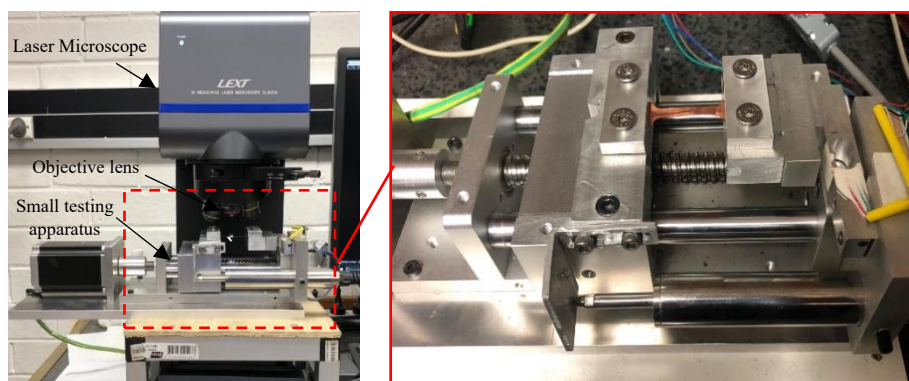


Figure 6.21: The testing apparatus under the laser microscope.

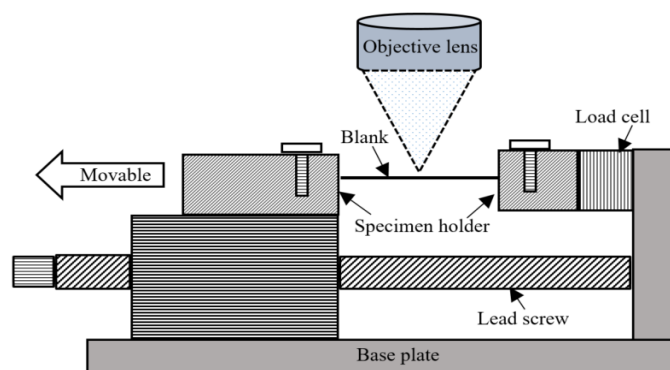


Figure 6.22: Schematic illustration of testing setup.

During the in-situ micro observation, a large region of stretched blank surface was observed by 3D laser-confocal microscope by using high magnifying lens. A constant distance was maintained between the stretched surface and the objective lens during testing. The surface roughness was measured at the same area in four stages by using a high magnifying lens (5X: $0.45\mu\text{m}$). The evaluated three-dimensional surface profiles of tested sample are shown in Figure 6.23. It observed that the surface roughness increase with the increase of plastic strain ' ϵ '. From these three-dimensional surface profiles, it is determined that in micro metal forming the local necking occurs in a very narrow region that is actually formed by free surface roughening, mainly causes the ductile fracture and the developed UTM is an appropriate device to examine this mechanism under the microscope for better understanding. Finally, it is confirmed that the surface roughness is one of the crucial factor affecting the fracture behaviour of metal foils in micro metal forming.

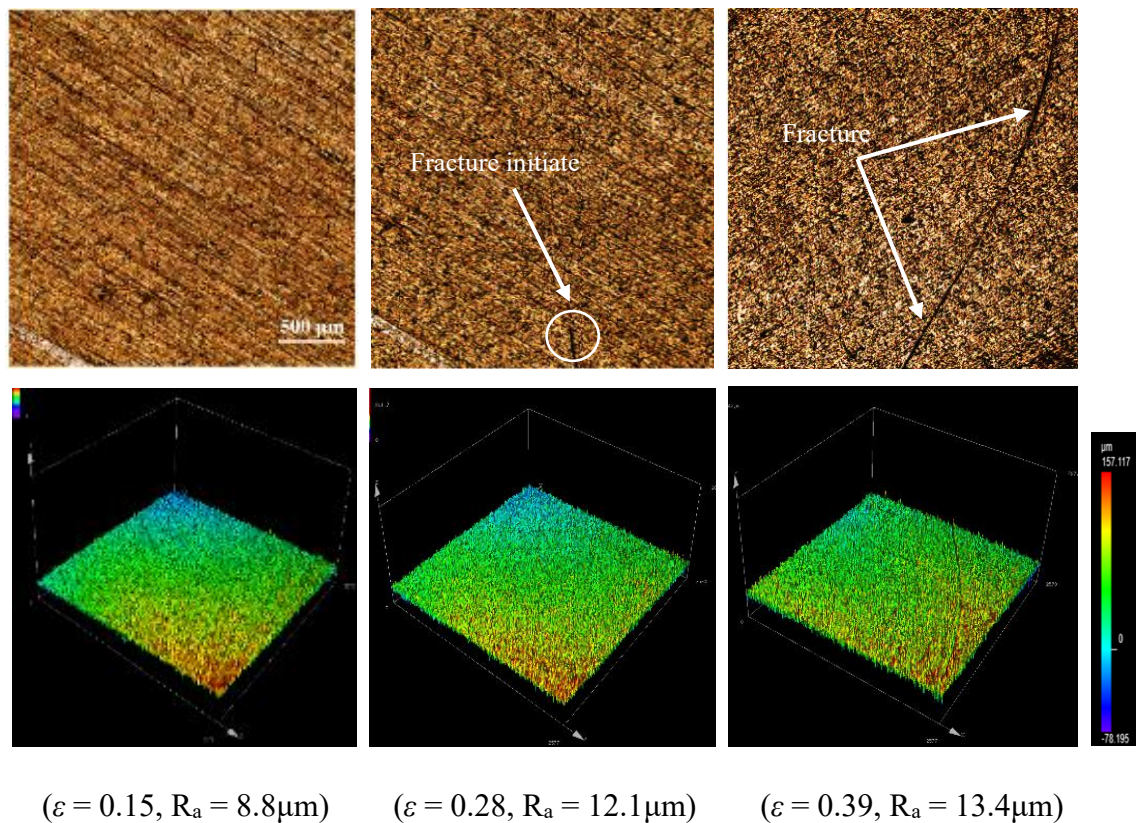


Figure 6.23: 3D surface profile of copper foil ($t = 0.05$ mm) obtained from laser microscope.

6.5 Summary

This chapter described a method to design and develop a portable miniaturised UTM. The newly designed apparatus has the capability to obtain displacement as small as 0.01 mm and maximum loads of 100 N. The mechanical properties of a 50 μm thick copper foil were

measured on this device and all the results were compared with the mean values obtained from commercial Instron machine. The reported results and the performance of developed testing machine indicate that it is an appropriate instrument to obtain reliable mechanical properties of thin and soft materials. The main advantage of this testing machine is the lower cost and smaller size compared to other commercial machines. Furthermore, an important feature of this device is the simplicity to exchange components (load cell and fixtures) according to the user requirements. This new testing system can be used on a 3D laser-confocal microscope, in order to evaluate the deformation behavior of materials on a microscale in real time. Future efforts will address the use of this equipment to obtain the mechanical properties of thin metallic films.

Chapter 7. Conclusion and recommendations for future work

This study was focused on size effects in micro metal forming operations, including micro tensile and micro V-bending testing. The experimentation offered basic data for micro metal forming technologies. The combination of experimentation and numerical modelling methods offered new vision into size effects controlling metal forming at the micro scales, and present test cases for further development of micro scale plasticity theories and models.

7.1 General conclusions

The general conclusions are presented as follows.

- i. Uniaxial micro tensile testing on micro scale copper specimens verified the existence of size effects as the T/D was limited in a certain range ($T/D > 1$). Together with the modifications made for the material model of hardening behaviour, the flow stress curves of copper samples were plotted. Due to the lack of adequately recovering of the strain-hardening behaviour of Cu the projected model with proposed modifications was only suitable up to first few plastic deformation points. This investigation provides a baseline for describing the deformation mechanisms that are truly important to micro metal forming operations.
- ii. The characteristics of three T/D ratios ($T/D > 1$, $T/D = 1$ and $T/D < 1$) were observed on the surface roughening behaviour of pure copper samples with uniaxial tensile testing. A significant increasing trend in the surface roughness was found with the reduction in the T/D ratio.
- iii. The observations of size effects in micro V-bending tests of copper specimens were done by considering the modified material intrinsic length (l_m) into the mixed constitutive model. The modified material intrinsic length was observed according to the average number of grains presented in the thickness direction of workpiece. Springback angle predicted by the mixed constitutive model with modified intrinsic length was in good agreement with experimental results. The results of classical metrical intrinsic length were also observed and could be replaced by modified material characteristic length. These results shed light on accurate modifications concern for micro metal forming.

- iv. A portable universal testing machine (UTM) has been designed and manufactured for measuring the mechanical properties of the miniaturised samples. The developed testing apparatus is compatible with a 3D laser-confocal microscope and it is suitable to investigate and provide a better understanding of the size effects in micro metal forming. A micro scale copper specimen was subjected to uniaxial tensile testing and the surface roughness process was successfully observed in detail.

7.2 Future work

- i. The grain orientation has an obvious size effect on the elastic and plastic deformation behaviours of the metal, its effect on springback can be studied in the future. The grain orientation information in three different T/D materials can be obtained by EBSD technology, and crystal plasticity finite element method (CPFEM) could be adopted to explore the size effects on springback.
- ii. To understand the relationship between surface roughness and technical parameters such as grain size, a constitutive model should be generated to simulate the surface evolution.
- iii. New testing apparatus can be used on a 3D laser-scanning microscope, to evaluate the deformation behaviours of other materials and miniaturised components. Not only is the developed apparatus suitable for metals, but also be used to test ceramics, composites, and polymers. In biomedical engineering, the new design and developed bone plates fractures can also be examined in detail with the help of this apparatus. Moreover, due to the novelty of this new compact testing apparatus, there is a potential for patent submission and commercialization.

References:

- [1] J. Jeswiet, M. Geiger, U. Engel, M. Kleiner, M. Schikorra, J. Duflou, R. Neugebauer, P. Bariani, S. Bruschi, Metal forming progress since 2000, *CIRP Journal of Manufacturing Science and Technology*. 1(1) (2008) 2-17.
- [2] S. Geißdörfer, U. Engel, M. Geiger, FE-simulation of microforming processes applying a mesoscopic model, 2006.
- [3] Y. Qin, Micro-forming and miniature manufacturing systems — development needs and perspectives, *Journal of Materials Processing Technology*. 177(1) (2006) 8-18.
- [4] A.R. Razali, Y. Qin, A Review on Micro-manufacturing, Micro-forming and their Key Issues, *Procedia Engineering*. 53 (2013) 665-672.
- [5] F. Vollertsen, D. Biermann, H.N. Hansen, I.S. Jawahir, K. Kuzman, Size effects in manufacturing of metallic components, *CIRP Annals*. 58(2) (2009) 566-587.
- [6] S. Mahabunphachai, M. Koç, Investigation of size effects on material behaviour of thin sheet metals using hydraulic bulge testing at micro/meso-scales, *International Journal of Machine Tools and Manufacture*. 48(9) (2008) 1014-1029.
- [7] U. Engel, R. Eckstein, Microforming—from basic research to its realization, *Journal of Materials Processing Technology*. 125-126 (2002) 35-44.
- [8] U. Engel, Tribology in microforming, 2006.
- [9] M. Geiger, M. Kleiner, R. Eckstein, N. Tiesler, U. Engel, Microforming, *CIRP Annals*. 50(2) (2001) 445-462.
- [10] M.W. Fu, J.L. Wang, A.M. Korsunsky, A review of geometrical and microstructural size effects in micro-scale deformation processing of metallic alloy components, *International Journal of Machine Tools and Manufacture*. 109 (2016) 94-125.
- [11] J.H. Deng, M.W. Fu, W.L. Chan, Size effect on material surface deformation behaviour in micro-forming process, 2011.
- [12] H.S. Kim, A quantitative study of the tribological size effect in microforming with a multi-region FEA model, *Tribology International*. 90 (2015) 104-112.

- [13] H. Li, X. Dong, Y. Shen, A. Diehl, H. Hagenah, U. Engel, M. Merklein, Size effect on springback behaviour due to plastic strain gradient hardening in microbending process of pure aluminum foils, *Materials Science and Engineering: A* 527(16) (2010) 4497-4504.s
- [14] J.Q. Ran, M.W. Fu, W.L. Chan, The influence of size effect on the ductile fracture in micro-scaled plastic deformation, *International Journal of Plasticity*. 41 (2013) 65-81.
- [15] W. Chan, M. Fu, and J. Lu, The size effect on micro deformation behaviour in micro-scale plastic deformation. *Materials & Design*, 2011. 32(1): p. 198-206
- [16] L.V. Raulea, A.M. Goijaerts, L.E. Govaert, F.P.T. Baaijens, Size effects in the processing of thin metal sheets, *Journal of Materials Processing Technology*. 115(1) (2001) 44-48.
- [17] H.N. Lu, D.B. Wei, Z.Y. Jiang, X.H. Liu, K. Manabe, Modelling of size effects in microforming process with consideration of grained heterogeneity, *Computational Materials Science*. 77 (2013) 44-52.
- [18] F.-K. Chen, J.-W. Tsai, A study of size effect in micro-forming with micro-hardness tests, *Journal of Materials Processing Technology*. 177(1) (2006) 146-149.
- [19] W.L. Chan, M.W. Fu, B. Yang, Experimental studies of the size effect affected microscale plastic deformation in micro upsetting process, 2012.
- [20] B. Meng, M.W. Fu, Size effect on deformation behaviour and ductile fracture in microforming of pure copper sheets considering free surface roughening, *Materials & Design*. 83 (2015) 400-412.
- [21] B. Guo, F. Gong, C. Wang, D.-b. Shan, Flow stress and tribology size effects in scaled down cylinder compression, 2009.
- [22] K. Suzuki, Y. Matsuki, K. Masaki, M. Sato, M. Kuroda, Tensile and microbend tests of pure aluminum foils with different thicknesses, *Materials Science and Engineering: A* 513-514 (2009) 77-82.
- [23] D. Anand, D.R. Kumar, Effect of Thickness and Grain Size on Flow Stress of Very Thin Brass Sheets, *Procedia Materials Science*. 6 (2014) 154-160.
- [24] H.M. Zbib, E.C. Aifantis, Size effects and length scales in gradient plasticity and dislocation dynamics, *Scripta Materialia*. 48(2) (2003) 155-160.

- [25] S.A. Parasiz, R. VanBenthysen, B.L. Kinsey, Deformation Size Effects Due to Specimen and Grain Size in Microbending, *Journal of Manufacturing Science and Engineering*. 132(1) (2010) 011018-011018-8.
- [26] Y. Sutou, T. Omori, K. Yamauchi, N. Ono, R. Kainuma, and K. Ishida, Effect of grain size and texture on pseudoelasticity in Cu–Al–Mn-based shape memory wire. *Acta Materialia*, 2005. 53(15): p. 4121-4133.
- [27] J.G. Liu, M.W. Fu, W.L. Chan, A constitutive model for modeling of the deformation behaviour in microforming with a consideration of grain boundary strengthening, *Computational Materials Science*. 55 (2012) 85-94.
- [28] C.-j. Wang, B. Guo, D.-b. Shan, L.-n. Sun, Effects of specimen size on flow stress of micro rod specimen, *Transactions of Nonferrous Metals Society of China*. 19 (2009) s511-s515.
- [29] Y. Sutou, T. Omori, N. Koeda, R. Kainuma, and K. Ishida, Effects of grain size and texture on damping properties of Cu–Al–Mn-based shape memory alloys. *Materials Science And Engineering: A*, 2006. 438: p. 743-746.
- [30] H. Ike, Surface deformation vs. bulk plastic deformation—a key for microscopic control of surfaces in metal forming, *Journal of Materials Processing Technology*. 138(1) (2003) 250-255.
- [31] Z.-w. Ma, G.-q. Tong, F. Chen, Deformation behaviour of materials in micro-forming with consideration of intragranular heterogeneities, *Transactions of Nonferrous Metals Society of China*. 27(3) (2017) 616-626.
- [32] M.W. Fu, W.L. Chan, Geometry and grain size effects on the fracture behaviour of sheet metal in micro-scale plastic deformation, *Materials & Design*. 32(10) (2011) 4738-4746.
- [33] C.J. Wang, D.B. Shan, J. Zhou, B. Guo, L.N. Sun, Size effects of the cavity dimension on the microforming ability during coining process, *Journal of Materials Processing Technology*. 187-188 (2007) 256-259.
- [34] S.-W. Baek, S.I. Oh, S.-H. Rhim, Lubrication for Micro Forming of Ultra Thin Metal Foil, 2006.
- [35] W. Wang, Y. Huang, K.J. Hsia, K.X. Hu, A. Chandra, A study of microbend test by strain gradient plasticity, *International Journal of Plasticity*. 19(3) (2003) 365-382.

- [36] Furushima, T.; Tsunozaki, H.; Hirose, Y., Fracture and surface roughening behaviors in micro metal forming. *Procedia Manufacturing*. 15 (2018) 1481-1486.
- [37] X. Lai, L. Peng, P. Hu, S. Lan, J. Ni, Material behaviour modelling in micro/meso-scale forming process with considering size/scale effects, *Computational Materials Science*. 43(4) (2008) 1003-1009.
- [38] L. Luo, Z. Jiang, D. Wei, Influences of micro-friction on surface finish in micro deep drawing of SUS304 cups, *Wear*. 374-375 (2017) 36-45.
- [39] W.T. Li, M.W. Fu, J.L. Wang, B. Meng, Grain size effect on multi-stage micro deep drawing of micro cup with domed bottom, *International Journal of Precision Engineering and Manufacturing*. 17(6) (2016) 765-773.
- [40] H.X. Zhu, B.L. Karihaloo, *Size-Dependent Bending of Thin Metallic Films*, 2008.
- [41] B. Song, G. Huang, H. Li, L. Zhang, G. Huang, and F. Pan, Texture evolution and mechanical properties of AZ31B magnesium alloy sheets processed by repeated unidirectional bending. *Journal Of Alloys And Compounds*. 489(2) (2010) p. 475-481.
- [42] T. Shimizu, M. Yang, K.-i. Manabe, Classification of mesoscopic tribological properties under dry sliding friction for microforming operation, *Wear*. 330-331 (2015) 49-58.
- [43] B. Bhushan, M. Nosonovsky, *Comprehensive Model for Scale Effects in Friction Due to Adhesion and Two- and Three-Body Deformation (Plowing)*, 2004.
- [44] Z. Jiang, J. Zhao, H. Xie, *Microforming Technology: Theory, Simulation and Practice*, 2017.
- [45] B. Klusemann, T. Yalçinkaya, Plastic deformation induced microstructure evolution through gradient enhanced crystal plasticity based on a non-convex Helmholtz energy, *Int. J. Plast.* 48 (2013) 168–188.
- [46] A. Haque, M.T.A. Saif, Saif M.T.A.: Strain gradient effect in nanoscale thin films. *Acta Mater.* 51, 3053-3061, 2003.
- [47] F. Vollertsen, Categories of size effects. *Production Engineering*, 2(4) (2008) p.377-383.
- [48] R. Eckstein, M. Geiger, and U. Engel. Specific characteristics of micro sheet metal working. in *Proceedings of the SheMet*, September. (1999).

- [49] H. Wicht and J. Bouchaud, NEXUS market analysis for MEMS and microsystems III 2005-2009. MST-news, Verlag VDI/VDE Innovation+ Technik GmbH, 5 (2005) p. 33-34.
- [50] J.L. Wang, M.W. Fu, S.Q. Shi, A.M. Korsunsky, Influence of size effect and plastic strain gradient on the springback behaviour of metallic materials in microbending process, *International Journal of Mechanical Sciences*. 146-147 (2018) 105-115.
- [51] J.-T. Gau, C. Principe, M. Yu, Springback behaviour of brass in micro sheet forming, *Journal of Materials Processing Technology*. 191(1) (2007) 7-10.
- [52] J. Del Valle and O. Ruano, Separate contributions of texture and grain size on the creep mechanisms in a fine-grained magnesium alloy. *Acta Materialia*, 55(2) (2007) p. 455-466.
- [53] R.K. Abu Al-Rub, G.Z. Voyiadjis, Analytical and experimental determination of the material intrinsic length scale of strain gradient plasticity theory from micro- and nano-indentation experiments, *International Journal of Plasticity*. 20(6) (2004) 1139-1182.
- [54] L. Llanes, A. Rollett, C. Laird, and J. Bassani, Effect of grain size and annealing texture on the cyclic response and the substructure evolution of polycrystalline copper. *Acta metallurgica et materialia* 41(9) (1993) p. 2667-2679.
- [55] S. Wang, W. Zhuang, D. Balint, J. Lin, A virtual crystal plasticity simulation tool for micro-forming, *Procedia Engineering*. 1(1) (2009) 75-78.
- [56] A.G. Evans, J.W. Hutchinson, A critical assessment of theories of strain gradient plasticity, *Acta Materialia*. 57(5) (2009) 1675-1688.
- [57] H. Mecking, U.F. Kocks, Kinetics of flow and strain-hardening, *Acta Metallurgica* 29(11) (1981) 1865-1875.
- [58] A. Molotnikov, R. Lapovok, C.H.J. Davies, W. Cao, Y. Estrin, Size effect on the tensile strength of fine-grained copper, *Scripta Materialia*. 59(11) (2008) 1182-1185.
- [59] Y.L. Chiu, A.H.W. Ngan, A TEM investigation on indentation plastic zones in Ni₃Al(Cr,B) single crystals, *Acta Materialia*. 50(10) (2002) 2677-2691.
- [60] X. Ma, R. Lapovok, C. Gu, A. Molotnikov, Y. Estrin, E. Pereloma, C. H. J. Davies, P. Hodgson, Deep drawing behaviour of ultrafine grained copper: Modelling and experiment, 2009.

- [61] A. Arsenlis, D.M. Parks, Crystallographic aspects of geometrically-necessary and statistically-stored dislocation density, 1999.
- [62] İ. Özdemir, T. Yalçinkaya, Modeling of dislocation–grain boundary interactions in a strain gradient crystal plasticity framework, *Comput. Mech.* 54 (2014) 255-268.
- [63] G.Z. Voyiadjis, R.K.A. Al-Rub, Gradient plasticity theory with a variable length scale parameter, *International Journal of Solids and Structures* 42(14) (2005) 3998-4029.
- [64] Li, H.; Dong, X.; Shen, Y.; Diehl, A.; Hagenah, H.; Engel, U.; Merklein, M., Size effect on springback behavior due to plastic strain gradient hardening in microbending process of pure aluminum foils. *Materials Science and Engineering: A*, 527(16) (2010) 4497-4504.
- [65] R.K. Abu Al-Rub, G.Z. Voyiadjis, Analytical and experimental determination of the material intrinsic length scale of strain gradient plasticity theory from micro- and nano-indentation experiments, *International Journal of Plasticity* 20(6) (2004) 1139-1182.
- [66] T. Yalcinkaya, W.A.M. Brekelmans, M. G. D. Geers, Non-convex rate dependent strain gradient crystal plasticity and deformation patterning, *Int. J. Solids Struct.* 49 (2012) 2625–2636.
- [67] T. Yalcinkaya, W.A.M. Brekelmans, M.G.D. Geers, Deformation patterning driven by rate dependent non-convex strain gradient plasticity, *J. Mech. Phys. Solids.* 59 (2011) 1–17.
- [68] S.-W. Lee, A study on the bi-directional springback of sheet metal stamping. *Journal of Materials Processing Technology*, 167(1) (2005) p. 33-40.
- [69] D. Fei and P. Hodgson, Experimental and numerical studies of springback in air v-bending process for cold rolled TRIP steels. *Nuclear engineering and design.* 236(18) (2006) p. 1847-1851.
- [70] Tekaslan, U. Şeker, and A. zdemir, Determining springback amount of steel sheet metal has 0.5 mm thickness in bending dies. *Materials & Design.* 27(3) (2006) p. 251-258
- [71] P.H. Hou, T.Y. Chen, An automatic tensile test measurement system for miniature specimens. *Experimental Techniques.* 29(4) (2005) 32-36.
- [72] Z. Ma, H. Zhao, H. Huang, L. Zhang, K. Wang, X. Zhou A Novel Tensile Device for In Situ Scanning Electron Microscope Mechanical Testing. *Experimental Techniques* 39(6) (2015) 3-11.

- [73] H. Kweon, S. Choi, Y. Kim, K. Nam Development of A new UTM (Universal Testing Machine) System for the Nano/Micro In-Process Measurement. *International Journal of Modern Physics B* 20 (25n27) (2006) 4432-4438.
- [74] G. Partheepan, D.K. Sehgal, and Pandey, R.K., Design and usage of a simple miniature specimen test setup for the evaluation of mechanical properties. *Inter. J. Microstructure and Materials Properties* (1) (2005) 38-50.
- [75] T. Furushima, Y. Hirose, Development of In-situ Observation Methods of Surface Roughening Behavior By Hand-size Stretching Test for Metal Foils. *Journal of Physics: Conference Series* 1063 (2018) 012130.
- [76] E. Huerta, J.H. Corona, A. Oliva, F. Aviles, J.H. González, J., Universal testing machine for mechanical properties of thin materials. *Revista mexicana de fisica* (56) (2010) 317-322.
- [77] T. Furushima, Y. Hirose, K. Tada, K. Manabe, Development of Compact Marchiniak Testing Apparatus for In-situ Microscopic Observation of Surface Roughening. *Procedia Engineering* (207) (2017) 1946-1951.
- [78] K.E. Clothier, Y. Shang, A Geometric Approach for Robotic Arm Kinematics with Hardware Design, Electrical Design, and Implementation. *Journal of Robotics* 2010.
- [79] ASTM E8 / E8M-16a, Standard Test Methods for Tension Testing of Metallic Materials, ASTM International, West Conshohocken, PA, 2016, www.astm.org.
- [80] ASTM D790-17, Standard Test Methods for Flexural Properties of Unreinforced and Reinforced Plastics and Electrical Insulating Materials, ASTM International, West Conshohocken, PA, 2017, www.astm.org.
- [81] ABAQUS User Manual, Version 6.13, Dassault Systèmes www.3ds.com.

Appendix-A

Appendix A-1 to A-2 demonstrate the Arduino sketching used for load cell and LVDT.

Appendix A-3 shows the modified Arduino coding of load cell and LVDT in one sketch.

```
#include "HX711.h"
// HX711.DOUT - pin #A1
// HX711.PD_SCK - pin #A0
HX711 scale(A1, A0); // parameter "gain" is omitted; the default value 128 is used by the library
void setup() {
  Serial.begin(9600);
  Serial.println("HX711 Demo");
  Serial.println("Before setting up the scale:");
  Serial.print("read: \t\t");
  Serial.println(scale.read()); // print a raw reading from the ADC
  Serial.print("read average: \t\t");
  Serial.println(scale.read_average(20)); // print the average of 20 readings from the ADC ___
  Serial.print("get value: \t\t");
  Serial.println(scale.get_value(5)); // print the average of 5 readings from the ADC minus the tare weight (not set yet)
  Serial.print("get units: \t\t");
  Serial.println(scale.get_units(5, 1)); // print the average of 5 readings from the ADC minus tare weight (not set) divided
  // by the SCALE parameter (not set yet)
  scale.set_scale(258.f); // this value is obtained by calibrating the scale with known weights; see the README for details
  scale.tare(); // reset the scale to 0
  Serial.println("After setting up the scale:");
  Serial.print("read: \t\t");
  Serial.println(scale.read()); // print a raw reading from the ADC
  Serial.print("read average: \t\t");
  Serial.println(scale.read_average(20)); // print the average of 20 readings from the ADC
  Serial.print("get value: \t\t");
  Serial.println(scale.get_value(5)); // print the average of 5 readings from the ADC minus the tare weight, set with tare()
  Serial.print("get units: \t\t");
  Serial.println(scale.get_units(5, 1)); // print the average of 5 readings from the ADC minus tare weight, divided
  // by the SCALE parameter set with set_scale
  Serial.println("Readings:");
}
void loop() {
  Serial.print("one reading:\t");
  Serial.print(scale.get_units(0, 1));
  Serial.print("\t\t| average:\t");
  Serial.println(scale.get_units(10, 1));
  scale.power_down(); // put the ADC in sleep mode
  delay(500);
  scale.power_up();
}
```

Appendix A-1: Arduino sketching for load cell.


```

/*
ReadAnalogVoltage

Reads an analog input on pin 0, converts it to voltage, and prints the result to the Serial Monitor.
Graphical representation is available using Serial Plotter (Tools > Serial Plotter menu).
Attach the center pin of a potentiometer to pin A0, and the outside pins to +5V and ground.

This example code is in the public domain.

http://www.arduino.cc/en/Tutorial/ReadAnalogVoltage
*/

// the setup routine runs once when you press reset:
void setup() {
  // initialize serial communication at 9600 bits per second:
  Serial.begin(9600);
}

// the loop routine runs over and over again forever:
void loop() {
  // read the input on analog pin 0:
  int sensorValue = analogRead(A0);
  // Convert the analog reading (which goes from 0 - 1023) to a voltage (0 - 5V):
  float voltage = sensorValue * (5.0 / 1023.0);
  // print out the value you read:
  Serial.println(voltage);
}

```

Appendix A-2: Arduino sketching for LVDT.

```

#include "HX711.h"

// HX711.DOUT - pin #A1
// HX711.PD_SCK - pin #A0

HX711 scale(A1, A0); // parameter "gain" is omitted; the default value 128 is used by the library
// initialize serial communication at 10000 bits per second:
void setup() {
  Serial.begin(9600);
  Serial.println("HX711 Demo");

  Serial.println("Before setting up the scale:");
  Serial.print("read: ");
  Serial.println(scale.read()); // print a raw reading from the ADC

  Serial.print("read average: ");
  Serial.println(scale.read_average(20)); // print the average of 20 readings from the ADC

  Serial.print("get value: ");
  Serial.println(scale.get_value(5)); // print the average of 5 readings from the ADC minus the tare weight (not set yet)

  Serial.print("get units: ");
  Serial.println(scale.get_units(5, 1)); // print the average of 5 readings from the ADC minus tare weight (not set) divided
  // by the SCALE parameter (not set yet)

  scale.set_scale(258.f); // this value is obtained by calibrating the scale with known weights; see the README for details
  scale.tare(); // reset the scale to 0

  Serial.println("After setting up the scale:");

  Serial.print("read: ");
  Serial.println(scale.read()); // print a raw reading from the ADC

  Serial.print("read average: ");
  Serial.println(scale.read_average(20)); // print the average of 20 readings from the ADC

  Serial.print("get value: ");
  Serial.println(scale.get_value(5)); // print the average of 5 readings from the ADC minus the tare weight, set with tare()

  Serial.print("get units: ");
  Serial.println(scale.get_units(5, 1)); // print the average of 5 readings from the ADC minus tare weight, divided
  // by the SCALE parameter set with set_scale

  Serial.println("Readings:");
}

void loop() {
  Serial.print("one reading:");
  Serial.print(scale.get_units(), 1);
  Serial.print(" average:");
  Serial.println(scale.get_units(10, 1));

  scale.power_down(); // put the ADC in sleep mode
  delay(500);
  scale.power_up();
  // read the input on analog pin 2:
  int sensorValue = analogRead(A2);
  // Convert the analog reading (which goes from 0 - 1023) to a voltage (0 - 5V):
  float voltage = sensorValue * (5.0 / 1023.0);
  // print out the value you read:
  Serial.println(voltage);
}

```

Appendix A-3: Modified Arduino sketching.